Identification of Cellular Interaction Partners of Adeno-associated Viruses

Dissertation

Frank Burkart

2014

DISSERTATION

SUBMITTED TO THE

COMBINED FACULTIES FOR THE NATURAL SCIENCES AND FOR MATHEMATICS OF THE

RUPERTO-CAROLA UNIVERSITY OF HEIDELBERG, GERMANY

FOR THE DEGREE OF

DOCTOR OF NATURAL SCIENCES

PRESENTED BY

FRANK BURKART, M.SC.

BORN IN PFORZHEIM, GERMANY

ORAL EXAMINATION: .....

Identification of Cellular Interaction Partners of Adeno-associated Viruses

Referees: Prof. Dr. Martin Müller

PD Dr. Oliver Müller

Declarations according to §8 of the doctoral degree regulations

I hereby declare that I have written the submitted dissertation independently and have not used other sources or materials than those particularly indicated. Furthermore I declare that I have neither applied for permission to be examined at any other institution, nor have I presented the same dissertation to another faculty, nor have I used this dissertation in any other form in another examination.

Heidelberg, Frank Burkart

Table of contents

Summary

Over the past decades, adeno-associated viruses (AAV) have evolved to be one of the most promising viral vectors for gene therapy. This great interest mainly rises from its non-pathogenicity, its simple organization and the fact that all viral genes are dispensable. Although these properties equip AAV as very safe vector, it is of great importance to further study the biology of AAV infection, which in part is still poorly understood. During the past years, many studies focused on the viral transduction, revealing mechanisms that facilitate viral infection. Upon those mechanisms, a key step in the AAV infection process is the conformational change of the capsid within the endosome, which leads to exposition of VP1/2 N-terminus. Analysis of the VP1/2 N-terminus makes specific domains accessible that play important roles during infection. In contrast, other studies demonstrated that modifications of the viral capsid by the host cell, such as phosphorylation and ubiquitination, affect and partially inhibit viral infection. Therefore, the underlying study aimed to identify cellular proteins that specifically interact with the unique N-terminus of the VP1/2 capsid proteins. For that, tandem affinity purification was performed using the VP1/2 N-termini of the AAV serotypes 2, 6, 8, 9 and 10. Double-tagged VP1/2 fusion proteins were overexpressed in and purified from HEK293TT cells, following mass-spectrometry to identify co-purified proteins. In total, 51 putatively interacting proteins were isolated. From those, 6 were identified with all of the serotypes used in the screen. Among the identified proteins that are involved in ubiquitination processes, SPOP, CAND1 and Cullin 3 were isolated. These proteins are known to form an ubiquitination machinery complex; hence they were used for further characterization. Interaction was confirmed by co-immunoprecipitation for SPOP and Cullin 3, as well as by indirect immunofluorescence analyzing, whether the proteins co-localize in transfected cells. Interestingly, when co-expressed with SPOP, VP1 was found in a speckled pattern localized in the nucleus, overlapping with SPOP, suggesting recruitment by SPOP. Sequence analysis of the VP1/2 N-terminus of all AAV serotypes revealed a putative SPOP binding consensus motif, which allowed mutational analysis for further characterization. Different AAV mutants showed a reduced transduction, as well as reduced binding to SPOP and differences in the subcellular localization. Overexpression of SPOP following infection with AAV did not change the level of transduction, suggesting endogenous SPOP levels to be sufficient to act on the infection. Knockdown experiments of SPOP, showed a slight increase in the transduction efficiency for AAV. Taken together, this study identified SPOP to be involved in the AAV life-cycle. Moreover it revealed cellular proteins that might be involved in the AAV infection process. Whether these proteins are captured by the virus to facilitate its infection or serve as host defense mechanism needs to be determined.

Zusammenfassung

Adeno-assoziierte Viren (AAV) entwickelten sich in den letzten Jahrzehnten zu den vielversprechendsten Vektoren für gentherapeutische Zwecke. Gründe hierfür sind unter anderem ihre Apathogenität, ihr einfacher Aufbau und die Tatsache, dass im Einsatz als Vektor auf alle viralen Gene verzichtet werden kann. Für eine sichere klinische Anwendung ist es unumgänglich, die Biologie des teilweise noch unbekannten Infektionsprozesses zu erforschen. Während der letzten Jahre wurden durch einige Studien wichtige Mechanismen der AAV Infektion aufgeklärt. Einer der wichtigsten Schritte ist die Konformations-Änderung des viralen Kapsids, die zur Exposition des VP1/2 N-Terminus führt. Durch Untersuchungen des VP1/2 N-Terminus wurden wichtige funktionelle und infektionsrelevante Domänen zugänglich gemacht. Im Gegensatz dazu zeigten andere Forschungsarbeiten, dass durch die Zelle bedingte Modifikationen des Kapsids, wie beispielsweise Phosphorylierung und Ubiquitinierung, die Infektion beeinflussen und zum Teil inhibieren können. Ziel der vorliegenden Arbeit war daher, zelluläre Proteine zu identifizieren, die spezifisch mit dem N-Terminus der Kapsid Proteine VP1/2 interagieren. Dazu wurde eine *Tandem Affinitäts-Aufreinigung* mit VP1/2 N-Termini von den AAV Serotypen 2, 6, 8, 9 und 10 durchgeführt. Doppelt markierte Fusionsproteine wurden in HEK293TT überexprimiert und aufgereinigt. Mittels Massenspektroskopie konnten insgesamt 51 mögliche Interaktionspartner identifiziert werden. Davon wurden sechs zelluläre Proteine mit allen im Screen verwendeten Serotypen isoliert. Unter den isolierten Proteinen, die an Ubiquitinierungsprozessen beteiligt sind, waren SPOP, CAND1 und Cullin 3. Von diesen Proteinen ist bekannt, dass sie zusammen einen Ubiquitinierungskomplex bilden, weshalb sie für weitere Experimente verwendet wurden. Die Interaktion konnte mittels Ko-Immunopräzipitation für SPOP und Cullin 3 bestätigt werden, in transfizierten Zellen wurde eine Ko-Lokalisation mittels indirekter Immunofluoreszenz beobachtet. Interessanterweise wurde VP1 in nukleären *speckles* gefunden, wenn es zusammen mit SPOP exprimiert wurde. Dies lässt auf eine Rekrutierung von VP1 durch SPOP schließen. Weiterhin konnte durch Sequenzanalyse von allen Serotypen ein mögliches SPOP-Bindemotiv im N-Terminus von VP1/2 identifiziert werden. Verschiedene Mutationen in diesem Motiv führten zu einer reduzierten Infektion und Bindung an SPOP sowie zu einer veränderten subzellulären Lokalisation. Eine Überexpression von SPOP führte zu keiner Änderung der Transduktion, was darauf hinweist, dass die endogenen SPOP Konzentrationen ausreichen, um die AAV Infektion zu beeinflussen. Im Gegensatz dazu führten verminderte SPOP Konzentrationen zu einem leichten Anstieg der Transduktionseffizienz. Zusammenfassend konnte mit dieser Arbeit gezeigt werden, dass SPOP im Lebenszyklus von AAV involviert ist. Des Weiteren wurden einige zelluläre Proteine isoliert, die möglicherweise ebenfalls während der Infektion eine Rolle spielen. Ob diese Proteine vom Virus selbst rekrutiert werden, um die Infektion zu erleichtern, oder ob sie der Zelle als Abwehrmechanismus dienen, muss in weiterführenden Studien untersucht werden.

1 Introduction

1.1 Biology of Adeno-associated viruses

Adeno-associated viruses (AAVs) are small, non-enveloped, single-stranded DNA viruses that were discovered in 1965 as contaminants in adenoviral stocks. AAVs belong to the *Parvoviridae* family and are classified as *Dependoviridae (Atchison 1965, Hoggan et al. 1966)*.

As already indicated by their genus, AAV depend on the co-infection of a helper virus for a replicative infection. Helper viruses have been identified to be adenovirus *(Atchison 1965)*, herpes simplex virus *(Georg-Fries et al. 1984)*, human cytomegalovirus *(McPherson et al. 1985)*, vaccinia virus *(Schlehofer et al. 1986)* and human papillomavirus *(Walz et al. 1997, Ogston et al. 2000)*. Upon co-infection, either of these viruses provides several essential functions necessary for AAV to undergo a productive infection. These functions are nuclear transport, formation of double-stranded DNA, conversion of circular DNA and activation of transcription *(Chang et al. 1989, Chang and Shenk 1990, Shi et al. 1991, Ferrari et al. 1996, Fisher et al. 1996, Duan et al. 1998, Duan et al. 1999, Xiao et al. 2002)*. Additionally, helper viruses support the transport, stability, splicing and translation of the AAV mRNAs *(Samulski and Shenk 1988, Janik et al. 1989, Mouw and Pintel 2000)* and finally facilitate AAV genome replication and AAV cell escape *(Carter et al. 1983, Huang and Hearing 1989, Ward et al. 1998, Geoffroy and Salvetti 2005)*. Besides the helper viruses, other studies suggested also cellular genotoxic stress, namely UV-light *(Yakobson et al. 1987, Yakobson et al. 1989)* or chemicals, such as hydroxyurea or cellular genotoxic stress *(Yalkinoglu et al. 1988)* to be able to provide helper functions that lead to a productive infection of AAV. In the absence of a helper virus (or other helper functions), AAV undergoes a latent infection, integrating site-specifically into chromosome 19 of the host cell genome *(Weitzman et al. 1994)* or maintaining as episomal state *(Cheung et al. 1980)*. Presence of a helper virus or cellular stress at later stages can reactivate DNA transcription and replication, converting AAV from its latent state to productive infection *(Grieger and Samulski 2012)*.

Since the first discovery in 1965, twelve different serotypes have been identified and isolated from human and primate tissues *(Muramatsu et al. 1996, Chiorini et al. 1997, Rutledge et al. 1998, Chiorini et al. 1999, Xiao et al. 1999, Mori et al. 2004, Schmidt et al. 2008)*. Natural hosts of AAV 1, 4, 7, 8, 11 and 12 are different primates, whereas humans are infected by the serotypes 2, 3, 5, 6 and 9. However, independent of their natural host, all AAV serotypes are able to infect different cell lines of human origin. Among these twelve serotypes, AAV2 is the best characterized and studied one and hence, considered as the prototype for AAV research.

Epidemiologically, AAV infections seem to be quite common, as anti-AAV antibodies have been detected in approximately 80% of the human population *(Moskalenko et al. 2000)*. However, as there is no human disease associated with AAV infection, AAVs are considered to be non-pathogenic *(Berns et al. 1975)*. During the past years, AAVs have emerged to turn into a very promising and the most frequently used viral vector for gene therapy, mainly due to its non-pathogenic behavior, but also its robustness and structural simplicity. To date, clinical trials at all phases are ongoing using different AAV serotypes to treat severe diseases, such as *Cystic Fibrosis* (AAV2), *Haemophilia B* (AAV2, AAV8) or *Muscular Dystrophy* (limb girdle, AAV1) *(Grieger and Samulski 2012)*.

1.2 Genome organization of AAV2

AAV2 carries a linear, single-stranded DNA genome of 4679 nucleotides (nt) length and is packaged in sense and antisense polarity at equal frequencies *(Srivastava et al. 1983, Daya and Berns 2008)*. The genome comprises the two viral genes *rep* and *cap* with three open reading frames (ORFs), encoding the non-structural Rep proteins, the structural Cap proteins, as well as a capsid assembly factor (Assembly Activating Protein; AAP; **Figure 1**) *(Rose et al. 1971, Hermonat et al. 1984, Sonntag et al. 2011)* and is flanked by two 145 nt long inverted terminal repeats (ITRs; **Figure 1 A**). The first 125 nt of the ITRs form the characteristic T-shaped hairpin structure mediated by three pairs of palindromic sequences, whereas the last 20 nt remain single-stranded and form the so called D-sequence *(Lusby et al. 1980)*. The ITRs are the only *cis*-acting elements in the AAV genome and serve with their 3'-OH overhang as primer during viral DNA replication. Beside their function in replication, the ITRs are recognized by the non-structural Rep proteins (**Figure 1 B**) at the Rep-binding elements triggering effective genome packaging, transcription, negative regulation in the absence of a helper virus and site-specific integration *(Daya and Berns 2008)*.

1.2.1 The Rep proteins

The *rep* gene encodes four non-structural proteins: Rep78, Rep68, Rep52 and Rep40 (named according to their respective molecular weight). Transcription of Rep78 and Rep68 is driven by the promoter p5 and both proteins are generated from the same mRNA by alternative splicing (Figure 1 **B**). As reviewed by *Grieger and Samulski (2012)*, these proteins seem to be important in almost every step during the viral life-cycle, including transcription, DNA replication and site-specific integration into the host cell genome. The smaller Rep proteins, Rep52 and Rep40, derive from a second mRNA, driven by the promoter p19. As for the two larger Rep proteins, Rep52 and Rep40 share a common mRNA and are generated by alternative splicing (**Figure 1 B**). These two proteins have been characterized to function in genome encapsidation into the preformed capsid *(King et al. 2001)*.

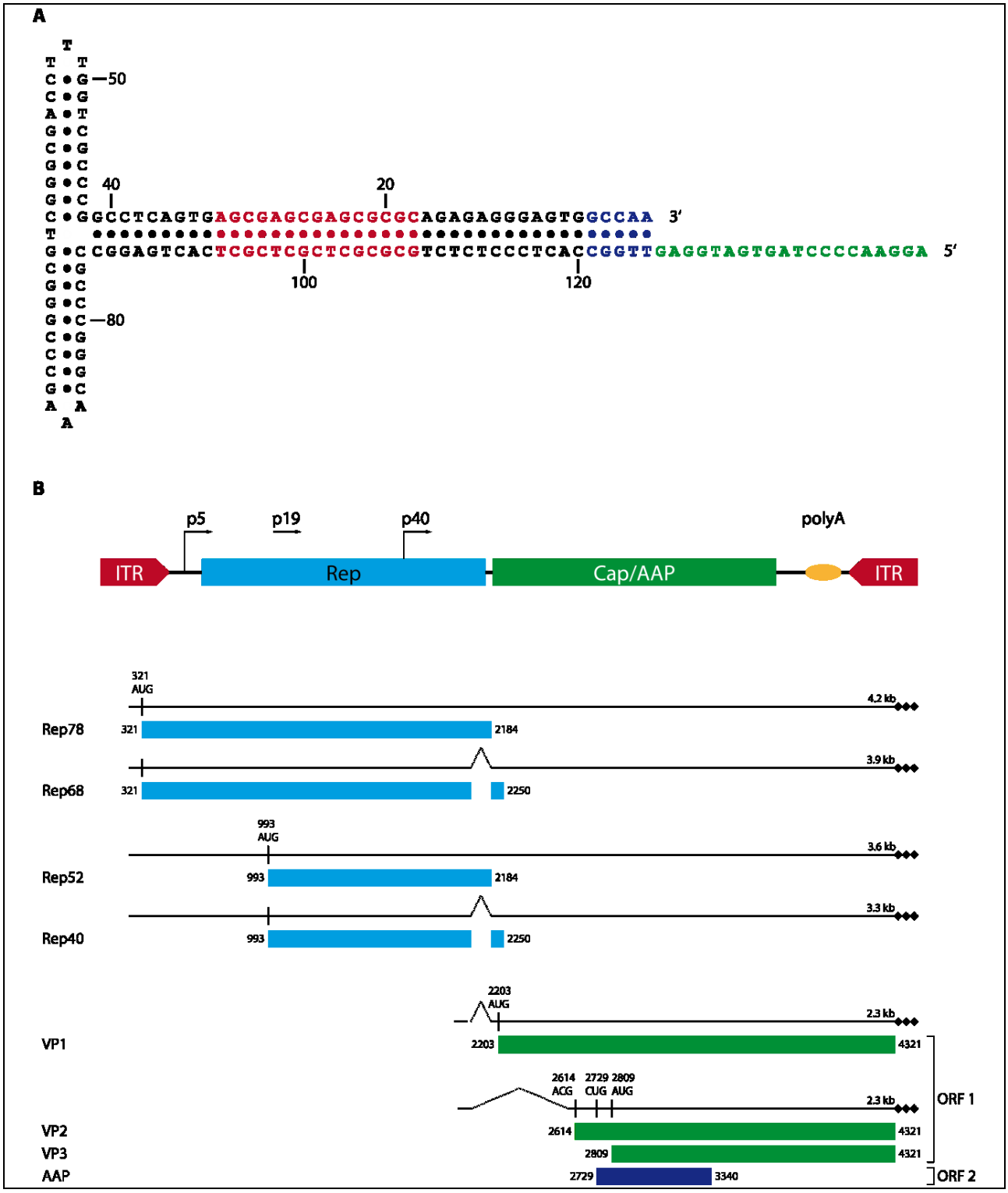

Figure 1: Genome organization of AAV2. A Secondary structure of the ITRs. The first 125 nt build the characteristic T-shaped hairpin with three palindromic sequences, the rep-binding-site (red) and a terminal resolution site (blue). The remaining 20 nt are single stranded and form the D-sequence (green; adapted from *Lusby et al. 1980*). **B** Complete AAV2 genome. The two genes rep (blue) and cap (green) are shown. Translation is driven by the three promoters p5, p19 and p40. Blue bars represent the four non-structural

regulatory (Rep) proteins, derived from two different mRNAs, while the green bars represent the three structural capsid proteins (Cap), encoded from the same mRNA. The dark blue bar represents the assembly activating protein (AAP) deriving from the second ORF that is located within the cap gene. Dotted lines represent the splicing sites and introns of the mRNAs and the three closed diamonds mark the polyadenylation sites. All start codons are shown and marked at the respective sites (adapted from *Naumer 2011)*.

1.2.2 The Cap proteins and AAP

The three structural proteins VP1 (87 kDa), VP2 (73 kDa) and VP3 (62 kDa), as well as the AAP (23 kDa) derive from two alternative spliced mRNAs initiated from the promoter p40. Different efficiencies of the splice acceptor sites result in the generation of a major and a minor mRNA species (**Figure 1 B**). Translation of the minor transcript results in the generation of VP1, whereas VP2 and VP3 are generated by translation of the major transcript, starting at the non-canonical start-codon ACG and the conventional start-codon AUG, respectively *(Rose et al. 1971, Becerra 1988)*. Due to the nature of the capsid protein synthesis of AAV2, all VP proteins share a common C-terminus and only differ in their N-terminal part, with VP1 having a unique N-terminus. In contrast to the three structural proteins, AAP is generated from an alternative open reading frame, using the non-canonical start-codon CUG (**Figure 1 B**). AAP seems to direct the newly synthesized VP proteins to the nucleoli of infected cells and drives the formation of the capsid assembly *(Sonntag et al. 2010)*.

Besides their function in the formation of the viral capsid (1.3), several functional domains have been identified on the VP1/2 N-terminus of the AAV2 capsid proteins (**Figure 2**). As for many other parvoviruses a phospholipase A2 (PLA2) domain was identified on the VP1 N-terminus, playing a major role during the infection (1.4.3) *(Zadori et al. 2001)*. It could be shown, that mutations in the PLA2 domain lead to reduced enzymatic activity, hence, attenuating viral infectivity *(Girod et al. 2002)*. Normally buried inside the viral capsid, the PLA2 domain of the VP1 N-terminus must be exposed during infection to exert its enzymatic activity. This conformational rearrangement of the capsid could be shown *in vitro* by heat treatment *(Kronenberg et al. 2001, Bleker et al. 2005, Kronenberg et al. 2005)*. *In vivo*, it is thought that the VP1 N-terminus exposure is induced by the low pH inside the endosomal compartment (1.4.3), in combination with the cellular proteases cathepsin B and L. The exact mechanism is still uncertain. Exposure occurs through the pores at the five-fold symmetry axis of the capsid (1.3) *(Bleker et al. 2005, Sonntag et al. 2006, Akache et al. 2007)*.

In addition to the PLA2 domain, three basic regions (BR) containing clusters of positively charged aminoacids are located within the VP1/2 N-terminus of the capsid proteins *(Grieger et al. 2006)*. While BR2 and BR3 are present in both, VP1 and VP2, BR1 is unique for the VP1 N-terminus

(**Figure 2**). The complete functions of the BRs are not fully known, however, their sequence seem to resemble nuclear localization signals. Recently, *Nicolson et al.* demonstrated that the BRs on VP1 and VP2 interact with importin-β mediating active nuclear transport through the nuclear pores (1.4.4). Mutations in the BRs lead to reduced binding of importin-β, thus resulting in a reduction of the infectivity *(Nicolson and Samulski 2013)*. In addition BR1, BR2 and BR3 are also involved in the translocation of newly synthesized capsid proteins into the nucleus, where capsid assembly occurs. Inside the nucleus, newly synthesized capsid proteins are supposed to be redirected into the nucleoli of infected cells by AAP for capsid assembly *(Sonntag et al. 2006, Sonntag et al. 2010)*.

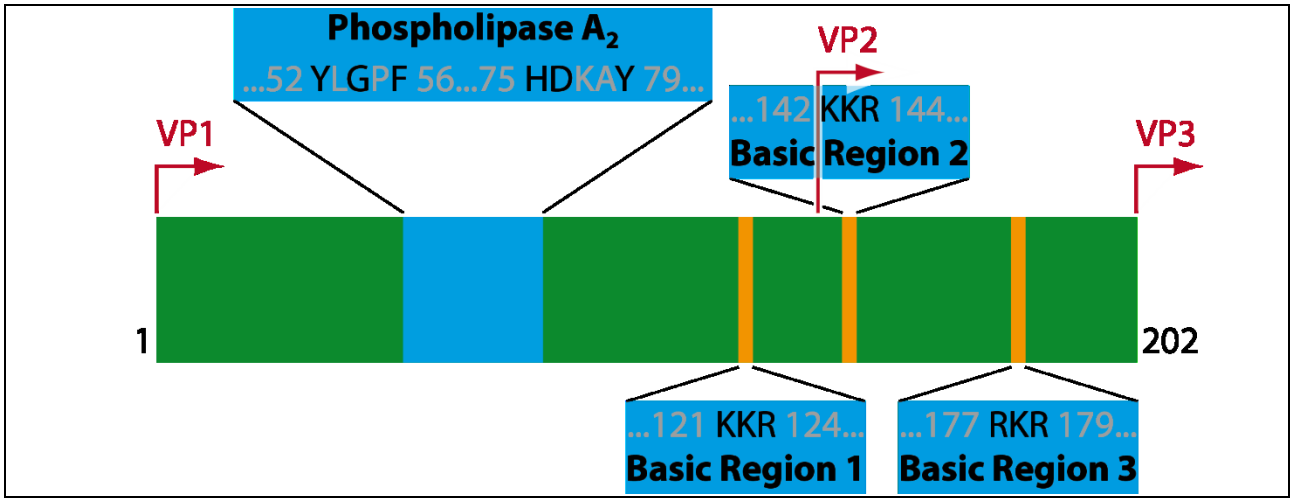

Figure 2: Overview of the AAV2 VP1/2 N-terminus. A phospholipase A2 domain in the unique VP1 N-terminus has been identified, comprising the aminoacids 52-79 (blue), followed by three basic regions (orange) that resemble nuclear localization signals. (adapted from *Popa-Wagner 2011)*

1.3 Capsid organization of AAV2

The AAV2 capsid is formed by the three capsid proteins VP1, VP2 and VP3. In total, 60 subunits of these proteins, arranged in T=1 symmetry, build the icosahedral capsid with approximately 25 nm in diameter *(Mitchell et al. 2010)*. The before mentioned major and minor mRNA transcripts, as well as the use of the non-canonical start-codon ACG for the generation of the capsid proteins (1.2.2), lead to a protein distribution into a molar ratio of VP1:VP2:VP3 of 1:1:10 *(Rose et al. 1971, Kronenberg et al. 2001)*, resulting in 50 copies of VP3 and five copies of VP1 and VP2 per capsid, respectively *(Grieger and Samulski 2012)*. The atomic structure of the capsid has been resolved in 2001 by cryo-electron microscopy at a resolution of 10.5 Å and using X-ray crystallography at a resolution of 3 Å in 2002 *(Kronenberg et al. 2001, Xie et al. 2002)*. The capsid is formed by 20 triangular faces formed by trimers of the structural proteins VP1, VP2 or VP3 (**Figure 3**, right panel). Identical interaction sites between these faces result in 2-fold, 3-fold and 5-fold symmetry axes *(Xie et al. 2002)*. All of the capsid proteins have a conserved eight-stranded anti-parallel β-barrel motif. Interspersed with

insertions of large loops, these β-strands contribute with about 60% to the capsid structure leading to the characteristic surface topology of depressions at the 2-fold axes, spikes at the 3-fold axes and cylindrical pores around the 5-fold axes (**Figure 3**) that have been shown to be important during infection for the externalization of the VP1 N-terminus (1.4.3) *(Bleker et al. 2005, Kronenberg et al. 2005)*.

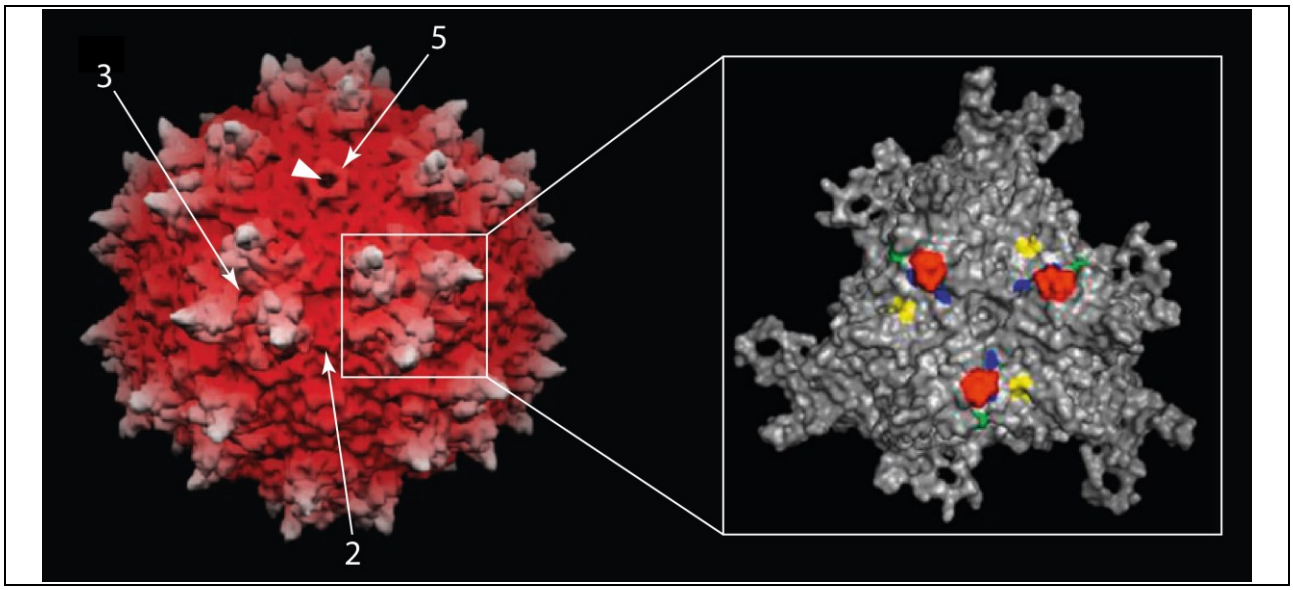

Figure 3: Surface topology of the AAV2 capsid. Characteristic symmetry axes are indicated by arrows and numbers: 2-fold axes, 3-fold axes with spikes and 5-fold axes with a cylindrical channel (arrow head). **Enlarged:** Triangular face of the three capsid proteins. Colored regions indicate the receptor binding sites at the protrusions along the 3-fold axes. (Taken and modified from Xie et al. (2002) and Michelfelder and Trepel (2009))

Recently, a study identified a so called "pH quartet" on the AAV capsid consisting of four aminoacids that are highly conserved among the AAV serotypes. It has been shown that this region undergoes a pH-dependent conformational change within the endosome *(Nam et al. 2011)*. Mutational analysis of this region employing AAV8 serotype, suggested that the capsid proteins additionally contribute to second-strand synthesis and transcription of the incoming genome via these four aminoacids *(Salganik et al. 2014)*.

1.4 AAV2 infection cycle

The AAV infection cycle can be divided into five steps: cell surface attachment (1.4.1), cellular uptake (1.4.2), intracellular trafficking (1.4.3), nuclear import and genome release (1.4.4). All steps are described in more detail in the following chapters.

1.4.1 Cell surface attachment

AAV2 infection is initiated by the binding of the virion to its primary receptor, which has been identified to be heparan sulfate proteoglycan (HSPG) *(Summerford and Samulski 1998)*. Interaction of the virion with a secondary receptor is a prerequisite for efficient cellular entry. Several studies proposed integrin $\alpha_v\beta_5$, integrin $\alpha_v\beta_1$, fibroblast growth factor receptor I, laminin receptor and hepatocyte growth factor receptor as secondary receptors for AAV2 *(Qing et al. 1999, Summerford et al. 1999, Kashiwakura et al. 2005, Akache et al. 2006, Asokan et al. 2006)*. However, the identification of several co-receptors for AAV, with none of them showing an essential role, has led to the general view, that AAV requires proteoglycan conjugates (HSPG for AAV2, AAV3 and AAV6) or O- or N-linked sugars (AAV1, AAV5, AAV6 or AAV9) as primary receptor, combined with one of the aforementioned secondary receptors for an efficient cell surface attachment (reviewed in *Nonnenmacher and Weber 2012)*. Additionally, it was shown that binding of AAV2 to HSPG also triggers a conformational change of the capsid locking the virus at the surface. This state is supposed to increase the binding affinity of the virus to the co-receptor thereby inducing endocytosis *(Levy et al. 2009)*.

1.4.2 Cellular uptake

Following cell surface attachment, internalization of the AAV-receptor complexes takes place via endocytosis. This process begins with invagination of the plasma membrane, followed by scission, forming a new vesicle containing the virus that is released into the cell. It has been demonstrated that cellular uptake is rather fast, 60-85% of the bound particles are internalized within 30-60 minutes after attachment *(Duan et al. 1999, Bartlett et al. 2000)*. Hence, this step is not considered to be rate-limiting during infection. The pathway that AAV uses to enter the cell is discussed controversially. First studies suggested clathrin-mediated endocytosis, dynamin negative cells showed a strong inhibition of AAV2 uptake *(Duan et al. 1999, Bartlett et al. 2000)*. However, *Sanlioglu and colleagues* demonstrated that inhibition of RacI, a GTPase inhibiting clathrin-mediated endocytosis and effector of macropinocytosis, dramatically reduces AAV2 uptake, suggesting a pathway independent of clathrin-mediated endocytosis. Furthermore, they showed that RacI mediated uptake leads to an activation of a phosphatidylinositol-3 kinase pathway that is necessary for the intracellular movement of the virus to the nucleus *(Sanlioglu et al. 2000)*. The most recent study by *Nonnenmacher et al.* however, could neither confirm the clathrin-mediated endocytosis, nor the RacI pathway for viral uptake. Moreover, they identified the recently characterized clathrin-independent carriers/GPI-enriched endocyctic compartment (CLIC/GEEC) pathway for AAV2 to enter the cell, also independtly from caveolin and macropinocytosis *(Nonnenmacher and Weber 2011)*. Furthermore, their data were confirmed by a genome-wide small interfering RNA screen that identified several

proteins of the CLIC/GEEC pathway to be essential for AAV2 transduction, such as ARHGAP10, Arf1 or GRAF1 *(Wallen et al. 2011)*. A possible explanation for this discrepancy with previous studies might be that modifications of cell homeostasis have occurred by the use of adenoviral vectors for protein overexpression. Taken together, these observations suggest, that AAV is able to use different mechanisms for internalization by the host cell(summarized in **Figure 4**) that either directs it to an infectious pathway entering the nucleus (1.4.4), a non-infectious pathway targeting it for proteasomal or lysosomal degradation or transcytosis, transporting it across epithelial cells; thereby irreversibly determining the viral fate *(Nonnenmacher and Weber 2012)*.

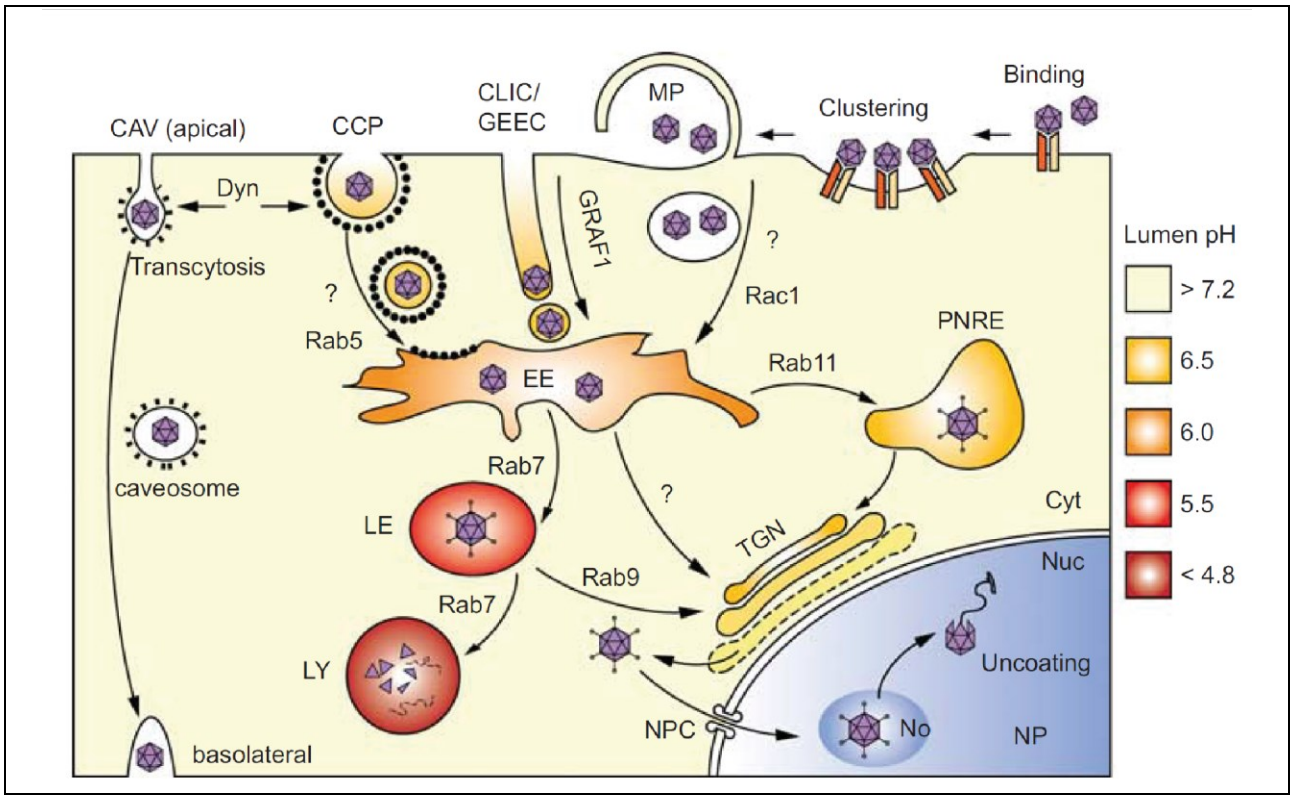

Figure 4: Illustration of entry and intracellular trafficking of AAV. After interaction with its primary and secondary receptor, AAV is internalized via one of the following endocytosis routes: macropinocytosis (MP), clathrin-independent carriers/GPI-enriched endocyctic compartment (CLIC/GEEC), clathrin-mediated (CCP), caveolar-mediated (CAV). AAV is trafficked towards the trans-Golgi network (TGN) via the early endosomes (EE), followed by the late endosomes (LE) and/or perinuclear recycling endosomes (PNRE). After exposure of the phospholipase A2 domain (spikes) on its N-terminus, AAV is released into the perinuclear space and imported into the nucleus (Nuc) through the nuclear pore complex (NPC), where it accumulates in the nucleolus (No), before genome uncoating occurs in the nucleoplasm (NP). Some of the depicted steps are hypothetical and still not completely proven. *(Taken from Nonnenmacher and Weber (2012)*

1.4.3 Intracellular trafficking

Intracellular trafficking is a slow and inefficient process during AAV infection and postulated as rate-limiting step *(Bartlett et al. 2000, Douar et al. 2001)*. Independent of the internalization mechanism (1.4.2), AAV is trafficked inside endosomes through the cytoplasm, thereby exploiting the cellular microtubule network *(Xiao and Samulski 2012)* and either released directly or via the Golgi apparatus into the perinuclear space *(Nonnenmacher and Weber 2012)*. The transport within the endosome is a crucial step during AAV infection, as the capsid undergoes a conformational change, leading to the externalization of the VP1/2 N-terminus *(Kronenberg et al. 2005, Sonntag et al. 2006)*. The low pH inside the endosome alone is not sufficient to mediate N-terminus exposition. However, the two cellular proteases cathepsin B and L have been shown to interact with the capsid facilitating the structural rearrangement and "priming" the capsid for genome release (1.4.4) at later stages of the infection *(Akache et al. 2007)*. Furthermore, *Salganik and colleagues* identified a pH-dependent protease activity within the AAV capsid that might also be involved in the conformational change *(Salganik et al. 2012)*. The exact mechanism of the structural change however, is still poorly understood. Following externalization, the PLA2 domain (1.2.2) exerts its enzymatic activity, mediating endosomal escape of the capsids into the perinuclear space *(Girod et al. 2002, Stahnke et al. 2011)*.

1.4.4 Nuclear import and genome release

AAV capsids are suggested to enter the nucleus as intact capsids through the nuclear pore complex (NPC) prior to genome release *(Bartlett et al. 2000, Sanlioglu et al. 2000, Nicolson and Samulski 2013)*. Additionally, it was demonstrated that AAV interacts with importin-β at its basic regions for active nuclear import. In contrast to these findings, a recently published study suggested that parvoviruses, including AAV, interact with key nuclear proteins leading to structural rearrangement of the capsids, which in turn mediates nuclear envelope breakdown. For AAV2 this effect was only observed when the capsids were exposed to pH 5.2 as it is known to be the milieu in late endosomes. This scenario allows parvoviruses to enter the nucleus independently from mitosis *(Porwal et al. 2013)*.

Inside the nucleus, capsids are directly transported to the nucleolus, where they interact with nucleolar proteins, such as B23/nucleophosmin *(Bevington et al. 2007)*. The role of the nucleolar localization is barely understood and even seems to be disadvantageous, as knockdown of the nucleolar proteins increases AAV transduction. Furthermore, as unmodified particles are released from the nucleoli into the nucleoplasm, where genome uncoating occurs, it seems that nucleolar localization is dispensable for AAV infection *(Johnson and Samulski 2009)*.

1.5 The ubiquitination-proteasome system

Protein turnover in cells is controlled by two major systems: the lysosomal system and the ubiquitination-proteasome system (UPS). The UPS is a highly regulated system that selectively marks individual proteins or entire protein populations for proteasomal degradation by the addition of chains of the 7 kDa molecule ubiquitin *(Hershko and Ciechanover 1998)*. Ubiquitination of proteins occurs through an E1-E2-E3 cascade, in which E1 is an ubiquitin-activating enzyme, E2 an ubiquitin-conjugating enzyme and E3 an ubiquitin-ligase *(Schulman and Harper 2009, Wenzel et al. 2011, Metzger et al. 2014)*. Among the E3 ubiquitin-ligases, the Cullin-RING E3 ligases (CRLs; 1.5.1) form the biggest family, responsible for approximately 20% of the protein turnover in cells *(Petroski and Deshaies 2005, Lydeard et al. 2013)*.

1.5.1 Cullin-RING E3 ligases

In mammals, seven different Cullins have been identified (Cul1, Cul2, Cul3, Cul4a, Cul4b, Cul5 and Cul7; **Figure 5**), all of them having a conserved Cullin homology domain *(Sarikas et al. 2011)*. In the UPS, Cullins organize the Cullin-RING E3 ligase complexes by acting as protein scaffold forming two modules. Via the C-terminal globular domain, Cullins bind a RING (really interesting new gene) E3 ligase which then recruits ubiquitin-loaded E2 enzymes mediating ubiquitin transfer to the substrate. The substrate-targeting unit is formed at the N-terminus by the recruitment of a substrate-receptor protein that is linked to an adaptor protein; i.e. Cul1 binds Skp1 as adaptor protein, allowing the recruitment of F-box-containing proteins as substrate-receptor proteins. This complex is considered as prototype and called SCF (Skp, Cullin, F-box containing complex; **Figure 5**).

In contrast to all other Cullins, Cul3 is the only scaffold that does not require a separate adaptor protein for the formation of the CRL (CRL3). Instead, it directly interacts with the substrate recognition protein via a BTB (Bric-a-brac, Tramtrack, Broad-complex) domain, located on the substrate recognition protein *(Sarikas et al. 2011, Genschik et al. 2013, Lydeard et al. 2013)*.

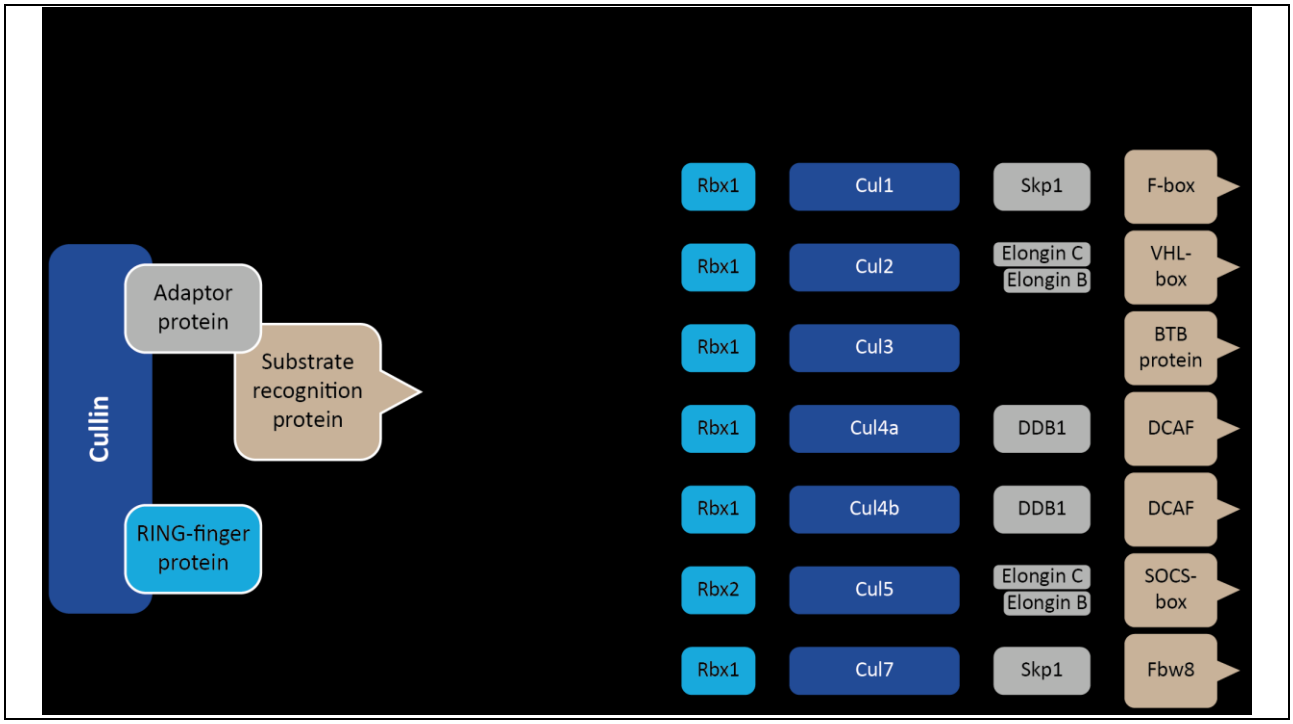

Figure 5: Architecture of the Cullin-RING E3 ligases. Left panel: Organization of a CRLs complex. Cullin binds a RING E3 ligase via its C-terminal domain (CTD) that mediates ubiquitin transfer to the substrate. The N-terminus binds an adapter protein that recruits a specific substrate recognition protein for substrate binding. **Right panel:** Single Cullins and their composition of the CRLs. ROC: Regulator of Cullins, Skp1: S-phase kinase associated protein 1, DDB1: DNA damage-binding protein 1, VHL-box: von Hippel-Lindau box, BTB: Bric-a-brac, Tramtrack, Broad-complex domain, DCAF: DDB1-Cul4 associated factor, SOCS-box: Suppressors of cytokine signaling-box, Fbw8: F-box and WD repeat domain protein 8, Rbx: RING-box protein. (adapted from *Sarikas et al. 2011)*

Over the past years, CRL3 has been demonstrated to be involved as key regulator in major cellular and developmental processes. Alterations in the function of CRL3s have been shown to lead to muscle and nerve degeneration, metabolic disorders or even cancer (reviewed by *Genschik et al. (2013)*. Besides targeting cellular proteins for proteasomal degradation, CLR3s also function in protein trafficking, late endosome maturation and subcellular localization of substrates. The best characterized Cul3 substrate recognition protein is Keap1, regulating the turnover of Nrf2, a transcription factor in oxidative stress response pathways *(McMahon et al. 2003)*. Another BTB substrate recognition protein for Cul3 that gained great interest during the past years is the BTB/MATH domain containing Speckle-type POZ protein (SPOP, 1.5.2). It has been shown that SPOP-mediated ubiquitination of the histone MacroH2A acts in a non-proteolytic manner leading to proper localization of MacroH2A within the inactive X chromosome *(Hernandez-Munoz et al. 2005)*. Furthermore, SPOP is supposed to control Daxx (death-associated protein) turnover, thereby regulating transcriptional processes and apoptosis *(Kwon et al. 2006)*.

1.5.2 The Cullin 3 substrate recognition protein Speckle-type POZ protein

Identified as protein localized in nuclear speckles, SPOP has been described to be substrate recognition protein for Cul3, mediating ubiquitination of substrates. SPOP contains three functional domains: A MATH (Merpin and TRAF homology) domain at the N-terminus mediating substrate interaction, an internal BTB domain for Cul3 binding and a C-terminal NLS. Moreover, analysis of the SPOP substrates Daxx, Puc, Ci and MacroH2A resulted in identifying a common 5-residue SPOP binding consensus motif (SBC): non-polar – polar – Serine – Serine/Threonine – Serine/Threonine (**Figure 6**) *(Zhuang et al. 2009)*. During the past years SPOP has been discovered to play a major role as tumor-suppressor, mainly demonstrated by its interaction and regulation with the oncogenic co-activator SRC-3/AIB1 or breast cancer metastasis suppressor 1 (BRMS1)*(Kim et al. 2011, Li et al. 2011)*.

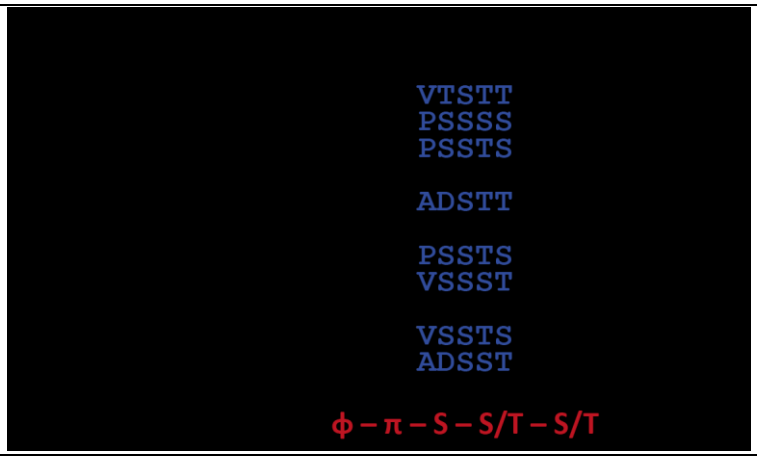

Figure 6: Identification of a SPOP binding consensus motif. Sequence analysis of known SPOP interaction partners revealed a common 5-residue SPOP binding consensus motif. φ: non-polar, π: polar, S: Serine, T: Threonine. (adapted from *Zhuang et al. 2009)*

1.5.3 Cullin-RING E3 ligase regulation

As CRLs function in protein regulation (1.5.1), these complexes need to be tightly regulated in a time and space dependent manner, allowing to directly reacting on the cellular needs at every stage of the cell-cycle. Recent studies suggest that CRLs alternate in cycles of "on" and "off" states, also considered as active and inactive. The current model (**Figure 7**) suggests, that Nedd8, an ubiquitin-like protein, tags Cullins by employing a cascade similar to ubiquitination, and thereby converts the CRLs into their active state, allowing substrate ubiquitination *(Petroski and Deshaies 2005)*. The reverse reaction, deneddylation of the Cullins, leads to the inactivation and subsequent disassociation of the CRL complex from the substrate recognition protein. This reaction is driven by the COP9 signalosome (CSN), in particular the CSN5 subunit *(Duda et al. 2008, Saha and Deshaies 2008)*. In

the deneddylated form, CAND1 (Cullin-associated neddylation dissociated protein 1) is able to bind the Cullins *(Liu et al. 2002, Zheng et al. 2002)*. Initially thought to inactivate the CRLs, recent studies suggest a catalytic role for CAND1, allowing to facilitate substrate recognition protein exchange. In reality, this regulative cycle is much more complex and still poorly understood *(Chua et al. 2011, Sarikas et al. 2011, Genschik et al. 2013, Lydeard et al. 2013)*.

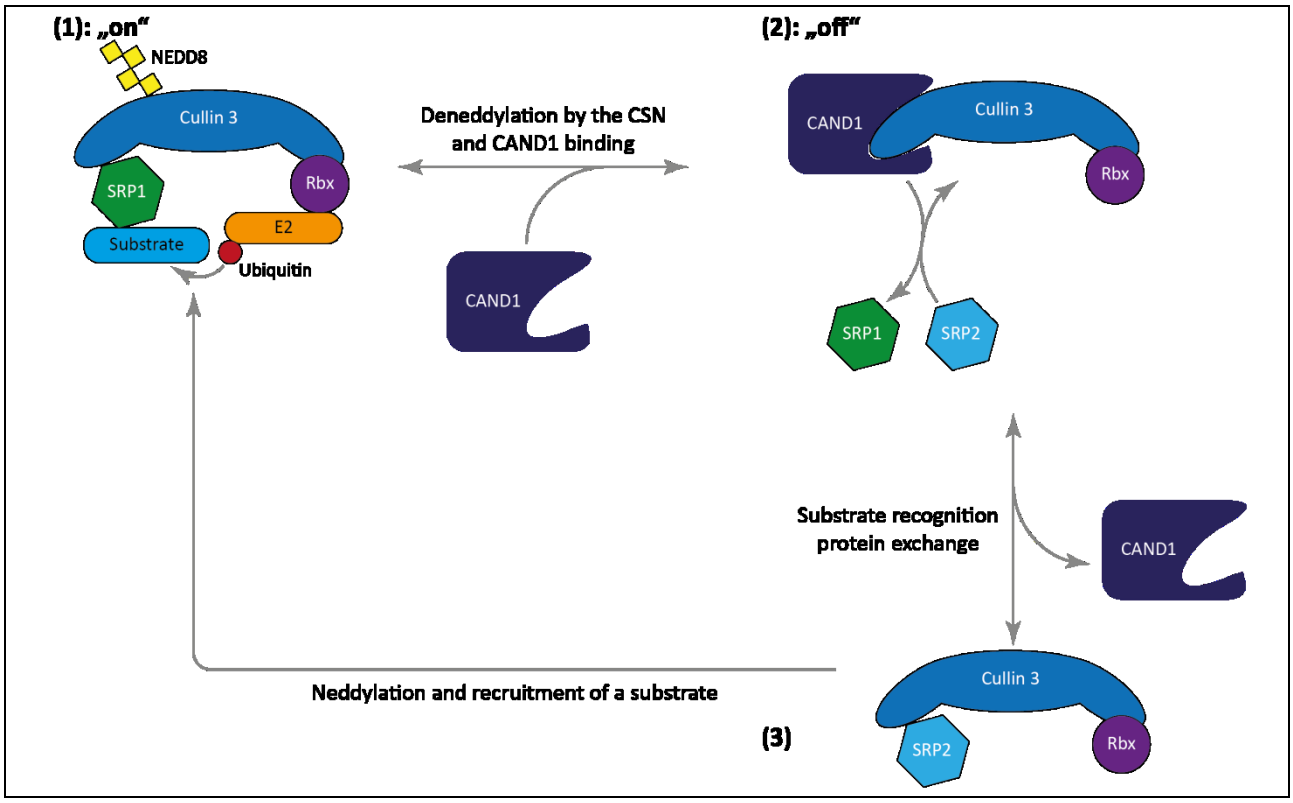

Figure 7: Simplified model for activation and inactivation of CRLs. Activated CRL3 interacts with a substrate for ubiquitination via a substrate recognition protein (SRP1) (1). Upon deneddylation by the signalosome the CRL complex dissociates allowing the binding of CAND1 (2). CAND1 facilitates the exchange of substrate recognition proteins thereby regulating the substrate specificity. Dissociation of CAND1 enables the newly formed CRL complex to be activated by neddylation (3) and recruit substrates for ubiquitination (1). SRP: substrate recognition protein, Rbx: RING-box protein, CAND1: Cullin-associated neddylation dissociated protein 1, E2: ubiquitin conjugating enzyme. Yellow squares: neddylation residues, red circles: ubiquitinatin residue. (modified from *Lydeard et al. 2013)*

1.6 The ubiquitination-proteasome system and viruses

The UPS provides a strong regulation for a number of cellular processes to maintain the cellular metabolism. Additionally, the UPS has been shown to interfere with viral proteins to defend the cell from viral infection. However, as viruses co-evolved with their hosts, they have gained strategies to exploit the UPS at several steps during infection to overcome the cellular defense and facilitate their

own infection. Some of these steps are entry, trafficking, replication or egress (reviewed in *Boname (2008)*.

Over the past years, several studies revealed mechanisms that are used by viruses to efficiently use the UPS for their infection. It has been shown that many viruses use CRLs (1.5.1) to target cellular proteins. For example, E1B-55K and E4orf6, two adenoviral proteins interact with Cul5 as substrate recognition proteins to target p53 for degradation, thereby preventing apoptosis, allowing Adenovirus to efficiently infect the cell *(Harada et al. 2002, Blanchette et al. 2004)*. Also Paramyxoviruses take advantage of the cellular CRLs. Expression of their "V" proteins interferes with the Jak/STAT pathway by interaction with Cul4a and DDB1, mediating degradation of either STAT1 or STAT2 and thus, preventing activation of transcription of distinct genes encoding for proteins that defend the cell against the viral infection *(Ulane and Horvath 2002, Precious et al. 2005)*. For HIV-I several research groups demonstrated that the viral HIV-I virion infectivity factor (Vif) forms an SCF E3 ligase complex with Cul5 and elongin B and C (**Figure 5**) to target the antiviral proteins APOBEC3G and APOBEC3F. In case Vif fails to completely neutralize the action of the two APOBECs, a second HIV-I protein, Vpr, is able to form a complex with either Cul1 or Cul4a targeting the cellular uracil DNA glycosylase (UNG) for degradation. These interactions allow HIV-I to overcome the host defense for efficient replication and generation of viral progeny *(Sheehy et al. 2003, Yu et al. 2003, Mehle et al. 2004)*.

In contrast to virus-mediated degradation of host proteins, Vaccinia Virus takes advantage of ubiquitination and proteasomal degradation. A study conducted by *Mercer et al.* demonstrated that newly synthesized core proteins are ubiquitinated during assembly. These ubiquitin residues are hidden inside the envelope and only get accessible after entering into a cell during infection. Ubiquitinated cores mediate proteasomal degradation, subsequently leading to genome release. A second round of ubiquitination by Cul3 allows the virus to efficiently replicate *(Mercer et al. 2012)*.

Many other studies demonstrated the involvement of the UPS in viral infection suggesting to play an important role for viruses to efficiently enter, replicate and egress the host cells *(Boname 2008)*.

1.7 Natural modifications of the AAV capsid

During the past years, several groups demonstrated that natural modifications of the AAV capsid influence viral transduction. Namely, these modifications are ubiquitination (1.7.1) *(Duan et al. 2000, Douar et al. 2001, Yan et al. 2002)* and phosphorylation of tyrosine residues (0) *(Zhong et al. 2007, Zhong et al. 2008, Zhong et al. 2008)*.

1.7.1 Ubiquitination of AAV capsids

Initial studies with the proteasome inhibitor MG132 demonstrated a strong increase in viral transduction. This increase might be due to several functions of the proteasome inhibitor. In first studies it was shown that treatment with MG132 was accompanied with stabilization and increased amounts of viral DNA, indicating that a fraction of incoming virus is ubiquitinated and targeted for proteasomal degradation *(Douar et al. 2001)*. However, further studies with other proteasome inhibitors showed an increased transduction, but only minor elevated levels of the viral DNA inside the host cell that cannot account for the strong increase in transduction. Together, these studies suggest that the increase in transduction using proteasome inhibitors cannot be explained by blocking the proteasomal degradation of the virus alone. Also, other effects such as enhanced trafficking to the nucleus and ER stress or stabilization of cellular proteins, also triggered by MG132, are potentiating viral transduction *(Duan et al. 2000, Yan et al. 2002, Zhong et al. 2007, Johnson et al. 2011)*. These off-target effects of the drug are discussed to have a much stronger influence on the transduction than the proteasome inhibition itself. However, *Mitchell et al.* recently characterized a new proteasome inhibitor (carfilzomib) that is supposed to specifically inhibit the chymotrypsin-like proteasome activity with no off-target effects on other proteases. Compared to the "old" inhibitors, carfilzomib showed similar results, supporting the other studies that demonstrated a proteasome-specific effect on AAV transduction *(Mitchell and Samulski 2013)*. However, even though carfilzomib is specific on the inhibition of the proteasome, off-target effects on other cellular components such as the stabilization of cellular proteins cannot be excluded. These effects might also influence the transduction, therefore a proteasome-specific effect on AAV transduction is still not shown completely.

The role of capsid ubiquitination during infection is nonetheless poorly understood. It is still controversially discussed whether ubiquitination is beneficial or detrimental for viral infection *(Nonnenmacher and Weber 2012)*. From an evolutionary point of view, one would assume that if ubiquitination was disadvantageous for the virus, natural selection would have led to escape mutants. Additionally, it has been shown that exchange of lysine residues, the targets of ubiquitination (1.5), did not show enhanced transduction. Further studies also demonstrated that in a cell free environment ubiquitination of capsids is less efficient than on denatured capsid proteins, suggesting that in cells a conformational change of the capsid during infection must occur leading to the exposure of these target lysine residues *(Wu et al. 2006, Yan et al. 2002, Kern et al. 2003, Opie et al. 2003)*. Unpublished bioinformatical data of *Nonnenmacher et al.* corroborate this hypothesis, indicating that potential lysine targets are located on the VP1/2 N-terminus which is exposed inside the endosome during infection.

1.7.2 Phosphorylation

Tyrosine-phosphorylation has been shown to impede viral transduction in a series of studies. Pioneer studies on a cellular phosphoprotein, single-strand D-sequence binding protein, demonstrated this protein shown to block second-strand synthesis by binding to the ITRs in a phosphorylation-dependent manner *(Qing et al. 1998)*. Inhibition of tyrosine-phosphorylation by either genistein or tyrphostin-23 led to dephosphorylation of this protein and a strong increase in viral transduction. It could be demonstrated that inhibition of phosphorylation results in enhanced nuclear transport of the virus. Additionally, epidermal growth factor receptor-protein tyrosine kinase (EGFR) was found to phosphorylate intact AAV2 capsids *in vitro*, resulting in a decrease in transduction independent of second-strand synthesis *(Zhong et al. 2007)*. As specific inhibition of EGFR with tyrphostin-23 did not show additive effects with MG132 it was postulated, that these drugs act on the same pathway, where phosphorylation is supposed to serve as positive signal for capsid ubiquitination *(Zhong et al. 2008)*. In concordance, tyrosine mutants of the AAV2 capsid showed a strong increase in transduction that was not further enhanced by treatment with either tyrphostin 23 or MG132, hence supporting the hypothesis that capsid phosphorylation is linked to ubiquitination *(Zhong et al. 2008)*.

As for ubiquitination, the biological role of capsid phosphorylation is still not completely understood. However, the mutational analysis of the tyrosine residues strongly supports the involvement of tyrosine phosphorylation during the infection of AAV.

1.8 Aim of the study

Complete understanding of the AAV infection cycle, beginning with receptor attachment, followed by cellular entry and trafficking to the nucleus where replication and transcription occurs, is a prerequisite for save usage of AAV vectors in gene therapy. Although more and more details of the AAV life-cycle have been described and identified over the last decades, many molecular mechanisms still remain unclear. Endosomal escape and nuclear transport seem to be a major rate-limiting step during viral infection. Here, a critical step is the conformational change of the capsid, exposing its VP1/2 N-terminus to mediate endosomal release. Some functional domains, such as the PLA2 or the three basic regions on the VP1/2 N-terminus, respectively, have already been identified to be involved during these crucial steps in the infection process. However, it is likely that the dramatic capsid rearrangement for the VP1/2 N-terminus exposure also allows cellular components to bind and interact with the capsid with either being detrimental or beneficial for the virus.

The objective of the underlying PhD project was to identify and characterize host cell proteins that might interact with the VP1/2 N-terminus of different AAV serotypes and play a role in the AAV life-cycle. In this regard, the following questions were addressed and examined in detail:

1) Are host cell proteins interacting with the VP1/2 N-terminus of AAV?

2) Are differences in the interacting proteins between the various AAV serotypes?

3) If host cell proteins interact with the VP1/2 N-terminus, what are the specific characteristics of the interaction and how do they influence the viral life-cycle?

Answering these questions should contribute to a broader understanding of the AAV life-cycle and thereby facilitating its use for clinical applications.

2 Material

2.1 Biological Materials

2.1.1 Mammalian cell lines

HeLa

HeLa cells are human epithelial cervix adenocarcinoma cells containing the HPV 18 genome. These cells were cultured in supplemented Dulbecco's modified Eagle's medium (DMEM).

HEK 293T/HEK 293TT

293T (293TT) cells are human embryonic kidney cells expressing the simian virus T-antigen in one (293T) or two (293TT) copies, respectively. These cells were cultured in DMEM containing 62.5 µM Hygromycin B.

FlpIn™ 293

FlpIn™ 293 cells are human embryonic kidney cells, containing a single stably integrated FRT site. These cells were cultured in DMEM.

293 SPOP K1/K5

293 SPOP K1/K5 are two clones of the parental FlpIn™ 293 cell line stably expressing human SPOP. These cells were cultured in DMEM containing 62.5 µM Hygromycin B.

2.1.2 Bacteria

Strain	*Genotype*
E.coli MxDH10? (Invitrogen)	*F- mcrA Δ(mrr-hsdRMS-mcrBC)Ψ80lacZΔM15 ΔlacX74 recA1 endA1 araD139 Δ(ara, leu)7697 galU galK λ- rpsL nupG tonA*
E.coli SoloPack (Agilent Technologies)	*Tet^r Δ(mcrA)183 Δ(mcrCB-hsdSMR-mrr)173 endA1 supE44thi-1 recA1 gxrA96 relA1 lac Hte [F' proAB lacI^qZΔM15 Tn10 (Tet^r Amy Cam^r]*
E.coli XL-Gold® (Agilent Technologies)	*endA1 glnV44 recA1 thi-1 gyrA96 relA1 lac Hte Δ(mcrA)183 Δ(mcrCB-hsdSMR-mrr)173 tetR F'[proAB lacIqZΔM15 Tn10(TetR Amy CmR)]*
E. coli RosettaTM	*F- ompT hsdS_B (r_B- m_B-) gal dcm pRARE (Cam^R)*
E.coli DB3.1	*F- gyrA462 endA1 glnV44 Δ(sr1-recA) mcrB mrr hsdS20(rB-, mB-) ara14 galK2 lacY1 proA2 rpsL20(Smr) xyl5 Δleu mtl1*

2.1.3 Viruses

Viruses were generated by transfection of the respective plasmids (numbered). A description of the plasmids is given in 2.2.1.

2.2 Molecular biological materials

Reporter virus	*Plasmids*
AAV2 renilla	#2288 + #2311
AAV2 YFP	#2288 + #2861
AAV2 renilla	#2772 + #2311 + #1814
AAV2 YFP	#2772 + #2861 + #1814
AAV2 PASSS renilla	#3098 + #2311 + #1814
AAV2 PASSS YFP	#3098 + #2861 + #1814
AAV2 PAASS renilla	#3099 + #2311 + #1814
AAV2 PAASS YFP	#3099 + #2861 + #1814
AAV2 PDASS renilla	#3096 + #2311 + #1814
AAV2 PDASS YFP	#3096 + #2861 + #1814
AAV2 PDAAS renilla	#3097 + #2311 + #1814
AAV2 PDAAS YFP	#3097 + #2861 + #1814
AAV2 PESSS renilla	#3183 + #2311 + #1814
AAV2 PESSS YFP	#3183 + #2861 + #1814

2.2.1 Plasmids

Designation	*Description*	*Reference*
1814	pDGΔVP,AAV2/Ad-helper plasmid without cap-gene	A. Sacher
2288	pDP2 --> AAV wt cap without ITRs, with helper functions	A. Sacher
2311	pdsRenilla: AAV construct for packaging ds Renilla Luciferase	A. Sacher
2767	AAV2 VP1 TAP-Tag C-terminal (in pZomeC)	this thesis
2768	AAV5 VP1 TAP-Tag N-terminal (in pZomeN)	this thesis
2769	AAV6 VP1 TAP-Tag C-terminal (in pZomeC)	this thesis
2770	AAV6 VP1 TAP-Tag N-terminal (in pZomeN)	this thesis
2785	AAV2 VP1 TAP-Tag N-terminal (in pZomeN)	this thesis
2786	AAV2 VP2 TAP-Tag N-terminal (in pZomeN)	this thesis
2787	AAV9 VP1 TAP-Tag N-terminal (in pZomeN)	this thesis
2788	AAV8 VP1 TAP-Tag N-terminal (in pZomeN)	this thesis
2789	AAV9 VP1 TAP-Tag C-terminal (in pZomeC)	this thesis
2859	AAV5 VP1 TAP-Tag C-terminal (in pZomeC)	this thesis
2860	AAV8 VP1 TAP-Tag C-terminal (in pZomeC)	this thesis
2861	dsYFP for AAV packaging	D. Grimm
2894	pZomeN containing AAP2 (AAP2N)	this thesis
2926	pZomeC containing AAV10 (AAP10C)	this thesis

2947	Cullin3 cDNA (open) in pENTR223 (Gateway compatible)	GPCF, DKFZ
2948	MAD2L2 cDNA (closed) in pENTR221 (Gateway compatible)	GPCF, DKFZ
2949	MAD2L1 cDNA (closed) in pENTR221 (Gateway compatible)	GPCF, DKFZ
2950	CAND1 cDNA (closed) in pENTR221 (Gateway compatible)	GPCF, DKFZ
2951	SPOP cDNA (closed) in pENTR221 (Gateway compatible)	GPCF, DKFZ
2952	CDK1 cDNA (closed) in pENTR221 (Gateway compatible)	GPCF, DKFZ
2953	Importin5 cDNA (closed) in pENTR221 (Gateway compatible)	GPCF, DKFZ
2954	CDK2 cDNA (closed) in pENTR221 (Gateway compatible)	GPCF, DKFZ
2955	Calpain2 cDNA (closed) in pENTR221 (Gateway compatible)	GPCF, DKFZ
2956	Cullin4a cDNA (open) in pENTR221 (Gateway compatible)	GPCF, DKFZ
2957	pDEST15 E.coli expression vector (GST-Tag); Gateway compatible	GPCF, DKFZ
2958	MycN, Gateway compatible vector (DEST)	GPCF, DKFZ
2959	FlagN, Gateway compatible vector (DEST)	GPCF, DKFZ
2960	pDEST ohne Tag, Gateway compatible (DEST)	GPCF, DKFZ
2969	N-GST-Mad2L1 (#2949 in pDEST15 #2957 / Gateway)	this thesis
2970	N-GST-CAND1 (#2950 in pDEST15 #2957 / Gateway)	this thesis
2971	N-GST-CDK1 (#2952 in pDEST15 #2957 / Gateway)	this thesis
2972	N-GST-CDK2 (#2954 in pDEST15 #2957 / Gateway)	this thesis
2973	N-GST-Calpain2 (#2955 in pDEST15 #2957 / Gateway)	this thesis
2974	N-Myc-Mad2L1 (#2949 in MycDEST #2958 / Gateway)	this thesis
2975	N-Myc-CAND1 (#2950 in MycDEST #2958 / Gateway)	this thesis
2976	N-Myc-SPOP (#2951 in MycDEST #2958 / Gateway)	this thesis
2977	N-Myc-CDK1 (#2952 in MycDEST #2958 / Gateway)	this thesis
2978	N-Myc-CDK2 (#2954 in MycDEST #2958 / Gateway)	this thesis
2979	N-Myc-Calpain2 (#2955 in MycDEST #2958 / Gateway)	this thesis
2980	N-Flag-Mad2L1 (#2949 in FlagDEST #2959 / Gateway)	this thesis
2981	N-Flag-CAND1 (#2950 in FlagDEST #2959 / Gateway)	this thesis
2982	N-Flag-SPOP (#2951 in FlagDEST #2959 / Gateway)	this thesis
2983	N-Flag-CDK1 (#2952 in FlagDEST #2959 / Gateway)	this thesis
2984	N-Flag-CDK2 (#2954 in FlagDEST #2959 / Gateway)	this thesis
2985	N-Flag-Calpain2 (#2955 in FlagDEST #2959 / Gateway)	this thesis
2986	Mad2L1 without Tag (#2949 in #2960 / Gateway)	this thesis
2987	CDK1 without Tag (#2952 in #2960 / Gateway)	this thesis
2988	CDK2 without Tag (#2954 in #2960 / Gateway)	this thesis
2989	N-GST-SPOP (#2951 in pDEST15 #2957 / Gateway)	this thesis
2990	Importin5 without Tag (#2953 in #2960 / Gateway)	this thesis
2991	N-Flag-Mad2L2 (#2948 in FlagDEST #2959 / Gateway)	this thesis
2992	Mad2L2 without Tag (#2948 in #2960 / Gateway)	this thesis
2993	CAND1 without Tag (#2950 in #2960 / Gateway)	this thesis
2994	Calpain2 without Tag (#2955 in #2960 / Gateway)	this thesis
2995	N-Myc-Importin5 (#2953 in MycDEST #2958 / Gateway)	this thesis
2996	N-Flag-Importin5 (#2953 in FlagDEST #2959 / Gateway)	this thesis
2997	SPOP without Tag (#2951 in #2960 / Gateway)	this thesis

2998	N-GST-Mad2L2 (#2948 in pDEST15 #2957 / Gateway)	this thesis
2999	N-GST-Importin5 (#2953 in pDEST15 #2957 / Gateway)	this thesis
3000	N-Myc-Mad2L2 (#2948 in MycDEST #2958 / Gateway)	this thesis
3013	Cullin3 cDNA (closed) in pENTR223 (Gateway compatible); contains BciVI site after Stopcodon	this thesis
3014	N-GST-Cullin3 (#3014 in pDEST15 #2957 / Gateway)	this thesis
3015	N-Myc-Cullin (#3013 in MycDEST #2958 / Gateway)	this thesis
3016	N-Flag-Cullin3 (#3013 in FlagDEST #2959 / Gateway)	this thesis
3017	Cullin3 without Tag (#3013 in #2960 / Gateway)	this thesis
3029	#3014 (GST-Cul3) in MxDH10	this thesis
3030	GST-Cul3 delta C-term.: #3014 cut with PsiI&SmaI, religated and transformed in MxDH10. deletion: 1047bp	this thesis
3035	#3030 subcloned in rosetta	this thesis
3096	AAV2 (2772) with mutation in putative SPOP-Motif (PDSSS): PDASS	this thesis
3097	AAV2 (2772) with mutation in putative SPOP-Motif (PDSSS): PDAAS	this thesis
3098	AAV2 (2772) with mutation in putative SPOP-Motif (PDSSS): PASSS	this thesis
3099	AAV2 (2772) with mutation in putative SPOP-Motif (PDSSS): PAASS	this thesis
3101	Myc-C Gateway compatible vector (DEST)	GPCF, DKFZ
3103	AAV5/6 chimera TAP (pZomeC); PCR for chimeric construct, cut with EcoRI and BsrGI, cloned into AAV6C (#2769; cut with EcoRI and BsrGI)	this thesis
3104	pKEX-VP1	J. Kleinschmidt
3109	pcDNA5/FRT/TO (Invitrogen; for FlpIn System)	Invitrogen
3110	pOG44 (Invitrogen; Flippase)	Invitrogen
3119	SPOP in pcDNA/FRT/TO (#3109) for stable cell line	this thesis
3132	pKEX VP1 (#3104) with mutation in putative SPOP motif (Quick Change): PDAAS	this thesis
3133	pKEX VP1 (#3104) with mutation in putative SPOP motif (Quick Change): PAASS	this thesis
3134	pKEX VP1 (#3104) with mutation in putative SPOP motif (Quick Change): PDASS	this thesis
3135	pKEX VP1 (#3104) with mutation in putative SPOP motif (Quick Change): PASSS	this thesis
3141	pDONR221 (Gateway)	GPCF, DKFZ
3172	pKEX VP1 N-terminus (until Start of VP3); CMV Promoter	this thesis
3182	pKEX VP1 (#3104) with mutation in putative SPOP motif (Quick Change): PESSS	this thesis
3183	AAV2 (2772) with mutation in putative SPOP-Motif (PDSSS): PESSS	this thesis

2.2.2 Oligonucleotides

2.2.2.1 TAP-Tag primer for pZomeC (VP1/2 N-terminus; different serotypes)

AAV1 (Containing BamHI restriction site, start-codon and Kozak-sequence):

Fwd.: 5' – TTTTGGATCCGCCACCATGGCTGCCGATGGTTATCTTCC – 3'
Rev.: 5' – TTTTGGATCCTGGTGCGCCACCGCCTGAA – 3'

AAV2 (Containing BamHI restriction site, start-codon and Kozak-sequence):

Fwd.: 5' – TTTTGGATCCGCCACCATGGCCGATGGTTATCTTCCAGATTGG – 3'
Rev.: 5' – TTTTGGATCCCGTATTAGTTCCCAGACCAGAGGGGG – 3'

AAV5 (Containing BglII restriction site, start-codon and Kozak-sequence):

Fwd.: 5' – TTTTAGATCTGCCACCATGTCTTTTGTTGATCACCCTCCAGATTGG – 3'
Rev.: 5' – TTTTAGATCTTGTATCAGCTCCCAAACTTGAGGCTGG – 3'

AAV6 (Containing BamHI restriction site, start-codon and Kozak-sequence):

Fwd.: 5' – TTTTGGATCCGCCACCATGGCTGCCGATGGTTATCTTCCAGATTGGC – 3
Rev.: 5' – TTTTGGATCCTGTAGTAGGTCCCACAGCAGCGGGGG – 3'

AAV8 (Containing BamHI restriction site, start-codon and Kozak-sequence):

Fwd.: 5' – TTTTGGATCCGCCACCATGGCTGCCGATGGTTATCTTCCAGATTGGC – 3'
Rev.: 5' – TTTTGGATCCTGTATTAGGTCCCACACCAGAGGGCGC – 3'

AAV9 (Containing BamHI restriction site, start-codon and Kozak-sequence):

Fwd.: 5' – TTTTGGATCCGCCACCATGGCTGCCGATGGTTATCTTCCAGATTGGC – 3'
Rev.: 5' – TTTTGGATCCGCCACCATGGCTGCCGATGGTTATCTTCCAGATTGGC – 3'

AAV10 (Containing BamHI restriction site, start-codon and Kozak-sequence):

Fwd.: 5' – TTTTGGATCCGCCACCATGGCTGCCGATGGTTATCTTCC – 3'
Rev.: 5' – TTTTGGATCCTGGAGCGCCACCGCCT – 3'

AAV5-6 chimera (Containing BsrGI and EcoRI restriction site, start-codon and Kozak-sequence):

Part 1 fwd.: 5' – TTTTTGTACACCCTAAGCCTCCGCCT – 3'
Part 1 rev.: 5' – TTTTTGGAAAGTGGTCGTCTATCCGCTTTCCGGTAGGAGCCGTCTTAGCACCTTC – 3'
Part 2 fwd.: 5' – TTTTCGGATAGACGACCACTTTCCAAAAAGAAAGACAGGCCAGCAGCCCGCTAAAA – 3'
Part 2 rev.: 5' – TTTTGAATTCCTAATTAGCGTCTACTTTCGGCGC – 3'

2.2.2.2 cDNA cloning of identified proteins

Introduction of Stop-codon into Cullin3

Fwd.: 5' – TTTTGTATACACATATGTAGCATAGTATCCAACTTTCTTG – 3'

Rev.: 5' – CCGCTTCCCTCATGATGTTTAAC – 3'

2.2.2.3 Cloning of pKEX VP1/2 N-terminus

Amplification of VP11/2 N-terminus

Fwd.: 5' – TTTTGGTACCCTCGAGATCCCAAATCAGGTATG – 3'
Rev.: 5' – TTTTTGGCCATTACGTATTAGTTCCCAGACCAGAGGGGG – 3'

2.2.2.4 Site-directed mutagenesis of putative SPOP binding motif in AAV2 VP1 N-terminus (Quick Change)

AAV2 PASSS:

Fwd.: 5' – CTGTGGAGCCAGCCTCCTCCTCGGG – 3'
Rev.: 5' – CCCGAGGAGGAGGCTGGCTCCACAG – 3'

AAV2 PAASS:

Fwd.: 5' – CCTGTGGAGCCAGCCGCCTCCTCGGGAAC – 3'
Rev.: 5' – GTTCCCGAGGAGGCGGCTGGCTCCACAGG – 3'

AAV2 PDASS:

Fwd.: 5' – TGTGGAGCCAGACGCCTCCTCGGGAAC – 3'
Rev.: 5' – GTTCCCGAGGAGGCGTCTGGCTCCACA – 3'

AAV2 PDAAS:

Fwd.: 5' – GTGGAGCCAGACGCCGCCTCGGGAACCG – 3'
Rev.: 5' – CGGTTCCCGAGGCGGCGTCTGGCTCCAC – 3'

AAV2 PESSS:

Fwd.: 5' – CTGTGGAGCCAGAATCCTCCTCGGG – 3'
Rev.: 5' – CCCGAGGAGGATTCTGGCTCCACAG – 3'

2.2.2.5 Generation of a cell line stably expressing SPOP

Flp-InTM System (Invitrogen)

Fwd.: 5' – TTTTGGATCCATGTCAAGGGTTCCAAGTCCTCC – 3'
Rev.: 5' – TTTTGATATCTCAGGATTGCTTCAGGCGTTTGC – 3'

2.2.3 siRNA sequences

Hs-SPOP-2 (GeneSolution siRNA, Qiagen)

CAGGCUCACAAGGCUAUCUUA

Hs-SPOP-2 (GeneSolution siRNA, Qiagen)
UACCUCUGCCAAGGCAAGUAA

Hs-SPOP-2 (GeneSolution siRNA, Qiagen)
UAGUGAGAGUUGGUGCUACA

Hs-SPOP-2 (GeneSolution siRNA, Qiagen)
AAGGCUCCAAACCUAGACAAA

2.3 Media and supplements

2.3.1 Mammalian cell culture

Media

Dulbecco's modified Eagle's medium (suppl. with 10% FCS, 1% P/S, 1% L-glutamine)	Sigma-Aldrich, Deisenhofen, Germany

Cryomedium

60% DMEM, non-supplemented
30% FCS
10% DMSO

Hygromycin B

Used at a final concentration of 62.5 µM

Doxycyclin

Used at a concentration of 0.25 µg/ml

Supplements

FCS	PAN Biotech, Aidenbach and Gibco, Paisleyy, UK
Penicillin/Streptomycin	GIBCO, Eggenstein, Germany
L-glutamine	Sigma-Aldrich, Deisenhofen, Germany

Transfection reagents

TurboFect™ transfection reagent	Thermo Scientific, Waltham, USA
HiPerFect® transfection reagent	Qiagen, Hilden, Germany

Further solutions

0.05% and 0.25% Trypsin	Gibco, Eggenstein, Germany

Bacteria culture

LB medium

10 g Tryptone
5 g yeast extract
5 g NaCl
Adjust final volume to 1 l with H_2O bidest., pH 7.5, autoclave

NZY⁺ medium

10 g casein hydrolysate
5 g yeast extract
5 g NaCl
Adjust final volume to 1 l with H_2O bidest., pH 7.5, autoclave

LB agar plates

98.5% LB medium (v/v)
1.5% bacto-agar (w/v)
Autoclaved, antibiotics added below 50°C

Antibiotics

Ampicillin	final concentration: 100 µg/ml
Kanamycin	final concentration: 25 µg/ml
Spectinomycin	final concentration: 100 µg/ml
Chloramphenicol	final concentration: 20 µg/ml

2.4 Preparation, manipulation and analysis of DNA

2.4.1 Mini preparation

Glucose Mix

50 mM Glucose
10 mM EDTA
25 mM Tris HCl, pH 8.0

Alkali lysis buffer

1% SDS
0.2 M NaOH

3M NaAc

pH 5.2, adjusted with concentrated acetic acid

TE buffer

10 mM Tris HCl, pH 7.4
1 mM EDTA
In H_2O bidest., pH 8.0

Roti® Phenol / Chloroform / Isoamyalcohol	Roth, Karlsruhe, Germany

2.4.2 Agarose gel-electrophoresis

1% Agarose gel

1g agarose dissolved in 100 ml TAE running buffer. 70 µg ethidiumbromide added when solution reached 60°C.

1x TAE running buffer

40 mM Tris
5.71% acetic acid (v/v)
10% 0.5 M EDTA, pH 8 (v/v)
In H_2O bidest.

70% Ethanol

70% ethanol in H_2O (v/v)

6x loading buffer	Thermo Scientific, Waltham, USA

2.4.3 Enzymes

Calf Intestinal Alkaline Phosphatase (CIP)	NEB Biolabs, Schwalbach, Germany
KOD HiFi DNA polymerase	TYOBO Novagen, Darmstadt, Germany
Rnase I	Roche, Mannheim, Germany
T4 Ligase	NEB Biolabs, Schwalbach, Germany
Topoisomerase I	NEB Biolabs, Schwalbach, Germany

Restriction enzymes

All restriction enzymes that were used during the course of this thesis were purchased at NEB Biolabs, Schwalbach, Germany.

Further materials and chemicals

6x loading buffer	Thermo Scientific, Waltham, USA
Lambd/HindIII DNA ladder	NEB Biolabs, Schwalbach, Germany
100 bp DNA ladder plus	NEB, Schwalbach, Germany
20 mM dNTP mix	Roche, Mannheim, Germany

10 mg/ml ethidiumbromide	Roth, Karlsruhe, Germany
25 mM $MgCl_2$	TYOBO Novagen, Darmstadt, Germany

2.5 Materials for protein analysis

2.5.1 GST-protein purification

Buffer IV (lysis buffer)

200 mM NaCl
20 mM HEPES pH 7.2
200 mM KAc
2 mM MgAc
0.01% Tween80
1 mM DTT (freshly added)
Protease inhibitor cocktail tablet (freshly added), pH 7.6

Washing buffer

50 mM Tris, pH 8.0

Elution buffer

50 mM Tris, pH 8.0
10 mM glutathione

Regeneration buffers

a) 6 M guanidinehydrochloride
b) 50 mM Tris, pH 7.5
c) 1x PBS
d) 20% EtOH

Purification column

1 ml GSTrap 4B	GE Healthcare, Buckinghamshire, UK

2.5.2 Determination of protein concentration

Bradford reagent	BioRad, München, Germany
BSA standard (2 µg/µl)	Thermo Scientific, Waltham, USA

2.5.3 SDS-polyacrylamide gel electrophoresis

Preparation of SDS-polyacrylamide gels

Tris buffer, pH 6.8

1 M Tris
0.03% bromphenol blue
In H_2O bidest., pH 6.8

Tris buffer, pH 8.8

1M Tris
In H_2O bidest., pH 6.8

Acrylamide solution	Roth, Karlsruhe, Germany
TEMED	Sigma-Aldrich, Deisenhofen Germany

Recipe for five SDS-gels (mini-format)

Chemicals	*3% stacking gel*	*12.5% separation gel*	*15% separation gel*
30% acrylamide	1.5 ml	18.75 ml	25 ml
1 M Tris buffer	1.95 ml (pH 6.8)	16.88 ml (pH 8.8)	18.75 ml (pH 8.8)
H_2O	11.25 ml	8.48 ml	5.25 ml
10% SDS	150 µl	450 µl	500 µl
10% APS	150 µl	450 µl	500 µl
TEMED	22.5 µl	22.5 µl	25 µl

Sample preparation

3x protein loading buffer

30% glycerol
6% SDS
15% β-mercaptoethanol
0.03% bromphenol blue
187.5 mM Tris
In H_2O bidest., pH 6.8

Electrophoresis

1x TGS buffer (running buffer)

2.5 mM Tris
1.45% glycine
0.1% SDS
In H_2O bidest., pH 8.3

Prestained protein ladder color plus	NEB Biolabs, Schwalbach, Germany
Coomassie Solution GelCode®	Thermo Scientific, Waltham, USA

2.5.4 Silver staining

Ag-Fix (100 ml):

50 % methanol
12 % acetic acid
50 µl formaldehyde (37 % Stock)

50% Ethanol

50% ethanol in H_2O bidest.

Thiosulfatesolution, fresh

0.2g Na-thiosulfate 5x H_2O per liter in H_2O bidest.
($Na_2S_2O_3$ * 5 H_2O)

Silvernitratesolution (100 ml), fresh

0.2 g silvernitrate
75 µl formaldehyde (37 % Stock)

Sodiumcarbonatesolution (100 ml), fresh

6 g Na_2CO_3
50 µl formaldehyde (37 % Stock)
0.02 % thiosulfatesolution

Stopsolution

50 % methanol
12 % acetic acid

2.5.5 Western blot analysis

1x EMBL buffer

48 mM Tris
39 mM glycine
1.3 mM SDS
20% methanol
In H_2O bidest., pH 8.2

1x PBS-T (wash buffer)

0.3% Tween 20 (v/v)
In 1x PBS

Blocking agent

5% milk in PBS-T

Stripping buffer (nitrocellulose membrane)

100 mM NaOH
2% SDS
0.5% DTT

2.6 Materials for immunological methods

2.6.1 Antibodies

Designation	*Description*	*Reference*
A20	Raised against intact AAV2 capsids	J. Kleinschmidt
A69	Raised against the capsid proteins of VP1 and VP2 of different AAV serotypes	J. Kleinschmidt
B1	Raised against VP1, VP2 and VP3 of different AAV serotypes	J. Kleinschmidt
Anti-myc (9E10)	Mouse monoclonal, binds to the epitope EQKLISEEDL of the human oncogene c-myc	NEB, Biolabs
Anti-myc (71D10)	Rabbit monoclonal, binds to the epitope EQKLISEEDL of the human oncogene c-myc	NEB, Biolabs
Anti-flag (M2)	Rabbit monoclonal, recognizes the FLAG-tag: DYKDDDDK	Brizzard, B.L.
Anti-actin (C4)	Mouse monoclonal, recognizes the FLAG-tag: DYKDDDDK	Lessard, J.L.
Anti-SPOP (C14)	Goat polyclonal, binds to an epitope located at the C-terminus of human SPOP	Santa Cruz
Anti-SPOP (B8)	Mouse monoclonal, binds to the aminoacids 351-374 of human SPOP	Santa Cruz
Anti-Ub - HRP(P4D1)	Mouse monoclonal, raised against full-length bovine ubiquitin	Santa Cruz
HA-Probe (Y11)	Rabbit polyclonal, recognizes an internal region of influenza hemagglutinin protein	Santa Cruz
GAMPO	Goat-anti-mouse coupled with HRP	Dianova
GARPO	Goat-anti-rabbit coupled with HRP	Dianova
DAGPO	Donkey-anti-goat coupled with HRP	Santa Cruz
AlexaFlour 488 (anti mouse)	Goat-anti-mouse IgG coupled with AlexaFluor 488	Life Technologies
AlexaFlour 488 (anti rabbit)	Goat-anti-rabbit IgG coupled with AlexaFluor 488	Life Technologies

Alexa Flour 594 (anti mouse)	Goat-anti-mouse IgG coupled with AlexaFluor 594	Life Technologies
Alexa Flour 594 (anti rabbit)	Goat-anti-rabbit IgG coupled with AlexaFluor 594	Life Technologies
Alexa Flour 488 (anti goat)	Chicken-anti-goat IgG coupled with AlexaFluor 488	Life Technologies
Alexa Flour 594 (anti goat)	Chicken-anti-goat IgG coupled with AlexaFluor 594	Life Technologies

2.6.2 TAP-tag

Lysis buffer

10% Glycerol
50 mM Tris, pH 8.0
100 mM KCl
0.1% NP-40
2 mM DTT (added fresh)
In H_2O bidest., 1x protease inhibitor tablet (Roche) per 7 ml buffer added freshly before use

TEV-buffer

10 mM Tris, pH8.0
150 mM NaCl
0.1% NP-40
0.5 mM EDTA
1 mM DTT (added freshly)
In H_2O bidest.

Calmodulin binding buffer (CBP)

10 mM β-mercaptoethanol
10 mM Tris, pH 8.0
150 mM NaCl
1 mM MgOAc
1 mM Imidazole
0.1% NP-40
2 mM $CaCl_2$
In H_2O bidest.

Calmodulin wash buffer

50 mM NH_4HCO_3, pH 8.0
75 mM NaCl
1 mM MgOAc
1 mM Imidazole

2 mM $CaCl_2$

Beads

IgG Sepharose™ 6 Fast Flow	GE Healthcare, Buckinghamshire, UK
Calmodulin Sepharose 4B	GE Healthcare, Buckinghamshire, UK

2.6.3 Immunoprecipitation

Non-denaturing lysis buffer

20 mM Tris-HCl, pH 8.0
137 mM NaCl
10% Glycerol
1% NP40
2 mM EDTA
In H_2O bidest., 1x protease inhibitor tablet (Roche) per 7 ml buffer added freshly before use

NET-N

20 mM Tris-HCl, pH 7.5
100 mM NaCl
1 mM EDTA
1% NP40

Beads

GammaBind™ Plus Sepharose™	GE Healthcare, Buckinghamshire, UK

2.6.4 Immunofluorescence

Fixation

2% PFA in PBS

Quenching

50 mM Ammoniumchloride

Permeabilization

0.2% Triton in PBS

Blockingsolution

1% BSA in PBS

DAPI

100 mg/ml in PBS

Mounting medium	Dianova, Hamburg, Germany

2.7 Materials for virological methods

2.7.1 Solutions for vector production

AAV Lysis Buffer

50 mM Tris, pH 8.5
150 mM NaCl
In H_2O bidest., pH 8.5, autoclave

PBS-MK

1 mM $MgCl_2$
2.5 mM KCl
In PBS, filter-sterilized

PBS-MK/NaCl

1 M NaCl in PBS-MK, filter-sterilized

Iodixanol

60% Iodixanol	Sigma-Aldrich, Taufkirchen, Germany

2.8 General buffers and solutions

1x PBS

140 mM NaCl
2.7 mM KCl
8.1 mM Na_2HPO_4
1.5 mM KH_2PO_4
In H_2O bidest., pH 7.4, autoclave

Methanol	Sigma-Aldrich, Deisenhofen, Germany
Ethanol	VWR, Darmstadt, Germany
Butanol	Applichem, Darmstadt, Germany
Isopropanol	VWR, Darmstadt, Germany

2.9 Chemicals

All chemicals were purchased from Sigma-Aldrich (Taufkirchen), AppliChem (Darmstadt), Merck (Darmstadt), Roth (Karlsruhe), Serva (Heidelberg), Fluka (Neu Ulm), Gerbu (Gaiberg), VWR (Darmstadt) and Life Technologies (Karlsruhe).

2.10 Kits

Beetle-Juice	PJK, Kleinbittersdorf, Germany
Chemiluminescence kit	Applichem, Darmstadt, Germany
LR Clonase™ II enzyme Mix	Life Technologies, Karlsruhe, Germany
Luciferase passive lysis buffer	Promega, Madison, USA
Qiagen Maxi Kit	Qiagen, Hilden, Germany
QIAprep Spin Miniprep kit	Qiagen, Hilden, Germany
QIAquick Gel extraction kit	Qiagen, Hilden, Germany
QIAquick Nucleotide removal kit	Qiagen, Hilden, Germany
QIAquick PCR purification	Qiagen, Hilden, Germany
QuickChange® II XL Sit-directed mutagenesis	Stratagene Agilent Technologies, La Jolla, USA
Renilla Glow-Juice	PJK, Kleinbittersdorf, Germany
RNeasy mini kit	Qiagen, Hilden, Germany
RT² first strand kit	Qiagen, Hilden, Germany
RT² Profiler Array	Qiagen, Hilden, Germany
RT² SYBR Green qPCR Mastermix	Qiagen, Hilden, Germany
StrataClone Blunt PCR Cloning Kit	Stratagene Agilent Technologies, La Jolla, USA

2.11 Electrical equipment

Cell culture hoods

Bio GARD cell culture hood	The Baker Company, Sanford, USA
Steril GARD III Advance cell culture hood	The Baker Company, Sanford, USA

Centrifuges

Beckman XL70 Ultracentrifuge	Beckman Coulter GmbH, Krefeld, Germany
Multifuge 1 S-R	Heraeus, Hanau, Germany
Refrigerated Sorvall RC6+ centrifuge	Thermo Scientific, Waltham, USA
Refrigerated tabetop centrifuge 5417R	Eppendorf, Hamburg, Germany
Tabletop centrifuge 5415C	Eppendorf, Hamburg, Germany
Ultracentrifuge Sorvall Discovery 90 SE	Thermo Scientific, Waltham, USA

Varifuge RF	Heraeus, Hanau, Germany
Megafuge 1.0	Heraeus, Hanau, Germany
Centrifuge rotors	
F12-6 x 500	Thermo Scientific, Waltham, USA
JA 25.50, Ti50.2, Ti70.1	Beckman Coulter, Krefeld, Germany
Freezer and fridges	
Liebherr Comfort	Liebherr, Biberach, Germany
Liebherr MedLine	Liebherr, Biberach, Germany
Liebherr Premium	Liebherr, Biberach, Germany
Liebherr ProfiLine	Liebherr, Biberach, Germany
Ultra-low freezer	Heraeus, Hanau, Germany
Incubators	
Function Line incubator	Heraeus, Hanau, Germay
Labotect CO_2 incubator	Labotect, Göttingen, Germany
Sanyo CO_2 incubator	Sanyo/Panasonic Healthcare Company, Wood Dale, USA
Microscopes	
Leica DMIL	Leica Microsystems, Wetzlar, Germany
Leitz Diavert	Diavert Leitz, Wetzlar, Germany
Will Wilovert	Wilovert Hund, Wetzlar, Germany
Zeiss Cell Observer	Zeiss, Jena, Germany
Zeiss LSM700	Zeiss, Jena, Germany
Pipettes	
Integra pipetboy	Integra Biosciences GmbH, Fernwald, Germany
Plate readers	
1420 Multilable Counter Viktor3	Perkin Elmer, Norwalk, USA
Multiskan GO (ELISA reader)	Thermo Scientific, Waltham, USA
PreCision 50-1200 µl (multichannel)	Biozym, Hessisch-Oldendorf, Germany
Research Pro 1200 (multichannel)	Eppendorf, Hamburg, Germany
Research Pro 300 (multichannel)	Eppendorf, Hamburg, Germany
Shaker and Mixer	
Bacterial culture shaker	Informs AG, Bottmingen, Switzerland
Combimag Red/RET magnetic stirrer	IKA, Staufen, Germany
Test-tube-rotator	Snijders Scientific, Tilburg, Netherlands
Thermomixer 5436	Eppendorf, Hamburg, Germany

Thermomixer comfort	Eppendorf, Hamburg, Germany
Vibramax-VXR	IKA, Staufen, Germany
Vortex Genie 2™	Bender and Hobein, Ismaning, Germany

Waterbaths

GFC waterbath	Grant Instruments, Cambridge, UK
UC water bath	Julabo, Seelbach, Germany

Others

800 W microwave	Bosch, Gerlingen-Schillerhöhe, Germany
C1000 Touch Thermal Cycler	BioRad, Munich, Germany
Econo Pump	BioRad, Munich, Germany
Electrophoresis Chamber	Roth, Karlsruhe, Germany
Electrophoresis Gel Slides	Roth, Karlsruhe, Germany
Electrophoresis power supply ST 606 T	Gibco BRL, Eggenstein, Germany
Electrophoresis power supply ST PS 305	Gibco BRL, Eggenstein, Germany
French Press (Emulski Flex C5)	Avestin, Ottawa, Canada
Gel Doc EZ Imager	BioRad, Munich, Germany
Horizontal Gel Electrophoresis Horizon 11.14	Gibco BRL, Eggenstein, Germany
Ice maker	Hoshizaki, Willich-Munchheide, Germany
Impulse Sealer	RNS Corp., Taipei,Taiwan
MicroPulser™ Electroporator	BioRad, Munich, Germany
MilliQ ultra-pure water unit	Millipore Merck, Darmstadt, Germany
Nanodrop spectrophotometer	PegLab, Erlangen, Germany
Nitrogen tank Chrono	Messer, Krefeld, Germany
pH meter	Sartorius, Göttingen, Germany
Sartorius scale	Sartorius AG, Göttingen, Germany
Transblot SD chamber	BioRad, Munich, Germany
Western Blot developing machine	Agfa, Mortsel, Belgium
X-Ray cassette	Kodak, Stuttgart, Germany

2.12 Common use utensils

1.5 ml and 2.0 ml reaction tubes	Eppendorf, Hamburg, Germany
10 and 15 mm glass cover slips	Thermo Scientific, Waltham, USA
10 cm culture plates	Greiner, Frickenhausen, Germany
15 ml reaction tubes	TPP, Klettgau, Switzerland
25, 75 and 150 cm^2 Tissue culture flasks	TPP, Klettgau, Switzerland
50 ml reaction tubes	Greiner, Frickenhausen, Germany
6, 10 and 15 cm cell culture dishes	Sarstedt Inc., Newton, USA
6-, 12-, 24- and 48-well test plates	TPP, Klettgau, Switzerland
96-well LIA plate	Greiner, Frickenhausen, Germany
96-well plate	Costar Corning, USA

Ultracentrifuge tubes	Beckman Coulter GmbH, Krefeld, Germany
Cell lifter	Costar Corning
Chemiluminescence films	GE Healthcare Limited, Buckinghamshire, UK
Cryo tubes, 2 ml	Roth, Karlsruhe, Germany
Electroporation cuvettes (25 x 2 mm)	Peqlab, Erlangen, Germany
Glass slides	Thermo Scientific, Waltham, USA
Inoculating loop	Greiner, Frickenhausen, Germany
Nitrocellulose membrane	Schleicher & Schuell, Dassel, Germany
One-time use filter, 0.2/0.4 µm	Renner, Dannstadt, Germany
Parafilm "M"	American National Can, Chicago, USA
Pasteur pipettes	
Pipet tips	Greiner, Frickenhausen, Germany
Pipettes (1000, 200, 100, 20, 10 and 2 µl)	Gilson, Middleton, USA
Syringes and needles	BD Franklin Lakes, USA
Whatman filter paper 3MM paper	Schleicher & Schuell, Dassel, Germany

2.13 Software

Adobe CS4/CS6	Adobe, San Jose, USA
Clone Manager 9.0 for Windows	Scientific & Educational Software, Cary, USA
Endnote X5	Thomson Reuters, New York, USA
Graphpad Prism 5.0	GraphPad Software, La Jolla, USA
ImageJ 1.40	NIH, Bethesda, USA
Microsoft Office 2003, 2010	Microsoft, Redmont, USA
Microsoft Windows XP, 8	Microsoft, Redmont, USA
String 9.0 database	www.string-db.org
Wallac 1420 Workstation	Perkin Elmer, Norwalk, USA
ZEN Black	Zaiss, Jena, Germany

3 Methods

3.1 Cultivation and manipulation of mammalian cells

3.1.1 Cultivation of mammalian cell lines

All cell lines were incubated at 37°C, 90% humidity and 5% CO_2 in an incubator. Passaging was done twice a week by washing the cells once with PBS, detaching them by addition of trypsin and splitting in an adequate dilution.

3.1.2 Determination of cell number

The cell number was determined by counting the cells with the use of a Neubauer chamber.

3.1.3 Cryo-conservation

Cells from a 150 cm^2 bottle were trypsinyzed, centrifuged at 1900 rpm for 5 minutes and resuspended in 3 ml of cryo-medium (2.3.1). The cell suspension was transferred into three cryo-tubes, incubated at -80°C in an isopropanol tank and finally stored in liquid nitrogen.

3.1.4 Transfection of mammalian cell lines

Cells (293 FlpIn™, 293T, 293TT, HeLa, HepG2) were transfected with different expression plasmids to analyze the cellular distribution or co-localization of expressed proteins. Additionally, transfection of 293TT cells was required for the TAP-tag experiments (3.4.1) as well as for several virological methods such as described in 3.5. Transfection was carried out by using Turbofect™ (2.3) according to the manufacturer's protocol with the following adjustments:

Tissue culture plate	*Volume of medium, ml*	*Number of cells*	*Amount of DNA, µg*	*Amount of Turbofect, µl*
96-well plate	0,1	$1*10^4$	0,2	0,4
24-well plate	1	$7*10^4$	1	2
12-well plate	2	$1*10^5$	2	4
6-well plate	4	$2.5*10^5$	4	8
10 cm dish	10	$4*10^6$	18	45
15 cm dish	15	$6*10^6$	40	75

Cells were seeded 24h prior transfection. For the preparation of the transfection mix, the required volume of non-supplemented DMEM was mixed with the DNA. Subsequently, the Turbofect™ solution was added and the mixture was vortexed for 20 seconds. After 20 minutes of incubation at room temperature the transfection mix was added dropwise to the cells. Cells were incubated for 48 – 72 h, harvested (3.1.6) and used for subsequent experiments.

3.1.5 siRNA transfection

For the specific knockdown of the human SPOP gene, different siRNAs (2.2.3) were transfected into HeLa cells using HiPerFect® transfection reagent (Qiagen). Shortly before transfection (~2h), 1.5 x 10^4 cells were seeded in 2.3 ml supplemented DMEM into a 6-well plate. For the transfection mix, different amounts of siRNA (100 ng, 200 ng or 300 ng) were mixed with 100 µl non-supplemented DMEM and 12 µl HiPerFect® and incubated for 10 minutes at room temperature. Subsequently, the transfection mix was added dropwise to the cells and incubated for 48h at 37°C. After incubation, cells were harvested for western blot analysis (3.1.6.1).

3.1.6 Harvesting of transfected cells

3.1.6.1 Harvesting and preparation of cell lysates for Western Blot analysis (3.3.4)

For the preparation of cell lysates, cells were detached in an adequate volume of trypsin (according to the plate format) and washed once with 1x PBS (2.8). After removing the liquid, the pellet was resuspended in an appropriate volume of 1x PBS (according the cell number) followed by addition of 3x SDS buffer (2.5.5). The samples were boiled for 7 minutes at 95°C and immediately cooled down on ice. Lysates were either used directly for subsequent experiments or stored at -20°C until use.

3.1.6.2 Harvesting and preparation of cell lysates for immunoprecipitation (3.4.2)

For the preparation of cell lysates used for immunoprecipitation, cells from a 10 cm dish were trypsinized and collected in a 2 ml tube. The suspension was centrifuged at 3.000 rpm for 5 minutes at 4°C, the pellet was resuspended in 0.5 ml non-denaturing lysis buffer (2.6.3) and incubated on ice for 2 h while vortexing in between. To clear the lysate, the tubes were centrifuged at 13.000 rpm for 10 minutes at 4°C and the supernatant was subsequently added to sepharose beads coated with the respective antibody (2.6.1).

3.1.6.3 Harvesting for AAV particle extraction (3.5.2)

For the extraction of AAV particles from transfected cells, cells ware scratched off the dish using a cell scraper and transferred into a 50 ml centrifuge tube. Cells that remained on the cell culture dishes were collected by rinsing the dishes once with 1x PBS (2.8) and transferred into the same tube. After centrifugation for 10 minutes at 1.800 rpm, the supernatant was discarded and the pellet was washed once with 1x PBS for 10 minutes at 1.800 rpm. Subsequently, the pellet was resuspended in 5 ml AAV lysis buffer (2.7.1; for 5 -10 15cm dishes) followed by cell lysis via freeze-thaw-cycles (3.5.2).

3.1.7 Generation of mammalian cell lines stably expressing human SPOP

For the generation of a cell line stably expressing human SPOP, the Invitrogen FlpIn™-system was used following the manufacturer's instructions. Briefly, 293 FlpIn host cells were co-transfected with pOG44 and pcDNA5/FRT/TO in a ratio 9:1 using Turbofect™ (2.3.1). 24h after transfection the medium was substituted by fresh DMEM and the cells were incubated for 24h. Subsequently, the transfected cells were splitted into a fresh bottle at a confluence of approximately 25% and incubated until they were attached to the flask (3-4 h). The medium was replaced by fresh DMEM containing hygromycin B at a concentration of 250 µM and cells were incubated until hygromycin B resistant foci were visible (ca. 2 weeks) by changing the medium every 2 – 3 days. 10 clones were picked, cultivated and tested for their SPOP expression by western blot analysis (3.3.4) after induction with doxycycline (3.1.8). Positive clones were cryoconserved (3.1.3).

3.1.8 Induction of a stable cell line with doxycycline

To overexpress the stably transfected human SPOP protein, cells were treated for 48h with 0.25 µg/ml doxycycline 24h after seeding.

3.1.9 Synchronization of cells

Cells were synchronized 24h after seeding. The medium was completely aspirated, cells were washed once with 1x PBS and then incubated in serum-free DMEM (containing antibiotics) for 24h. After incubation, fresh FCS was added to a final concentration of 10%. Cells were used for further experiments 48h after the described procedure.

3.1.10 Transduction of mammalian cell lines with reporter viruses

For infection analysis of reporter viruses, cells were seeded in an appropriate plate 24 h prior infection. Infection was done at a MOI of 10^3 or 10^4 for 24-48h. Depending on the reporter gene, analysis was either done by determining the luciferase acitivity (3.5.5) or indirect immunofluorescence (3.4.3).

3.2 Molecular biology methods

3.2.1 Polymerase chain reaction (PCR)

PCR was used to amplify specific fragments of DNA and/or to insert enzyme restriction sites, start- or stop-codons. For the reaction, the template DNA, product specific primers, dNTPs, polymerase buffer and the polymerase (KOD Hot Start DNA polymerase; 2.4.3) were mixed and placed into a PCR thermal cycler for the reaction. The reaction was performed as follows:

Reaction mix:

10 – 50 ng	template DNA
3 µl	25 mM $MgCl_2$
5 µl	2 mM dNTPs (each)
1 µl fwd. primer	100 µM
1 µl rev. primer	100 µM
5 µl	10x buffer (#2)
1 µl	KOD polymerase (1U/µl)
Ad 50 µl	H_2O

PCR program:

1 x	98°C	2 min.	denaturation
30x	98°C	15 sec.	denaturation
	65-70°C	15 sec.	annealing
	72°C	20 sec.	extension
1x	72°C	7 min.	final extension

Analysis of the PCR product was done by agarose gel electrophoresis (3.2.5). The product was purified using the PCR purification kit, nucleotide removal kit or gel extraction kit (2.10) depending on the following steps.

3.2.2 StrataClone™ Blunt TOPO cloning

TOPO cloning was used to efficiently clone the amplified PCR product into the TOPO backbone vector for DNA sequencing analysis (3.2.13). For the reaction 3 µl of the PCR product, 2 µl buffer and 1 µl of the vector mix (Topoisomerase I covalently bound to the vector) were mixed and incubated at room-temperature for 15 minutes. Then, 1 µl of the mixture was pipetted to 50 µl of chemical-competent bacteria and incubated on ice for 20 minutes. After the incubation, transformation was done by heat-shock according to the manufacturer's protocol (3.2.9.1). 150 µl of the culture were plated on LB-amp plates containing 160 µg X-Gal to allow blue/white screening, where white colonies contain the plasmid with the PCR insertion. White colonies were picked and cultivated; DNA was isolated by mini-preparation (3.2.11.2) and subsequently sent for sequencing (3.2.13).

3.2.3 Gateway cloning

For the generation of full ORF expression clones all the cDNAs were ordered at the GPCF of the DKFZ. cDNAs were provided as complete Gateway®-compatible entry-vectors allowing to shuttle the gene of interest into a destination vector with the LR reaction. All the reactions were done using the Fast Gateway® LR protocol obtained from the GPCF. A single reaction was carried out in a 0.2 ml PCR reaction tube and prepared as follows:

Reaction mix:

2 µl	5x LR buffer Gateway®
3 µl	destination vector (150 ng/µl)
2 µl	entry vector (150 ng/µl)
1 µl	water
0.5 µl	Topoisomerase I (NEB)
1 µl	10x Topoisomerase I reaction buffer (NEB)
0.5 µl	LR clonase

The reaction was incubated over night at 25°C and subsequently transformed into electro-competent bacteria (3.2.9.2). At least 3 colonies were picked and analyzed by digestion (3.2.7) with BsrGI and agarose gel-electrophoresis (3.2.5). Clones containing the right insert were stored as a glycerol stock (3.2.10) at -80°C.

3.2.4 Site-directed mutagenesis, QuickChange®

To introduce specific mutations into a gene of interest, complement primers were designed containing the mutation in their sequence. The reaction was performed using the QuickChange® II XL Site-Directed Mutagenesis Kit (2.10), following the manufacturer's protocol. The reaction mix was prepared as follows.

Reaction mix:

5 µl	10x reaction buffer
4 ng	template DNA
125 ng	primer #1
125 ng	primer #2
1 µl	dNTP mix
3 µl	QuickSolution™ reagent
Ad 50 µl	H_2O
1 µl	PfuUltra HF DNA polymerase (2.5 U/µl)

PCR program:

1 x	95°C	1 min.	denaturation
18x	95°C	50 sec.	denaturation
	60°C	50 sec.	annealing
	68°C	7 min.	extension
1x	68°C	7 min.	final extension

To digest the parental DNA template, 1 µl of DpnI restriction enzyme (10 U/µl) were added to the PCR reaction and incubated at 37°C for 1h. Subsequently, 2 µl of the reaction were transformed into 45 µl of XL10-GOLD ultra-competent cells following the protocol provided with the kit.

3.2.5 Agarose gel-electrophoresis

To analyze DNA agarose gel-electrophoresis was used. Hereby, DNA fragments were separated by size in an electric field. Separation was done using a 1% agarose gel (0.33 g agarose in 33 ml TAE buffer (2.4.2) containing 3 µl of ethidiumbromide (10 mg/ml)). For DNA extraction, a preparative gel was prepared (1.3 g agarose dissolved in 130 ml 1x TAE buffer containing 8 µl ethidiumbromide (10 mg/ml)). The gel was placed in an electrophoresis chamber that was filled with 1x TAE buffer. Electrophoresis was done at 100 V for 30 min (analytical) or 60 min (preparative) per gel. For analytical gels, the DNA was visualized with UV light at 254 nm wavelength and for preparative gels at 366 nm to avoid DNA damage. Here, the desired bands were cut out with a scalpel.

3.2.6 DNA extraction from agarose gels

DNA extraction and purification from agarose gels was done using the QIAgen gel extraction kit (2.10) following the manufacturer's instructions. Briefly, DNA was excised from the gel and dissolved in 3 volumes of QC buffer for 10 minutes at 50°C in a shaker. 1 Volume of isopropanol was added and the mixture was loaded onto a provided column to bind the DNA. After several washing steps with the provided buffers, the DNA was eluted in 30 µl of water.

3.2.7 Restriction digest

Restriction digest was either used for cloning following ligation (3.2.8) or for analytical purposes. The digest was done in a total volume of 20 µl, containing the desired restriction enzymes (NEB), the respective buffer (diluted to 1x) and the DNA (~ 1 µg). Digestion was carried out for at least 1h at 37°C unless differently specified for the enzymes. To determine whether the digest was successful, agarose gel-electrophoresis was performed (3.2.5).

3.2.8 Ligation

To ligate a DNA fragment and a vector, approximately 500 ng of the vector and fragment were mixed in a molar ratio of 1:10. Ligation was done using the T4 ligase (2.4.3) for 20 minutes at room temperature. A standard ligation mix was prepared as follows:

Ligation mix:

100 ng	vector DNA
X ng	insert
2 µl	10x T4 ligase buffer
1 µl	T4 ligase
Ad 20 µl	H_2O

After the incubation, 1 µl of the ligation mix was transformed into electro-competent bacteria (3.2.9.2).

3.2.9 Transformation of E.coli

3.2.9.1 Heat-shock

For transformation of chemical competent bacteria, the DNA-bacteria mix (3.2.83.2.2) was incubated for 45 seconds at 42°C in a waterbath. Subsequently, the reaction was put on ice for 2

minutes and 300 µl of LB-medium were added. Then, it was incubated for 1 h at 37°C, plated on LB-agar plates containing the desired antibiotic and incubated at 37°C overnight to obtain colonies.

3.2.9.2 Electroporation

For the transformation of electro-competent bacteria, 1 µl of the ligation (3.2.8) was mixed with 40 µl of electro-competent bacteria and transferred into a cooled electroporation cuvette. Electroporation was done by pulsing with 2.5 kV for 5ms. 300 µl of LB-medium were added to the transformed bacteria and the mix was incubated at 37°C for 1h before plating 150 µl on a LB-agar plate with the respective antibiotic. The plate was incubated at 37°C overnight to obtain colonies.

3.2.10 Preparation of glycerol stocks

For long-term storage of bacteria containing a transformed plasmid, glycerol stocks were prepared. Here, 300 µl of sterile glycerol (100%) were mixed with 1 ml of an overnight bacteria culture and stored at -80°C.

3.2.11 DNA extraction from bacterial cultures

3.2.11.1 Mini-preparation using the phenol-chloroform extraction

To extract DNA from *E. coli* using the phenol-chloroform method, 1.5 ml bacteria culture grown over night were pelleted. The pellet was resuspended in 100 µl glucose mix (2.4.1) and incubated on a shaker for 5 minutes. Next, 200 µl of alkali buffer (2.4.1) were added and the mix was incubated on ice for 5 minutes. For neutralization, 150 µl NaAc were added and incubated on ice for 5 minutes. Subsequently, 450 µl phenol/chloroform were added and incubated on a shaker for 5 minutes followed by centrifugation at 13.000 rpm for 5 minutes. 450 µl isopropanol were pipetted into fresh tubes and 380 µl of the upper phase of the phenol-containing samples were added. The mixture was incubated for 10 minutes at -80°C and immediately centrifuged for 30 minutes at 0°C, 13.000 rpm. The pellet was washed with 500 µl of 70% EtOH and 500 µl of 100% EtOH, dried for 10 minutes and resuspended in 50 µl of water.

3.2.11.2 Mini-preparation using the Qiagen mini-prep kit

DNA preparation was done following the manufacturer's instruction. DNA was eluted in 30 µl H_2O and quantified by using the Nanodrop (3.2.12).

3.2.11.3 Maxi-preparation using the Qiagen maxi-prep kit

DNA preparation was done following the manufacturer's instruction. DNA was dissolved in 500 µl H_2O or TE buffer (2.4.1) and quantified at the Nanodrop (3.2.12).

3.2.12 DNA quantification

To determine the concentration of DNA preparations the Nanodrop was used. The spectrum of 1 µl sample was measured in relation to a blank sample.

3.2.13 DNA-Sequencing

Sequencing was performed by GATC Biotech in Konstanz, Germany.

3.3 Protein analysis methods

3.3.1 SDS-Polyacrylamide gel electrophoresis (SDS-PAGE)

To separate denatured proteins according to their molecular weight, SDS-PAGE was performed. Cell lysates were mixed with 3x SDS buffer (2.5.3) and boiled for 7 minutes at 95°C. Besides the denaturation of the proteins, the 3x SDS marker loads the proteins equally with negative charges. 10µl of the denatured lysates were loaded on a SDS gel (either 12.5% or 15% separation gel; 2.5.3). Electrophoresis was done in 1x TGS buffer (2.5.3) at 90 V for the stacking gel and 120 V for the separation gel. Due to their negative charges, proteins are separated by size, as they move towards the anode in an electric field and stop at a certain pore size depending to their molecular weight. Visualization of the protein bands was done by either coomassie- (3.3.2), silverstaining (3.3.3) or western blot (3.3.4).

3.3.2 Coomassie staining

To visualize proteins in a SDS gel after electrophoresis (3.3.1), the gel was washed in water twice for 30 minutes and subsequently incubated with Coomassie Solution GelCode® (2.5.3) solution for at least 1h at room-temperature. Then, the excess solution was washed out with water until clear bands, marking the proteins, were visible. Protein bands were monitored at the Gel Doc EZ Imager (2.11).

3.3.3 Silverstaining

For the visualization of proteins at very low concentrations in a SDS gel after electrophoresis (3.3.1), the gel was stained with a silver solution using the following protocol. Proteins were fixed with Ag-FIX (2.5.4) for 1h at room-temperature followed by three washing steps with 50% EtOH, 20 minutes each. To block the unspecific binding of silver ions, the gel was incubated for 1 minute in fresh thiosulfate solution (2.5.4) and washed three times with H_2O, 20 seconds each. Subsequently, the gel was incubated in silvernitrate solution (2.5.4) for 20 minutes and washed again three times with H_2O, 20 seconds each. To visualize the proteins, the gel was incubated in sodiumcarbonate solution (2.5.4) until the bands were visible and washed three times with H_2O. To stop the reaction, the gel was incubated in Ag-Stop solution for 10 minutes and finally washed for 20 minutes in 50% MeOH. Protein bands were monitored at the Gel Doc EZ Imager (2.11).

3.3.4 Western Blot analysis

To visualize and analyze a specific protein after the separation in a SDS gel (3.3.1), the proteins were blotted onto a nitrocellulose membrane using the semi-dry blot method. For this, a "sandwich" was prepared, starting with three Whatman papers (2.12) drenched in 1x EMBL buffer (2.5.5), then the nitrocellulose (drenched in 1x EMBL) membrane, the gel and three Whatman papers. The sandwich was put in the blotting chamber (2.11) and the transfer was performed at 120 mA for proteins with a molecular weight lower than 80 kDa and 240 mA for proteins with a molecular weight higher than 80 kDa per membrane. The membrane was blocked for 30 minutes in 5% milk PBS-T (2.5.5) at room temperature and then incubated with the desired primary antibody (2.6.1; diluted in 5% blocking milk) over night at 4°C. After incubation the membrane was washed three times for 10 minutes with PBS-T and incubated for 1h at room-temperature with the secondary antibody (2.6.1; diluted in 5% blocking milk). Then, the membrane was washed three times for 10 minutes with PBS-T and proteins were detected using the chemiluminescent kit (2.10) according to the manufacturer's protocol by adding 0.5 ml of each solution onto the membrane and incubate it for 1 minute at room-temperature. The chemiluminescence was detected using high performance X-ray films (2.12) in a dark room.

3.3.5 Stripping of the nitrocellulose membrane

For the specific detection of several proteins on a western blot the nitrocellulose membrane was stripped. For this, the membrane was incubated 30 min at 55°C in stripping buffer (2.5.5). Afterwards, it was washed once with PBS-T (2.5.5) and blocked with 5% milk in PBS-T. After incubation with the primary antibody western blot method (3.3.4) was carried out.

3.3.6 GST-Protein Purification

Protein purification was done in order to obtain proteins of interest for the production of a polyclonal serum in rats and guinea pigs. For this, a 400 ml E.coli rosetta (2.1.2) culture was grown (inoculated with 4 ml of an overnight culture) until an OD_{600} of ~ 0.5 (100 µl aliquot was taken for analysis; aliquot 1) and induced with 100 µM IPTG overnight at 27°C (aliquot 2). The induced culture was harvested for 10 minutes at 5.000 rpm and the pellet resuspended in 40 ml buffer IV (2.5.1; containing one tablet protease inhibitor). Cells were lysed using the French press with 3-4 passes at 15.000 psi (aliquot 3) and the lysate was cleared at 17.000 rpm and 4°C for 1h (aliquot 4). The purification was done at 4°C using GSTrap columns (2.5.1). Equilibration of the column was done with 20 ml of buffer IV at a speed of 1 ml/min. Subsequently, the cleared supernatant was loaded on the column and circulated overnight at a speed of 0.5 ml/ml. An aliquot of the flow-through was taken for further analysis (aliquot 5). Then, the column was washed with 20-40 ml buffer IV and 10 ml of 50 mM Tris (pH 8.0), both at 1 ml/min. Afterwards, the protein was eluted into 500 µl fractions using 5 ml of 10 mM glutathione in 50 mM Tris (pH 8.0) at room temperature. 1 ml was applied with a syringe and incubated for 10 minutes, and then the fractions were collected. To quantify the fractions, Bradford assay (3.3.7) as well as SDS-PAGE (3.3.1) following coomassie staining (3.3.2) was used. Similar concentrated fractions were pooled for dialysis (3.3.8).

Regeneration of the column was done with 5 ml 6M guanidine hydrochloride, 10 ml 50 mM Tris (pH 7.5), 10-20 ml PBS and 10 ml 20% EtOH. All these steps were performed at 4°C and 1 ml/min. The regenerated columns were stored in 20% EtOH at 4°C.

3.3.7 Bradford assay

A Bradford assay was used to quantify protein concentrations in a solution in reference to a BSA standard. Briefly, a BSA standard was titrated 1:2 in duplicates in a 96-well plate, starting with a concentration of 2 µg/µl. The fractions were titrated 1:2 in three different wells. Subsequently, 100 µl Bradford reagent (1:5 in water) were added per well, and the absorbance at 595 nm was measured. Protein concentrations were calculated in reference to the BSA standard.

3.3.8 Dialysis

To exchange the elution buffer from the fractions, proteins were dialyzed at 4°C overnight against 1x PBS containing 200 µM NaCl. Dialyzed fractions were collected and quantified by Bradford assay (3.3.7) and SDS-PAGE (3.3.1) followed by coomassie staining (3.3.2).

3.3.9 Mass-spectrometry

To identify potential binding partners of different AAV VP1/2 N-termini after the Tandem Affinity Purification (3.4.1), the eluted samples were subjected to mass-spectrometry. The whole sample was trypsinized and excised from a SDS-gel before the mass-spectrometry. The analysis was done by the GPCF of the DKFZ.

3.4 Immunological methods

3.4.1 Tandem-affinity purification (TAP-Tag)

To identify potential interaction partners of different AAV VP1/2 N-termini the TAP-tag method was used. Here, the target protein is fused to a double tag containing protein A and a calmodulin binding peptide. Both tags are separated by a TEV-cleavage site. The procedure was performed as follows: Unless indicated differently, washing steps were done for 2 minutes at 1.200 rpm and 4°C. For the purification, transfected 293TT cells (10x 15 cm dishes; 3.1.4) were collected using a cell-scraper and centrifuged at 1900 pm for 5 minutes. The pellet was resuspended in 5 ml cold lysis buffer (2.6.2) and incubated on ice for 30 minutes. Then, the lysate was distributed into four 1.5 ml reaction tubes and cleared at 13.000 rpm and 4°C for 10 minutes (aliquot 1). The cleared supernatants were pooled into a fresh 15 ml Falcon tube and incubated overnight at 4°C on a rotating wheel with 75 µl IgG-sepharose beads (2.6.2), which were washed 5 times with 1 ml lysis buffer. For the TEV-protease cleavage, the overnight reaction was cleared at 1.200 rpm and 4°C for 2 minutes (aliquot 2) and the supernatant was discarded. The pellet was washed three times in 1 ml lysis buffer followed by three washing steps in 1 ml TEV buffer. An aliquot of the beads was taken for further analysis (aliquot 3), and the washed pellet was resuspended in 225 µl TEV buffer (2.6.2). Subsequently, 75 µl TEV protease (0.7 mg/ml) were added and the reaction was incubated overnight at 4°C. After incubation, the reaction was cleared by centrifugation and the supernatant, containing the cleaved construct, was transferred into a fresh tube and resuspended in 300 µl TEV buffer. The reaction was centrifuged and the supernatant was collected into a fresh tube. This procedure was repeated three times in total to obtain a final volume of 900 µl (aliquot 4). The remaining IgG beads were resuspended in 1 ml TEV buffer and an aliquot for further analysis was taken (aliquot 6). The TEV cleavage procedure was stopped by adding 5 mM iodoacetamide and 7 µM $CaCl_2$ to the supernatant. Binding to the calmodulin beads was done by adding 75 µl of the beads (5 times washed with calmodulin binding buffer (2.6.2)) to the supernatant and incubation for 90 minutes at 4°C on a rotating wheel. For the elution, the reaction was cleared (aliquot 6) and the pellet was washed twice with calmodulin binding buffer and twice with calmodulin wash buffer (2.6.2; 1ml each). After

washing, 40 µl of 3x SDS buffer (2.5.3) were added and the sample was boiled at 95°C for 7 minutes. The purification was analyzed by SDS-PAGE (2.5.3) and western blot (2.5.5) of the aliquots. Successful purifications were further analyzed by mass-spectrometry (3.3.9).

3.4.2 Immunoprecipitation of over-expressed proteins

To examine the interaction between proteins of interest, immunoprecipitation was performed. Here, sepharose beads (2.6.3) were washed twice with NET-N (2.6.3, 1.200 rpm, 2 min, 4°C) and incubated with 500 µl of the VP1 specific antibody A69 (2.6.1, hybridoma supernatant) overnight at 4°C on a rotating wheel. The next day, transfected cells were harvested as described in 3.1.6.2. The pellet was resuspended in 500 µl protease inhibitor containing non-denaturing lysis buffer (2.6.3) and incubated on ice for 1h. Subsequently, lysis was carried out by passing the suspension 3 times through a 23G needle with a syringe. Lysis was confirmed by microscopy and the lysate was immediately cleared by centrifugation (13.000 rpm, 10 min, 4°C). An aliquot of the supernatant was taken for further analysis. The cleared supernatant was transferred to the antibody loaded sepharose beads and incubated overnight at 4°C on a rotating wheel. After incubation, the beads were washed five times with NET-N (1.200 rpm, 2 min, 4°C) and the proteins were eluted with 40 µl 3x SDS buffer (2.5.3) and boiled for 7 minutes at 95°C. Analysis of the input (aliquot of the supernatant) and the immunoprecipitation was done by western blot (2.5.5). For the analysis of several specific proteins the membrane was stripped as described in (3.3.5).

3.4.3 Indirect immunofluorescence

Immunofluorescence was done to detect and visualize specific proteins in cell culture by fluorescent microscopy. In the underlying thesis, immunofluorescence was used for co-localization studies, as well as for the analysis of the cellular distribution of specific proteins. Immunofluorescence was carried out as follows. Unless indicated differently, all steps were performed at room-temperature. HeLa cells (5x 10^4) were seeded on 10 mm glass cover slips in a 24-well plate and transfected with the expression plasmids of the proteins of interest as described in (3.1.4). 48h after transfection, the cells were washed once in 1x PBS (2.8) and subsequently fixed with 2% PFA (2.6.4) in PBS for 15 min at room temperature. To avoid artefacts of the dyes, the cells were quenched with 50 mM ammoniumchloride (2.6.4) twice for 10 minutes. Permeabilization was done with 0.2% Triton X100 (2.6.4) in PBS for 10 minutes following three washing steps with PBS. To avoid unspecific binding of the antibody, the cells were blocked with 1% BSA in PBS (2.6.4), followed by the incubation with the primary antibodies (2.6.1) for 1h at 37°C. Cells were washed 5 times in 1x PBS and subsequently incubated with the secondary antibody (2.6.1) and DAPI (2.6.4, 1:100) diluted in 1% BSA in PBS for 1h at 37°C. After five final washing steps, cells were mounted in mounting medium (2.6.4) on a

glass slide and sealed with nail polish for conservation. Analysis of the samples was either done at the LSM700 or the cell observer (2.11).

3.5 Virological methods

3.5.1 Production of AAV particles in 293TT cells

To produce AAV particles in a large-scale format, five 15 cm dishes with 293TT cells (each dish 6x 10^6 cells) were transfected with 42 µg (two-plasmid-system) or 36.5 µg (three-plasmid-system) of plasmid DNA per plate, repectively. DNA was diluted in 1.5 ml of unsupplemented DMEM and 36 µl Turbofect™ (2.3.1) were added. Then, the reaction mix was vortexed, incubated at room-temperature for 20 minutes and subsequently added dropwise to the cells. Cells were incubated at 37°C for 48h until they were harvested.

3.5.2 AAV particle extraction from transfected cells 293TT

For the extraction of AAV particles from transfected 293TT cells (3.1.4), cells were harvested as described in (3.1.6.3). The 5 ml cell suspension was lysed by 5 freeze-/thaw-cycles (liquid nitrogen – 37°C). Then, genomic DNA was removed by a benzonase digest (50 U/ml) for 30 minutes at 37°C. The lysate was cleared by centrifugation (5.000 rpm, 10 min) and used for the purification in an iodixanol step gradient (3.5.3).

3.5.3 AAV particle purification from 293TT cell extracts

To purify AAV particles from 293TT cell extracts (3.5.2) an iodixanol step gradient was performed. The gradient was generated by carefully pipetting the single layers into the bottom of a 13 ml quickseal ultracentrifugation tube (2.12) through a Pasteur pipette, starting with the lowest density layer (AAV particle containing supernatant). This layer was underlayed by 1.5 ml 15% iodixanol in PBS-MK + 1 M NaCl (2.7.1). Continuously, the following layers were pipetted using the same technique: 1.5 ml 25% iodixanol in PBS-MK (2.7.1) containing phenol red, 1.5 ml 40% iodixanol in PBS-MK and 4 ml 60% iodixanol containing phenol red to fill up the tube. Subsequently, the tube was sealed and centrifuged for 2h at 10°C and 50.000 rpm using the Ti70.1 rotor (2.11). Under these conditions, the AAV particles should move into the 40% iodixanol layer. For the isolation of the particles, the tube was supplied with air using a needle and the 40% layer was taken out with a needle and a syringe and stored at -80°C for further use. A small aliquot of the particles was quantified by quantitative real time PCR.

3.5.4 AAV particle quantification

The quantification of the genome titer of AAV productions was done using quantitative real time PCR. The procedure was conducted by the group of Barbara Leuchs (DKFZ, Heidelberg).

3.5.5 *In vitro* transduction assay

The *in vitro* transduction assay was performed to analyze the infectivity of reporter viruses (AAV2 wt and SPOP-binding mutants) on different cell lines at different conditions (untreated, siRNA knockdown, overexpression of a protein of interest). For this, cells were seeded (10.000/per well in 100 µl DMEM) one day prior transduction and incubated at 37°C. The transduction was done at different MOIs (1.000, 10.000) depending on the experiment. 24 h after transduction, the medium was discarded and the cells were incubated for 15 minutes at room-temperature with 25 µl 1x passive lysis buffer (2.10) and a shaker. Subsequently, 20 µl of the lysate were transferred into a white 96-well plate (LIA; 2.12). For the luciferase detection, 100 µl of renilla glow juice (2.10) with coelenterazine (1:50) were added to each well and the luminescence was monitored at the Wallac Work Station (2.11) and analyzed in Microsoft Excel (2.13).

4 Results

4.1 Isolation and identification of host cell proteins that interact with the VP1/2 N-termini of different AAV serotypes

Viral infection processes are rather complex procedures that require several molecular mechanisms to be successful. These processes include the overcoming of host cell barriers such as the anti-viral immune response, but also a tightly timed interplay between viral and host cell proteins. For AAV it has been demonstrated that one of the most crucial step is the conformational change within the endosome leading to the exposure of the VP1/2 N-terminus. Because functional domains on the VP1/2 N-terminus have been identified and described during the past years, it seemed obvious that this part of the viral capsid is assigned with a key function in the viral life-cycle. Hence the question arose, whether this domain is involved in the binding and also the regulation of particular cellular proteins helping facilitating the viral infection. To answer this question, the present study aimed on the identification and characterization of proteins that were so far unknown to be involved in the AAV life-cycle.

For the identification of cellular proteins interacting with the VP1/2 N-termini of different AAV serotypes, the Tandem-Affinity-Purification (TAP-tag) method was performed, as described by *Rigaut et al. (1999)*. In this procedure, tagged target proteins are overexpressed in and isolated from cells, followed by a two-step tag-specific affinity purification (3.4.1). Isolated complexes are subsequently subjected to mass-spectrometry analysis to determine their exact identity (**Figure 9 A**).

4.1.1 Cloning and characterization of TAP-tagged AAV VP1/2 N-termini

To generate the target proteins for the TAP-tag procedure, VP1/2 N-termini of the AAV serotypes 2, 5, 6, 8, 9 and 10 were each fused to a double-tag, composed of a calmodulin-binding-peptide (CBP) and protein A, separated by a cleavage site for TEV (Tobacco Etch Virus) protease. Therefore, the DNA sequences encoding for the VP1/2 N-termini of various AAV serotypes were inserted into the pZomeC vector (Cellzome, 2.2.1), resulting in C-terminally tagged constructs (**Figure 8 A**). Protein expression was tested by transfection of the constructs and their subsequent overexpression in HEK293TT cells following western blot analysis of the cell extracts (**Figure 8 B**).

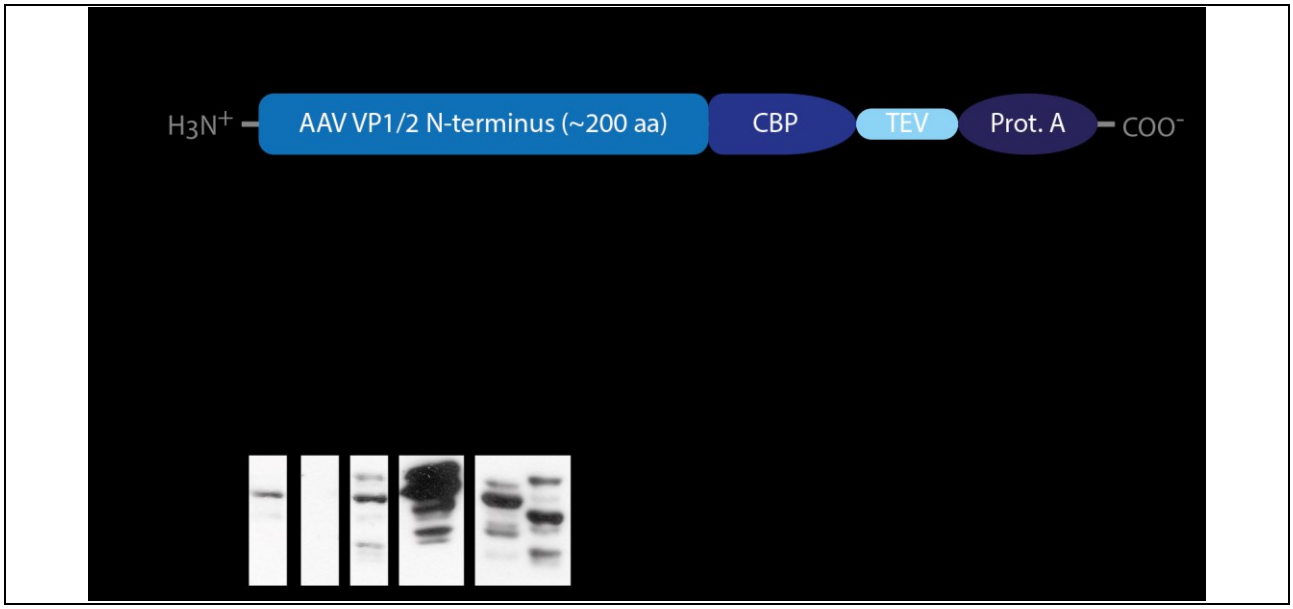

Figure 8: Expression analysis of the cloned TAP-tagged AAV VP1/2 N-termini. A Overview of the VP1/2 N-terminus fused to the TAP-tag. **B** Expression of the TAP-tagged VP1/2 N-termini from six AAV serotypes in HEK293TT cells. $3*10^5$ cells were transfected with the respective DNA for 48h. Cells were harvested and the 10 µl of the cell lysates were loaded on an SDS-gel for subsequent western blot analysis. Shown are the blots from independent experiments for each AAV serotype. Detection was done with the VP1-specific antibody A1 (2.6.1). aa: amino acids; CBP: calmodulin-binding peptide, TEV: Tobacco Etch Virus protease cleavage site, Prot. A: protein A

Expression was observed for all constructs, except AAV5, albeit at different levels, with AAV8 showing the strongest signal. Because expression of the C-terminally tagged AAV5 VP1/2 N-terminus could not be detected, (**Figure 8 B**, second lane), an N-terminally TAP-tagged AAV5 VP1/2 N-terminus construct was generated, using the pZomeN vector (2.2.1). However, also the N-terminally tagged AAV5 protein could not be expressed in HEK293TT cells (data not shown). Besides the band-specific VP1/2 N-terminus fusion protein with an expected molecular weight of ~45 kDa, for all expression constructs degradation products and also higher molecular weight aggregates could be detected (**Figure 8 B**). However, the specific fusion proteins were present at sufficient levels after small-scale transfections and therefore the respective expression constructs were considered to be suitable for use for the identification of host cell-specific AAV VP1/2 N-terminus binding proteins using the tandem-affinity purification method.

4.1.2 Tandem-affinity purification of AAV VP1/2 N-terminus-interacting protein complexes following expression in HEK293TT cells

To identify proteins that interact with the VP1/2 N-termini of different AAV serotypes, the TAP-fusion constructs described and analyzed above (4.1.1) were used for a large scale transfection of

HEK293TT cells for expression. For each construct $8*10^7$ cells were transfected with 400 µg of plasmid DNA. After 48h of incubation, cell lysates were prepared (3.1.6.1) and subjected to a first round of affinity purification using IgG sepharose beads, which bind specifically the protein A domain within the TAP-tag. After extensive washing, TEV protease was added to the beads in order to cleave the resin-bound TAP-tagged AAV VP1/2 N-terminus fusion proteins. Afterwards, the eluate was subjected to a second round of affinity purification using calmodulin-coupled beads which capture the CBP part of the TAP-tag. Elution was done by boiling the protein-bead complexes in 3x SDS loading buffer (**Figure 9 A**). The resulting eluate was then analyzed by SDS-PAGE, following either Coomassie or silver staining to determine the presence of protein bands different to the VP1/2 N-terminus (**Figure 9 B**), which present putative AAV VP1/2 N-terminus binding proteins.

Despite extensive washing, strong contaminating IgG bands deriving from the purification procedure were still present, which might have superposed additional protein bands. However, addition of an extra washing step after TEV protease cleavage, allowed to completely removing any remaining IgG beads, thus resulting in the loss of the bands of the heavy and light IgG chain (**Figure 9 C**, lane 7). To monitor the purification, aliquots were taken for western blot analysis at every single step during the TAP-tag procedure. An exemplary western blot of the AAV6 TAP aliquots is shown in **Figure 9 C**. As can be seen in this blot, expression of the fusion construct was strong (lane 1) and the fusion protein bound almost completely to the IgG beads (lane 3) because only a faint fusion protein-specific band could be detected in the supernatant (lane 2). After TEV protease treatment, the VP1/2-CBP protein was detected in the eluate shifted from ~45 kDa to ~32 kDa due to the cleavage of protein A (lane 4). In the IgG fraction no VP1-specific band could be observed anymore (lane 5) suggesting that the cleavage reaction was complete. The entire VP1/2-CBP construct bound to the calmodulin-coupled beads (lane 7) since it was not detected in the supernatant afterwards (lane 6).

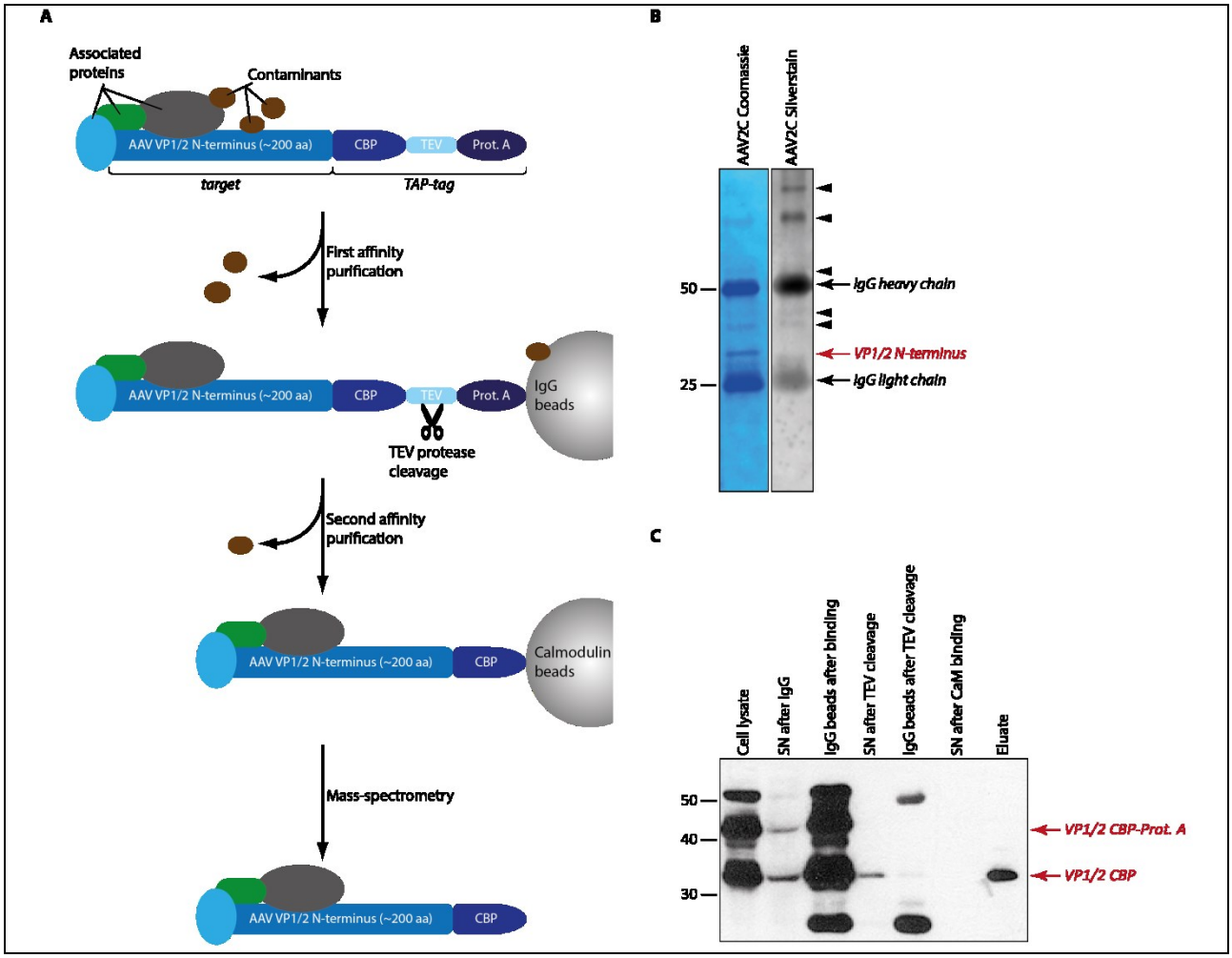

Figure 9: TAP-tag procedure. A Overview of the purification process. Overexpressed AAV VP1/2 N-terminus fusion proteins (blue bar) putatively interact with cellular proteins (light blue, green and grey). The resulting protein complexes are purified in two steps. In a first affinity purification step, the fusion protein is bound to IgG beads mediated by the protein A domain within the TAP-tag. Subsequent TEV protease cleavage facilitates the elution of the fusion protein. This is followed by a second affinity purification step using calmodulin beads that specifically bind the remaining CBP domain within the TAP-tag. Extensive washing after binding of the fusion protein to the beads (both steps) helps to remove unspecific, contaminating proteins and/or cellular debris (brown circles). **B** Analysis of the purified and eluted proteins. 10 µl of the protein eluates were analyzed by SDS-PAGE following either coomassie or silver staining. The gels revealed bands of co-purified proteins (arrowheads), indicating putatively interacting proteins. Left panel: Coomassie staining. Right panel: Silverstaining; both exemplarily for AAV2 VP1. **C** Purification control of the AAV6 VP1/2 N-terminus fusion construct. Samples of every single purification step were taken and analyzed by western blot. The blot confirms the presence of the purified and cleaved VP1/2 N-terminus construct in the eluate. Loading volumes were adjusted to the volumes during the purification. For the eluate however, a 10-fold higher volume was loaded. For detection, A1 hybridoma supernatant specific for the AAV VP1/2 N-termini was used. SN: supernatant, CBP: calmodulin-binding peptide.

Proteins eluted from the calmodulin matrix were analyzed by mass-spectrometry (3.3.9). As a negative control for the screening, different HPV-L2-TAP fusion constructs were transfected,

expressed and purified under the same conditions to exclude binding partners that unspecifically co-purified during the procedure, by comparing the mass-spectrometry results of the VP1 purifications and HPV L2 (data not shown).

4.1.3 Isolation of VP1/2-N-termini interacting proteins

As this work aimed on the identification of unknown cellular proteins interacting with the AAV VP1/2 N-termini of different AAV serotypes, the complete purified eluate (4.1.2) was trypsin-digested and used for mass-spectrometry analysis, without extracting specific bands from the SDS gel. Database analysis was done using the NCBI protein database once with the criteria "all taxa" to identify VP1-specific peptides, demonstrating the purification the VP1/2 fusion proteins and thereby indicating ag successful purification procedure. Furthermore the database analysis was done with the criteria "mammals" for identification of binding partners of mammalian origin. In each mass-spectrometry analysis, peptides of the respective VP1 proteins were identified, indicating a successful purification of the AAV VP1/2 N-terminus TAP-tag fusion proteins. Unspecific proteins, either deriving from the purification procedure (IgGs) or the handling itself (keratins), but also proteins from other species different to human origin, that were found with the database, were not further considered and eliminated from the identified proteins. In total, 102 proteins deriving from other species were eliminated, resulting in a final list of 51 different putatively interacting proteins from all five TAP-purifications. An overview on the proteins, as well as which proteins were co-eluted with which AAV serotype is depicted in **Table 1**. For all of these proteins, at least two different peptides were identified, thus fulfilling the standard criteria for mass-spectrometry. The selection criteria of candidates that were used for further experiments characterizing their function on AAV are described in detail in the following paragraphs.

As shown in **Figure 10 A**, seven of the identified proteins co-eluted with all of the five serotypes, whereas the other proteins were detected with four or fewer serotypes. Of these, AAV6 was found to interact with 39 of the isolated proteins, followed by AAV2 (25), AAV10 (22), AAV8 (19) and AAV9 (17, **Figure 10 B**). The high degree of divergence among these five purifications of the identified proteins might derive from differences in the VP1/2 N-terminus sequences, although the VP1/2 N-terminus is highly conserved among all serotypes (with AAV5 and AAV12 being the least conserved serotypes). Another reason might be technical issues of the purification, as the efficiency of the transfection as well as the recovered eluate was not equal among all purifications, hence variations regarding protein input have influenced the mass-spectrometry result. However, proof of principle that the purification method is suitable to identify potential AAV VP1/2 N-terminus interacting proteins might be the isolation of Cyclin-dependent kinase 2 (CDK2). CDK2 has been demonstrated in an *in vivo* high-throughput protein interaction screen to directly bind to AAV2 and

AAV8, negatively influencing their infection *(Murphy et al. 2008)*. In addition, speckle-type POZ protein (SPOP) was identified in a yeast-two-hybrid screen to interact with the AAV2 VP1/2 N-terminus, functional analysis however, is still lacking *(Popa-Wagner 2011)*. Moreover, a large siRNA screen on AAV2 infection suggested Calpain 2 to be involved during AAV2 infection *(Sommer and Hölscher, not published)*. However, this also implied that a specific interaction was not necessarily linked to a purification of proteins which co-eluted with all of the serotypes used in the screen. It rather demonstrated the importance of further characterization experiments to conclude on specific interactions with the respective VP1/2 N-termini. Taken together, the co-elution of already described proteins demonstrates the efficiency of the screen to allow the identification of novel putative interaction partners.

Table 1: Co-eluted proteins in the TAP-screen

Group and protein	AAV-Serotype(s)
Cell-cycle	
Calpain 2	**2, 6 ,8 ,9, 10**
Calpain 11*	2, 6, 8, 9, 10
Calpain small subunit 1*	2, 8, 9, 10
Cyclin-A2	2, 6, 8, 9, 10
Cyclin-dependent kinase 1	**2, 6, 8, 9, 10**
Cyclin-dependent kinase 2	**2, 6, 8, 9, 10**
Protein S100 A1	2, 6
Protein S100 A2	10
DNA replication	
DNA helicase II	6
Metabolism	
Delta 2-isopentenyl pyrophosphate transferase-like protein	6
Inositol-3-phosphate synthase 1*	6
Ornithine transcarbamylase	2
Phospholipid hydroperoxide glutathione peroxidase	6
Vacuolar sorting protein 26	6
Vacuolar sorting protein 35	6
Nuclear pore/import	
Importin 5*	**2, 6, 8, 9, 10**
Signal transduction	
Hippocalcin-like protein 1	2, 6, 9, 10
Insulin receptor substrate 4*	8
Microfibril-associated glycoprotein 4	2, 6, 10
Rig homolog	2, 6

Group and protein	AAV-Serotype(s)
Translation/Ribosomal	
S3 ribosomal protein	8, 9
40S ribosomal protein S10	6
40S ribosomal protein S20	6
60S acidic ribosomal protein P1*	6
60S ribosomal protein L23*	2, 6
78 kDa glucose-regulated protein*	2, 6, 8, 10
Elongation factor 1-alpha 1*	2, 6
Heat shock cognate 71 kDa protein*	2, 6, 9
Heat shock protein 60	2, 6
Heat shock protein 70-2*	6
Heat shock protein 90 kDa*	8
hnRNP U protein	2, 6, 8, 9
L11 ribosomal protein	2, 6
Mitochondrial heat shock protein 75*	6, 8, 10
RNA helicase A*	8
S10 ribosomal protein	8, 9
S5 ribosomal protein	6
Transport	
alpha-Tubulin*	8, 10
beta-Actin*	2, 9, 10
beta-Tubulin*	2, 6, 8, 9
Copine 1*	2, 6, 8, 9, 10
Copine 3*	2, 6, 9, 10
EH domain containing 2	6
Nestin	2, 10
Vimentin*	6
Ubiquitination	
26S proteasome non-ATPase regulatory subunit 12*	10
26S proteasome subunit 11*	6, 10
Cullin 3	**6, 10**
Cullin 4a*	6, 10
CAND1*	**2, 6, 8, 10**
SPOP	**6, 9**

The TAP-tag procedure with the five different AAV VP1/2 N-terminus fusion proteins identified 51 putatively interacting proteins. These proteins were classified according to their cellular function. The right column shows the serotype(s) that each protein co-eluted with. Proteins marked with an asterisk were also isolated with the HPV16 L2 TAP-tag purification. Proteins marked in bold represent the proteins chosen for further analyses (4.2).

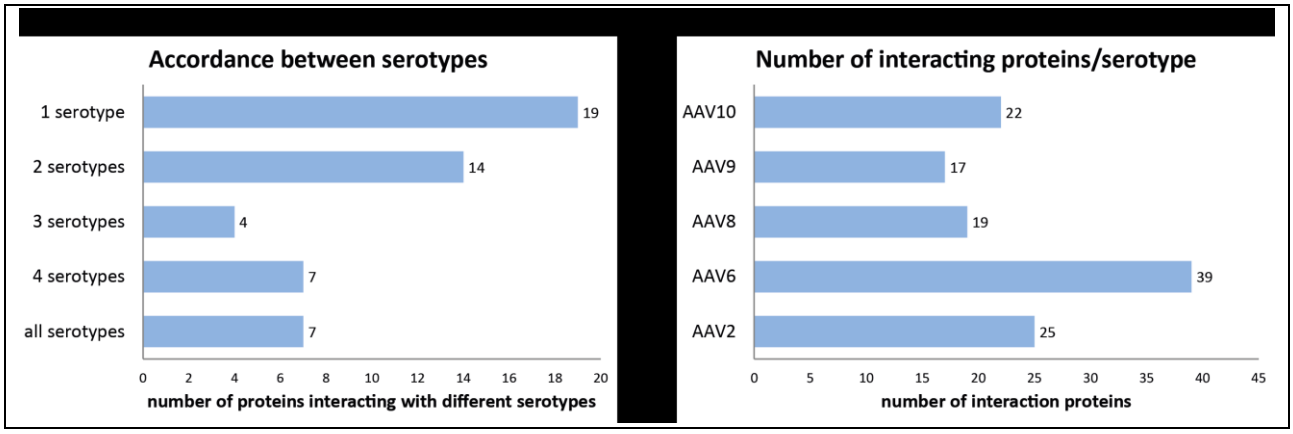

Figure 10: Overview on the interaction of the isolated proteins with the respective AAV serotype(s). A Abundance of identified proteins that either co-eluted with one, two, three, four or five serotypes. **B** Number of proteins that interacted with every single serotype used in the screen. Total number of isolated proteins: 51.

The identified proteins were classified into eight different categories, according to their cellular functions. These categories were: Cell-cycle, DNA replication, metabolism, nuclear pore/import, signal transduction, translation/ribosomal proteins, transport and ubiquitination (**Table 1, Figure 11**). Although Importin 5 also functions in transportation it was categorized separately, as its function in transportation is restricted to the nucleus. The largest category of the identified proteins, comprised of 17 different proteins, consisted of ribosomal and heat shock proteins. However, as nine proteins of this group were also found in the HPV16 L2 TAP-tag screen (negative control purification), and also the fact that these proteins are quite common in protein screens due to their abundance in the cell *(Nash et al. 2009)*, they were excluded from further characterization experiments. Furthermore, six out of eight of the identified proteins involved in cellular transportation were isolated with HPV16 L2 as well, hence this subset of proteins was not considered for further analyses.

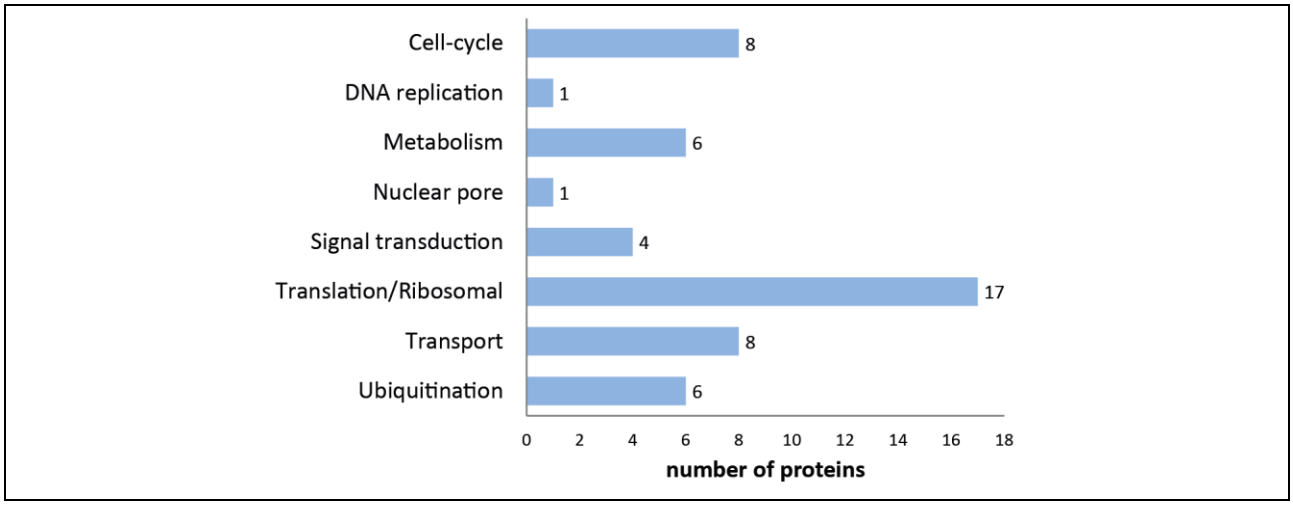

Figure 11: Functional diversity of the co-eluted proteins with the VP1/2 N-termini-TAP constructs. The identified proteins were grouped according to their cellular function into eight different categories.

As AAV does not depend on dividing cells to infect, it might be that it exploits cell-cycle proteins such as CDKs of the host cell to facilitate the infection. In concordance with this hypothesis, *Porwal et al. (2013)* demonstrated, that parvoviruses, including AAV, interact with key nuclear proteins to initiate nuclear envelope breakdown for their infection *(Porwal et al. 2013)*. Also, at the course of this screening, little was known about proteins being involved in nuclear capsid transport, however, it was postulated that AAV enters the nucleus as intact capsid. Despite the fact that Importin 5 was isolated with HPV16 L2 as well, its presence in the AAV TAP-tag purifications was a hint for an active transport of the capsids into the nucleus. Moreover, identification of several proteins of the ubiquitination-proteasome system further implied the influence of capsid ubiquitination on the AAV infection. For these reasons, the isolated proteins named above seemed to be promising interaction partners and hence were used for further characterization experiments on their specificity to AAV. In addition, the two orthologues (Mad2 L1 and Mad2 L2) of the spindle assembly protein Mad2 (mitotic arrest deficient 2) were included, because they were identified to be promising interaction partners of the AAV2 VP1/2 N-terminus in the aforementioned yeast-two-hybrid screen *(Popa-Wagner 2011)*. A list of the nine chosen proteins for further characterization is summarized in **Table 2**, including their function in the cell, as well as their subcellular distribution.

Table 2: Proteins of interest for further analysis

Protein	Localization	Function
Cell-cycle		
Calpain 2	Cytoplasm	Cell-cycle progression; Ca^{2+}-dependent
CDK1	Nucleus/Cytoplasm	Cell-cycle control; G2/M transition
CDK2	Nucleus/Cytoplasm	Cell-cycle control; G1/S transition
Mad2 L1	Nucleus	Control of metaphase-to-anaphase transition by ubiquitination
Mad2 L2	Nucleus	Control of metaphase-to-anaphase transition by ubiquitination
Nuclear pore/import		
Importin 5	Nucleus	Nuclear transport
Ubiquitination		
Cullin 3	Nucleus	Scaffold of Cullin-RING ligase 3, mediating ubiquitination
CAND1	Nucleus/Cytoplasm	Regulator of Cullin-RING ligases
SPOP	Nucelus	Substrate adaptor for Cullin 3 in ubiquitination processes

Chosen proteins with their subcellular localization (according to www.uniprot.org) and their cellular function.

4.2 Validation of the interaction between the nine chosen proteins and VP1

4.2.1 Cloning of proteins of interest into expression vectors

To confirm the specific interaction between the nine chosen proteins (**Table 2**) and VP1, co-immunoprecipitation as well as co-localization studies using indirect immunofluorescence were performed. For that, cDNAs encoding for the different proteins (obtained from the GPCF) were inserted into an expression vector (2.2.1) that contained a myc-tag located at the N-terminus of the respective protein. Expression of the proteins was analyzed by transfecting the expression constructs into HEK293TT cells for 48h. Lysates were prepared and subsequently analyzed by western blot (**Figure 12 A**). As a control for the myc-specific transfection, a lysate of untransfected cells was loaded. A positive control for the myc-antibody was a previously tested myc-expression construct.

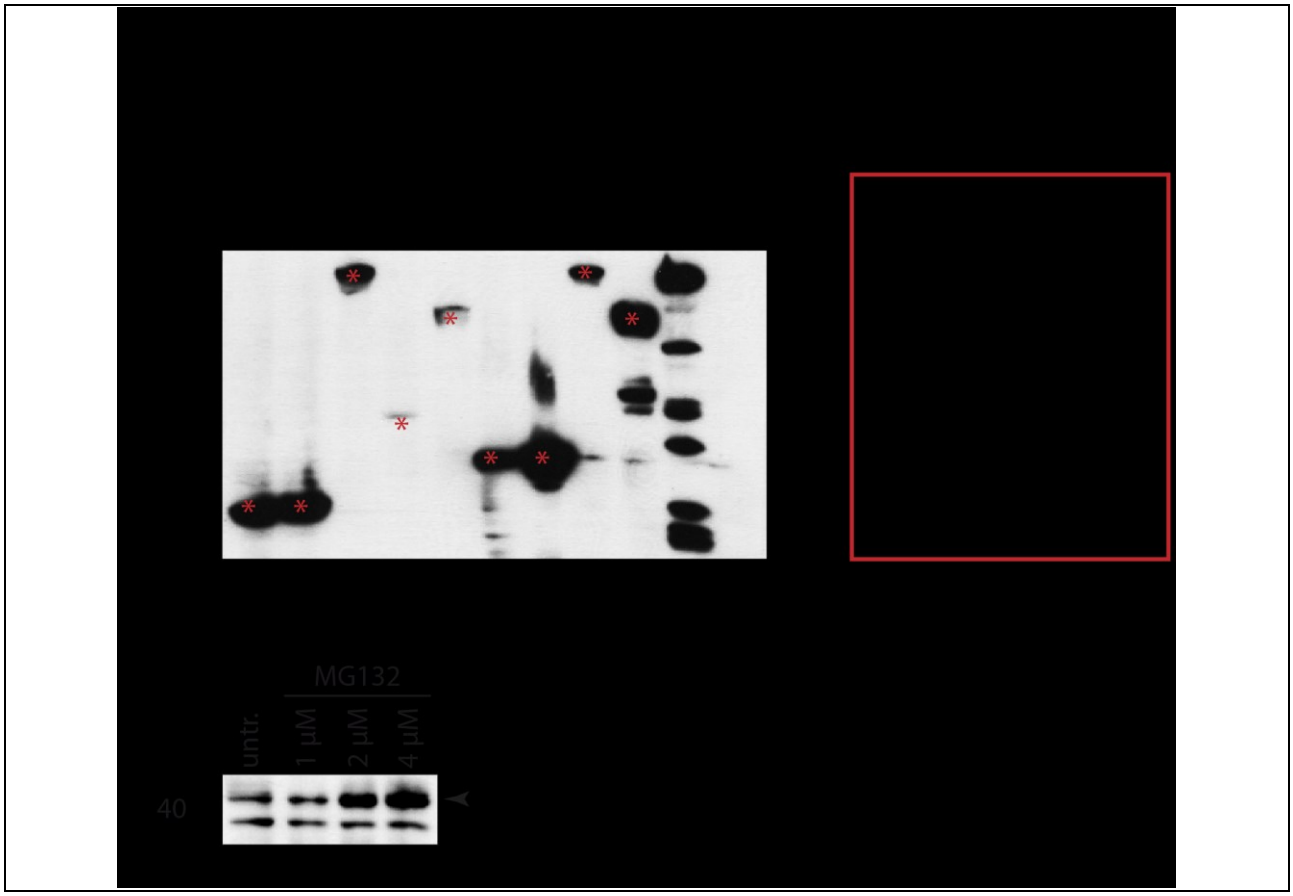

Figure 12: Overexpression of myc-tagged putative VP1/2 N-terminus interaction partners. A Proteins were overexpressed in HEK293TT cells ($1*10^5$ cells/construct) for 48h. Lysates were prepared and subsequently used for western blot analysis. Myc-specific bands in the transfected cell lysates were detected. Respective protein sizes are listed on the right (according to www.uniprot.org). SPOP detection was very weak (lane 4). Myc positive control: A previously validated myc-expression construct, provided by the group of T. Hofmann, DKFZ. **B** Treatment of SPOP transfected cells with different concentrations of MG132 led to a dose-dependent accumulation of SPOP, allowing overcoming the weak expression and thus its detection by western blot.

All proteins were detected with bands according to their molecular weight, albeit Calpain 2 also showed a band at ~50 kDa, indicating a certain degree of degradation. The low signal for SPOP might be due to a high turnover and strict regulation by the cell, as it functions in the ubiquitin-proteasome system (1.5.2). To rule out, whether this hypothesis was true, the overexpression of SPOP in HEK293TT cells was repeated in addition with different concentrations of the proteasome inhibitor MG132, preventing the proteasomal degradation of ubiquitinated proteins, and thereby leading to their accumulation. For this, cells were treated with MG132 4h prior harvest. As shown in **Figure 12 B**, inhibition of the proteasome led to a stabilization of SPOP in a dose-dependent manner, with the strongest signal at 4 µM. However, as this dose came along with a partial cytotoxic

effect, a more gentle concentration of 2 µM MG132 was used for further experiments. The strong expression of all of the proteins allowed using them for further characterization experiments.

4.2.2 Co-immunoprecipitation of proteins of interest and AAV2 VP1

The validation of the interaction with the chosen proteins, as well as all further experiments were conducted with AAV2 VP1 only, because it represents the prototype among all AAV serotypes. To proof the specific interaction between the isolated proteins and AAV2 co-immunoprecipitation (co-IP) were performed. Instead of only using the VP1/2 N-terminus, the full-length VP1 protein was overexpressed. For that a vector was used, in which the start codons of VP2 and VP3 were mutated, thereby facilitating the exclusive expression of VP1 alone (with only minor levels of VP3 probably due to a leaky repressor). Use of the full-length VP1 suggested resembling more physiological conditions, as it should be able to fold in its native conformation thereby mimicking the situation during infection and protein-synthesis. Precipitation was done using a VP1/2-specific antibody (A69) immobilized on sepharose beads (2.6.3). Co-IP was optimized and thus resulted in specific bands for the following proteins: Mad2 L2, CDK1, CDK2, Cullin 3 and Calpain 2, but it also led to the complete loss of Mad2 L1 and almost complete loss of CAND1 and Importin 5 (all of these proteins were precipitated in an initial co-IP experiment under less stringent conditions; **Figure 13**). Interaction of VP1 and CDK2 could not be confirmed by co-IP because a signal for CDK2 was also detected in the negative control (IP without VP1). However, CDK2 was described to interact with AAV2 and AAV8 previously *(Murphy et al. 2008)*. Raising the conditions to even higher stringencies would probably reduce the unspecific CDK2 binding on the one hand, but might also lead to the loss of more of the other proteins on the other hand. Also, CAND1 and Importin 5 showed faint bands in the IP, which might indicate a specific interaction. However, because the background was quite high, a clear conclusion was not possible. Although the expression of VP1 varied among the samples in the input, specific precipitation with the A69 antibody resulted in strong VP1 signals.

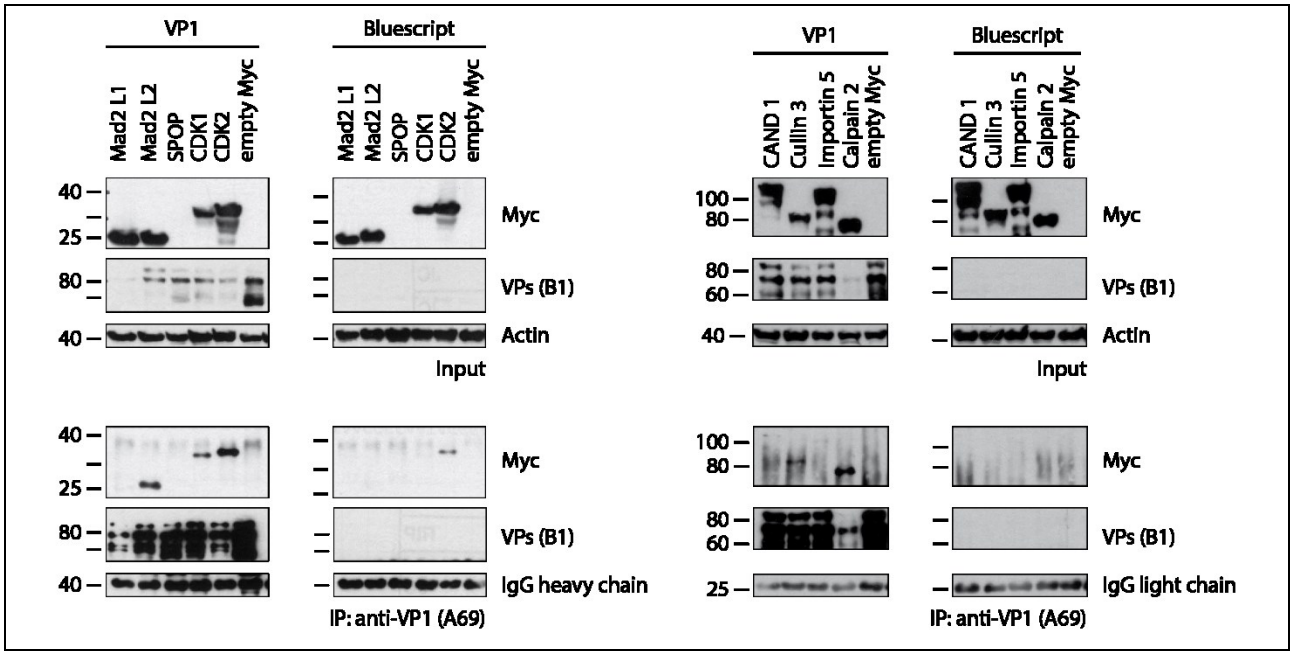

Figure 13: Co-immunoprecipitation of VP1 and the isolated proteins. HeLa cells ($6*10^6$ cells/construct) were transfected with expression plasmids. 48h after transfection, cells were harvested, lysed and 10 µl of the cell lysates were subsequently analyzed by western blot. Left panel: Low molecular weight proteins. Right panel: High molecular weight proteins. Overexpression was observed for all of the proteins except for SPOP in both, the VP1 samples and the negative control IP (upper panels). Specific co-IP was observed for Mad2 L2, CDK1, Cullin3 and Calpain 2 (lower panels). The reduced VP1 signal for Calpain 2 was considered as blotting artifact, as it was not observed in previous experiments. CDK2 was detected in the IP, as well as in the negative control, indicating an unspecific binding to the sepharose beads. Myc-control: empty myc-expression vector. Antibodies: A69 (IP), anti-myc, anti-VP (B1) anti-actin.

For SPOP no expression could be shown under these conditions. For this reason, the co-IP was performed in combination with treatment of 2µM MG132, as described before (4.2.1), prior to subjecting putative VP1-SPOP complexes to the IgG-loaded beads. Proteasome inhibition resulted in a strong expression of SPOP in both, the VP1 approach and the negative co-IP. A clear SPOP signal was detected in the co-IP for the VP1 sample, indicating an interaction between VP1 and SPOP. A SPOP-specific band was not detected for the negative control (**Figure 14**).

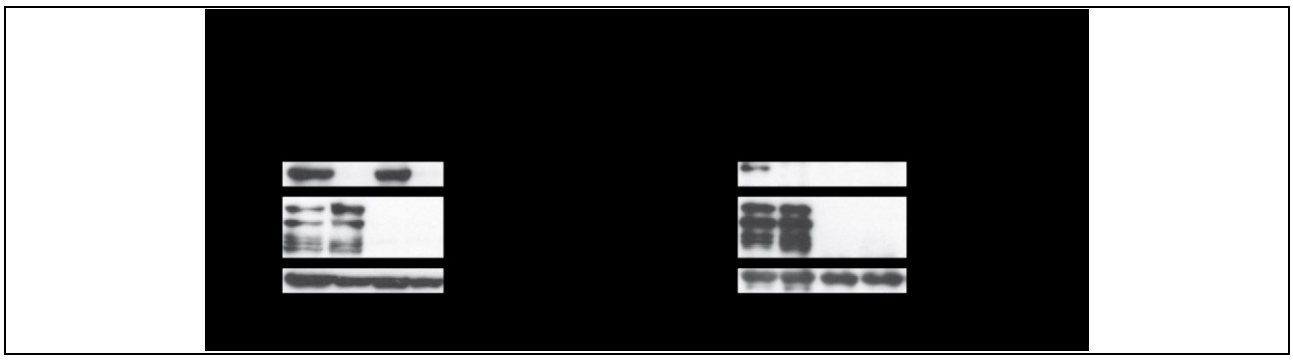

Figure 14: Co-immunoprecipitation of SPOP. HeLa cells ($6*10^6$ cells/construct) were transfected with expression plasmids. 44h after transfection, cells were treated with 2 µM MG132 for 4h and subsequently harvested and lysed. 10 µl of the cell lysates were analyzed by western blot. Co-IP was performed using the standard protocol. Strong overexpression of SPOP was observed, resulting in a SPOP-specific band in combination with VP1 (right panel).

Taken together, the co-IP results confirmed the interaction of Mad2 L2, SPOP, CDK1, Cullin3 and Calpain 2 with VP1 (**Table 3**). Furthermore, although CDK2 was also detected in the negative control, together with the previous identification *(Murphy et al. 2008)* it was considered to be specific.

4.2.3 Cellular distribution of AAV2 VP1 and the proteins of interest

To further confirm the specific interaction between the nine identified proteins and the N-terminus of AAV2 VP1, cellular localization between the proteins was analyzed by indirect immunofluorescence (3.4.3). To be able to draw conclusions on the co-localization, or to determine if co-expression of VP1 and the proteins leads to a redistribution of either, the subcellular localization of the identified proteins as well as of VP1 was analyzed. For that, HeLa cells were transfected with expression plasmids encoding either for the VP1 or one of the identified proteins and stained with fluorescently labelled antibodies to visualize their cellular distribution. Microscopy was done on a fluorescence microscope (**Figure 15**).

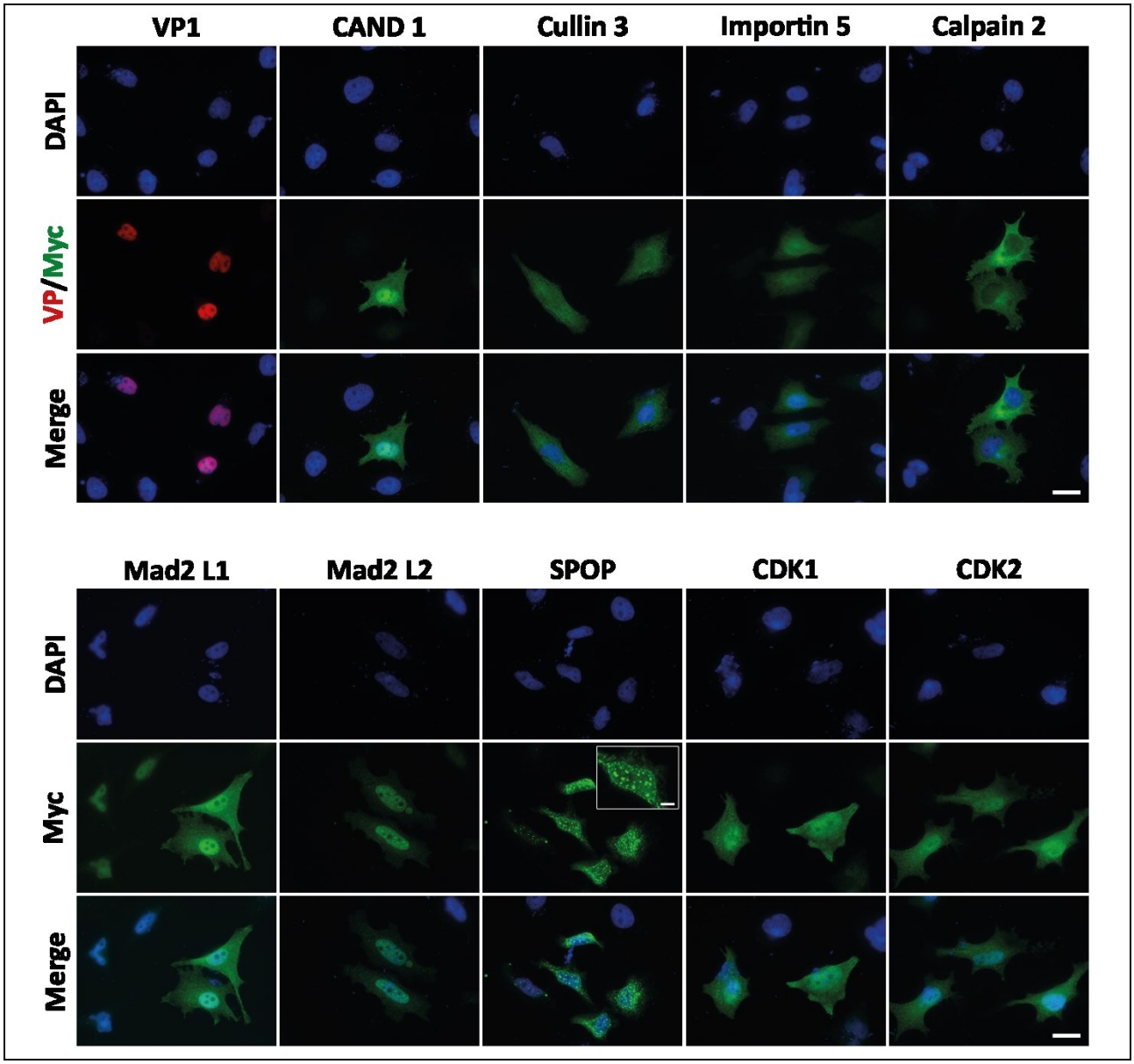

Figure 15: Subcellular distribution of VP1 and the putative AAV VP1/2 N-terminus binding proteins. Myc-tagged constructs (green), or VP1 (red) were overexpressed in HeLa cells, fixed and stained with fluorescently labelled secondary antibodies (VP1: Alexa fluor 594; Myc: Alexa fluor 488). DAPI was used for the visualization of the nucleus (blue). The speckled phenotype, postulated for SPOP, is demonstrated in the enlarged window (scale bar: 5 µm). Primary antibodies: A69 (VP1), anti-myc (proteins of interest). The experiment was performed twice. Scale bar: 20 µm

As already described before, VP1 mainly localizes to the nucleus when overexpressed in cells. In the current experiment in a few cells the distribution of VP1 was diffuse covering the cytoplasm and nucleus, but the majority of the cells showed a clear nuclear distribution. This observation coincides with a study performed by *Popa-Wagner (2011)* revealing that approximately 70% of VP1 transfected cells show a nuclear localization, whereas 30% are cytoplasmic-nuclear. Except for Cullin 3 and Importin 5, the subcellular distribution of the identified proteins reflected the phenotypes that are

published in the literature (**Table 2**). Cullin 3 and Importin 5 were both postulated to only localize in the nucleus. However, the results of the current experiment show a diffuse localization of both proteins in the cytoplasm and the nucleus. This observation might be explained by the fact that the compared to the physiological levels highly elevated protein concentrations within the cell, induced by the transfection of expression constructs, interfere with the natural protein localization. Furthermore, the subcellular distribution might also be affected by the addition of the myc-tag. Also, both orthologues of Mad2 showed a faint staining in the cytoplasm, the majority however, localized to the nucleus. The nuclear speckled phenotype that was described for SPOP could be confirmed (**Figure 15**; enlarged), also indicating a specific staining for the myc-expression constructs.

4.2.4 Co-localization of AAV2 VP1 and the putative interaction partners

To analyze, whether VP1 co-localizes with either of the proteins of interest, co-expression experiments following visualization by indirect immunofluorescence were performed. The previously determined subcellular localization of the proteins and VP1 (**Figure 15**) facilitated the analysis of whether the distribution of either VP1 or the proteins changed when co-expressed. The results are depicted in **Figure 16**. For all proteins under investigation overlapping localization with VP1 could be observed. Because most of the proteins, as well as VP1 were mainly localized within the nucleus (**Figure 15**) it was not clear whether this result reflected a specific interaction. However, co-expression of SPOP altered the localization of VP1. When expressed alone, VP1 was detected in a diffuse distribution in the nucleus and/or the cytoplasm (**Figure 15**, **Figure 23 A**), whereas SPOP localized in a typical speckled pattern within the nucleus (**Figure 16**). In combination though, the VP1 signal overlapped with the nuclear speckles formed by SPOP, suggesting that SPOP recruits VP1 into its speckles. This result might indicate a direct interaction between SPOP and VP1.

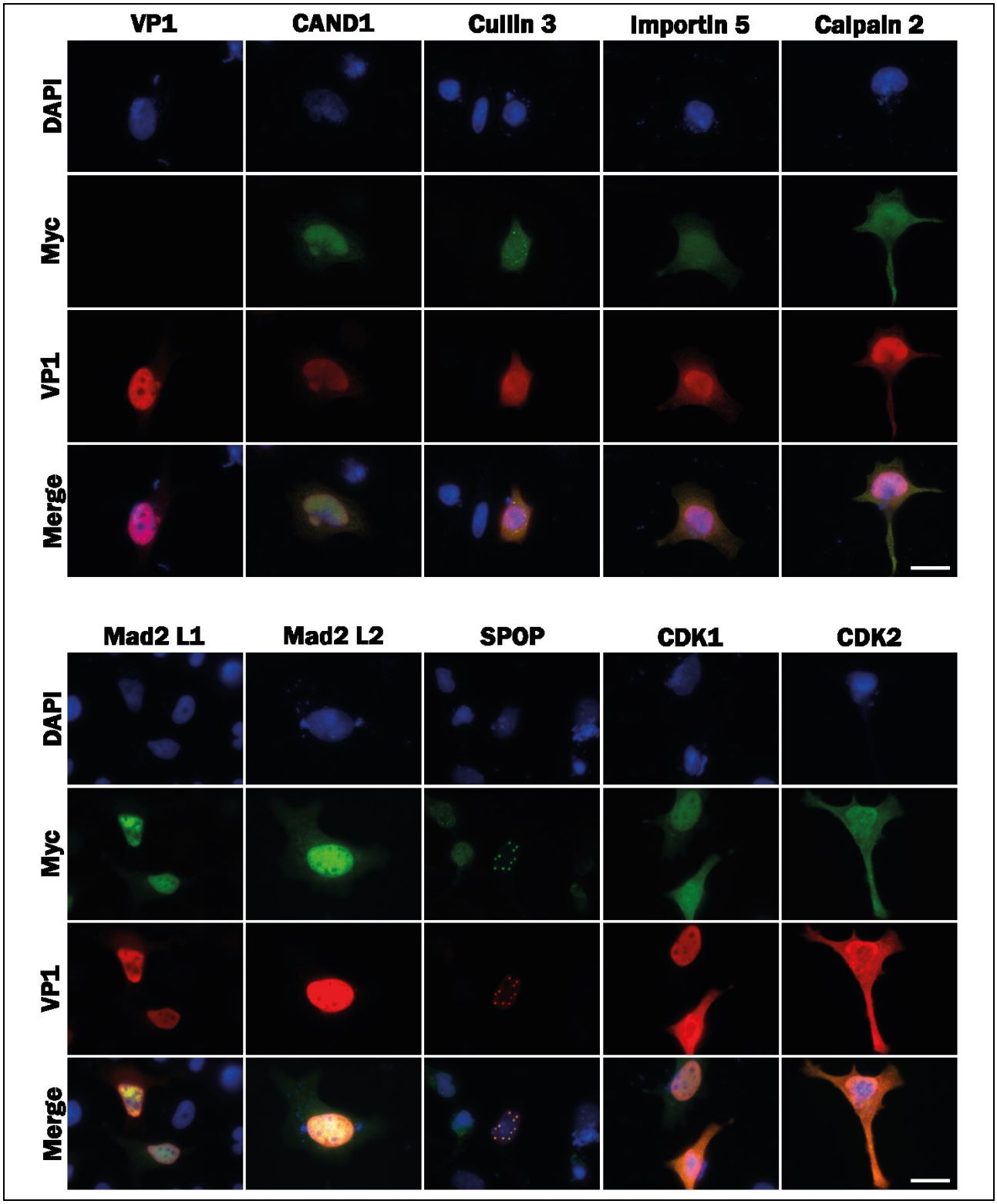

Figure 16: Analysis of the cellular localization of AAV2 VP1 and potential interaction partners after co-expression. VP1 was co-expressed in HeLa cells for 48h in combination with one of the putative interaction partners, fixed and stained with fluorescently labelled secondary antibodies (VP1: Alexa fluor 594; Myc: Alexa fluor 488). DAPI was used to visualize the nucleus (blue). Primary antibodies: A69 (VP1), anti-myc (proteins of interest). The experiment was performed three times. Scale bar: 20 µm

To further confirm that the potential interaction between SPOP and VP1 was mediated by the VP1/2 N-terminus, co-localization between SPOP and VP3 was analyzed. VP3 is the shortest of the three capsid proteins and is lacking the unique N-terminus. Therefore, it can be considered as natural N-terminus truncation mutant and hence it should not localize into the speckles, if interaction is dependent on the presence of the VP1/2 N-terminus. HeLa cells were transfected with either of the constructs for 48h. Subsequently, cells were harvested and prepared for immunofluorescence. For the detection of the capsid proteins VP1 and VP3, the B1 antibody was used, which recognizes an epitope located at the C-terminus of VP1, VP2 and VP3. As observed before, VP1 was found in a speckled pattern when overexpressed in combination with SPOP. In contrast, VP3 showed a diffuse distribution all over the cell, which was not changed when SPOP was overexpressed. In total, 365 cells were imaged of which 80 were transfected with SPOP (22%). Out of these, 41 cells were co-transfected with VP3 (51%). In all cases, Vp3 and SPOP never co-localized. This result might indicate that the interaction between SPOP and VP1 was specific to VP1, and binding is supposed to occur at the VP1/2 N-terminus (**Figure 17**).

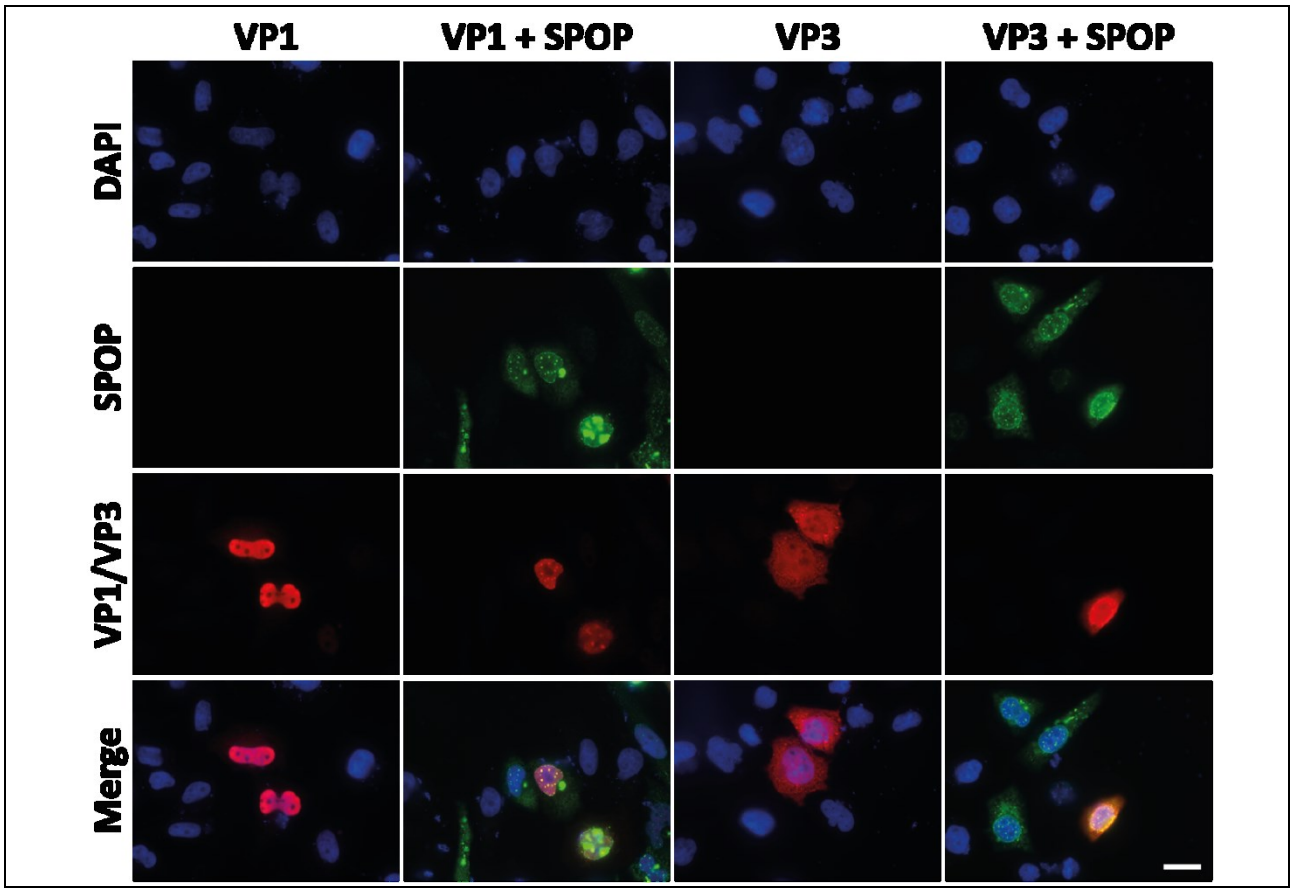

Figure 17: VP1 but not VP3 co-localized with SPOP after overexpression in HeLa cells. HeLa cells were transfected either with VP1 or VP3 alone or in combination with SPOP, fixed and stained with specific antibodies. Detection of the capsid proteins was done using the B1 antibody, SPOP was detected with the

anti-myc antibody. Visualization was done with fluorescently labelled secondary antibodies (VP1/3: Alexa fluor 594; Myc: Alexa fluor 488). DAPI was used to visualize the nucleus (blue). The experiment was performed in duplicates. Scale bar: 20 µm

To investigate whether the redistribution of VP1 into a distinct speckled phenotype when co-expressed with SPOP has an effect on the cellular localization of the other potential VP1 interacting proteins, a triple transfection of VP1, SPOP and each of the myc-tagged proteins was performed. If the proteins bind to the VP1 protein, they might co-localize with VP1 within the SPOP speckles. To be able to distinguish between the SPOP protein and the potentially interacting VP1 protein a non-tagged expression construct encoding for SPOP was transfected and the analysis was restricted to cells that showed the speckled phenotype of VP1, assuming that these cells were successfully co-transfected with the SPOP construct. Results are depicted in **Figure 18**. Under these conditions Mad2 L1, Cullin 3 and Calpain 2 were found to be localized in nuclear speckles that overlapped with the speckled VP1 phenotype, suggesting a specific interaction of these three proteins with VP1.

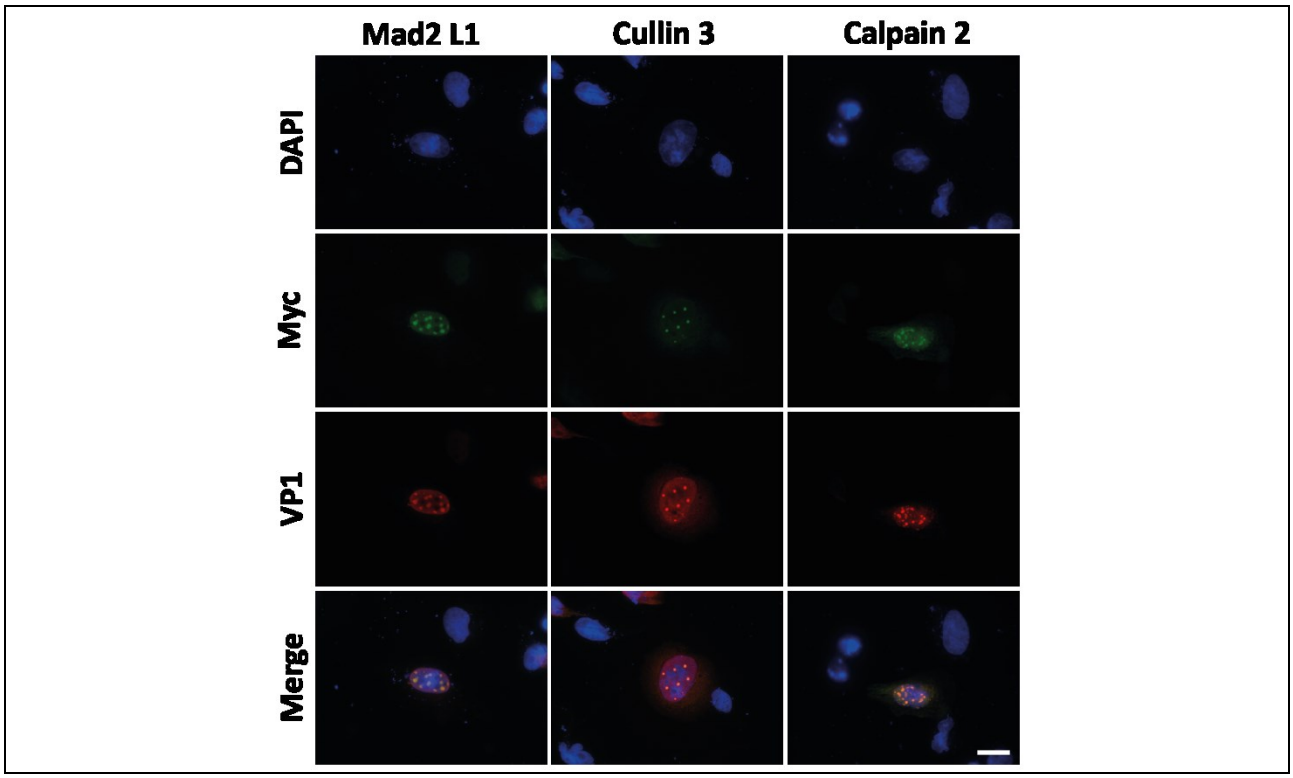

Figure 18: Analysis of the sub-cellular localization of VP1, Mad2 L1, Cullin 3 and Calpain 2 in the presence of SPOP overexpression. HeLa cells were transfected with VP1 (red), un-tagged SPOP and myc-tagged constructs of Mad2 L2, Cullin 3 and Calpain 2 (green). Visualization was done with fluorescently labelled secondary antibodies (VP1: Alexa fluor 594; Myc: Alexa fluor 488). DAPI was used to stain the nucleus (blue). Primary antibodies: A69 (VP1), anti-myc (proteins of interest). The experiment was performed twice. Scale bar: 20 µM

Taken together, the immunofluorescence data confirmed the interaction between VP1 and Mad2L1, SPOP, Cullin 3 or Calpain 2, respectively. A summary of the validation and the characterization data of the identified proteins and AAV2 VP1 is listed in **Table 3**.

Table 3: Summary of the results of the experiments to confirm the interaction of the identified host cell proteins with the AAV2 VP1/2 N-terminus

	Yeast-two hybrid*	MS	Co-IP	Co-localization
Cell-cycle				
Calpain 2	-	+	+	+
CDK1	-	+	+	-
CDK2	-	+	+ ‡	-
Mad2 L1	+	-	-	-
Mad2 L2	+	-	+	+
Nuclear pore/import				
Importin 5	-	+	tbd	-
Ubiquitination				
Cullin 3	-	+	+	+
CAND1	-	+	tbd	-
SPOP	+	+	+	+

Shown are the results of a number of experiments to determine AAV2 VP1/2 N-terminus interacting host cell proteins. Experiments performed were yeast-two hybrid *(Popa-Wagner 2011)*, mass-spectrometry, co-immunoprecipitation following co-expression and analysis of co-localization within the cell. '+': results suggest interaction with VP1/2 N-terminus; '-': results did not confirm a specific interaction with VP1; tbd: results were inconclusive, requires further analysis. MS: mass-spectrometry; tbd: to be determined. ‡: also detected in the negative control. *Performed by *Popa-Wagner (2011)*

As SPOP was identified and confirmed with all approaches, the following experiments aimed at further analysis and characterization of its function with regard to AAV2 infection. Also, the isolation of Cullin 3 and CAND1, two proteins involved in the ubiquitin-proteasome system (1.5.1), indicated the involvement of the UPS in the AAV2 life-cycle, hence providing a promising approach for further studies.

4.3 Influence of SPOP on the AAV2 life-cycle

4.3.1 Biological function of SPOP, CAND1 and Cullin 3

To get an idea on the biological function of SPOP, CAND1 and Cullin 3 within the cell, a *functional protein association network analysis* using the String 9.1 database (www.string-db.org) was performed. String 9.1 allows the analysis of protein interactions on the basis of known data, but also on bioinformatics prediction. It includes information about direct physical interactions and also indirect functional interactions that are derived from published data, high-throughput screens, co-expression studies or genomic context. To date, this database comprises more than five million proteins from 1133 different organisms. For the candidate VP1 interaction partners, the database revealed a direct interaction between SPOP and Cullin 3, as well as between Cullin 3 and CAND1 on the basis of published data (**Figure 19 A**). In agreement with this, previously published data showed that these proteins form an ubiquitination machinery complex called Cullin-RING-ligase 3 (CRL3, 1.5.1; reviewed in *Genschik et al. (2013)*). In this complex, neddylated Cullin 3 acts as scaffold, binding a RING E3 ligase at its C-terminus, which in turn recruits an ubiquitin-loaded E2 enzyme, mediating ubiquitin transfer to a substrate. On the N-terminus, Cullin 3 binds a specific substrate recognition protein that recruits substrates for ubiquitination. SPOP has been postulated to act as Cullin 3-specific substrate recognition protein, binding Cullin 3 via a BTB domain (1.5.2). In contrast, CAND1 binds to de-neddylated Cullin 3 in order to mediate substrate recognition protein exchange. Transferring this model to the results obtained with the TAP-tag screen (4.1.3, **Table 1**), VP1 might be recruited by SPOP to Cullin 3 through a direct interaction, in order to be ubiquitinated. This hypothesis would propose that in the course of the TAP-tag procedure a complex of VP1-SPOP-Cullin 3 was isolated. During substrate recognition protein exchange, intermediate states of Cullin 3, the substrate recognition protein (SPOP) and CAND1 can potentially occur. This further leads to the hypothesis that during turnover of VP1 in the TAP-tag experiment these intermediate states were present, because of the purification and detection of CAND1. A simplified summary of this model is shown in (**Figure 19 B**).

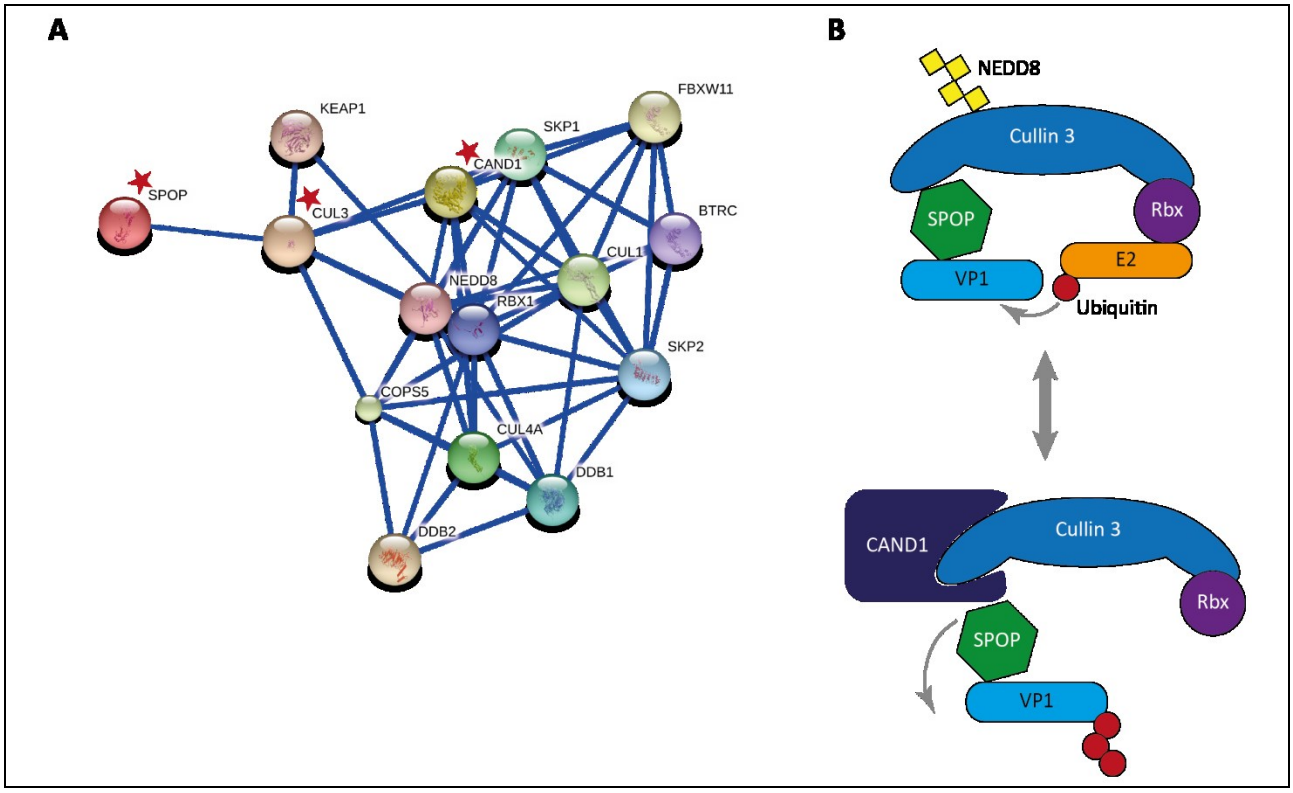

Figure 19: Biological function of SPOP, CAND1 and Cullin 3. A String 9.1 analysis revealed a direct interaction between SPOP and Cullin 3, as well as CAND1 and Cullin 3 (marked with asterisks). String 9.1 parameters: Confidence view, confidence interval of 0.7. **B** Proposed schematic model of the Cullin-RING ligase 3. Upper panel: Neddylation of Cullin 3 converts it in its active state. Cullin 3 recruits an ubiquitin-loaded E2 enzyme via its bound RING E3 ligase (Rbx) to mediate ubiquitination of substrates, recruited through SPOP. Lower panel: Inactive Cullin 3 (de-neddylated). CAND1 binds to Cullin 3 mediating substrate recognition protein exchange. SPOP, as well as the ubiquitinated substrate dissociate from Cullin 3. Rbx: RING-box protein

4.3.2 VP1/2 N-terminus sequence alignment reveals a putative SPOP binding motif

The fact that SPOP mediates the recruitment of certain substrates to the CRL3 complex suggests that these substrates must bear a specific SPOP recognition sequence. Analysis of binding properties of previously described SPOP substrates, identified a 5-residue SPOP binding consensus (SBC) motif, consisting of a non-polar – polar – serine – serine/threonine – serine/threonine amino acid sequence (position 1 -5: φ – π – S – S/T – S/T; *Zhuang et al. (2009)*). If the model described above accounts for VP1, VP1 should possess an SBC motif within its amino acid sequence. To determine, if SPOP binding of AAV VP1 occurred via an SBC motif, the VP1 sequences of the 13 described serotypes were aligned and screened for the published SBC motif. Interestingly, all serotypes except for AAV5 and 12 (the two least conserved serotypes among AAV) revealed a 5-residue sequence of proline – aspartate – serine – serine – serine/threonine (Pro Asp Ser Ser Ser/Thr), representing a putative SBC motif in their VP1/2 N-terminus, suggesting that interaction with SPOP might occur at this site

(**Figure 20**). Different to the other serotypes, AAV9 displayed an alanine at position 5 of the putative SBC motif. Depending on the AAV serotype the identified SBC motif is located at amino acid position 152 – 156 or 153 – 157 within VP1. Further screenings of the VP1 sequence excluded the presence of any additional similar motifs, indicating this motif to be the only site SPOP might interact with. Albeit AAV9 harbors an alanine at position 5 it still might resemble a functional SBC motif, given that SPOP was co-purified with AAV9 in the TAP-tag procedure (Table 1). The fact that AAV5 does not contain the putative SBC motif raised the question, whether SPOP could be identified in the TAP-tag with AAV5 or not. AAV5 was previously excluded from the TAP-tag procedure and analysis because transfection of the respective expression construct did not yield high expression levels (**Figure 8 B**). Nevertheless, new findings for the other AAV serotypes motivated to perform the TAP-tag procedure, regardless of the low expression levels (**Figure 8 B**) and with the hope that the sensitivity of the subsequent mass-spectrometry analysis is sufficient to identify even very low amounts of a certain protein. However, the presence of AAV5 VP1 could not be detected and therefore further analysis is necessary to investigate this particular question (data not shown).

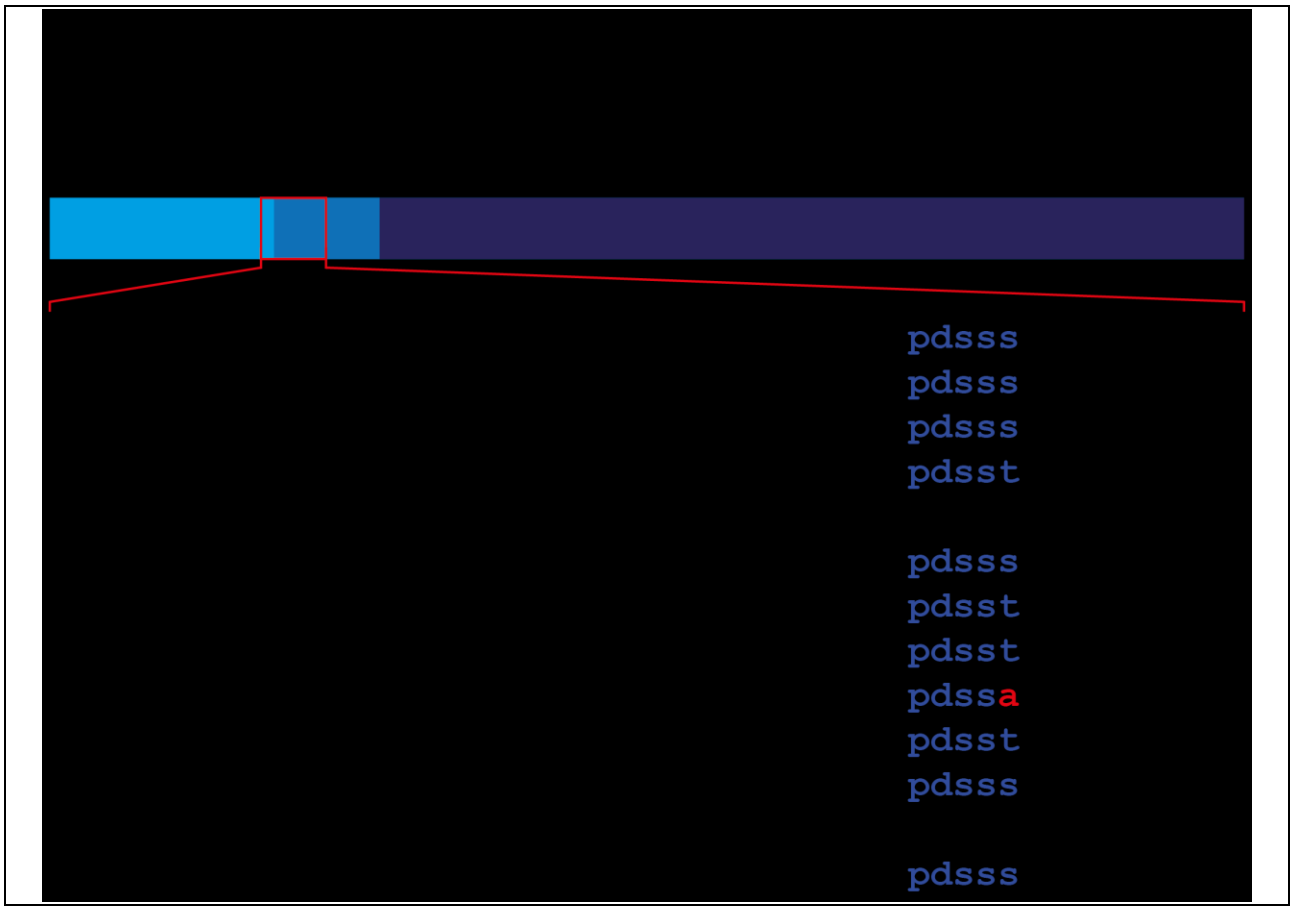

Figure 20: Identification of a putative SPOP binding motif within the VP1/2 N-terminus of AAV1-13. Sequence alignment of the VP1 proteins of the AAV serotypes 1-13 revealed a putative SPOP binding

consensus motif located within the N-terminus of VP1/2. The two least conserved serotypes did not comprise this region. φ: non-polar, π: polar, Ser: Serine, Thr: Threonine.

4.3.3 Site-directed mutagenesis of the putative SBC motif

To determine whether the predicted SBC motif mediates the binding of VP1 to SPOP, different VP1 expression constructs with distinct mutations within this motif were generated. Using site-directed mutagenesis (3.2.4) five different mutants were generated that either encoded for a one or two amino acid exchange (**Figure 21 A**). For four of these mutants the original amino acid(s) (aa 153 – 157) were exchanged for alanine, while for the other, aspartate was replaced by glutamate (D154E), to retain SPOP binding, as both amino acids have similar chemical properties. The mutations were verified by DNA sequence analysis and the constructs were subsequently used for analysis of SPOP binding by co-IP, co-localization, as well as ubiquitination. In addition to the mutations in the VP1 expression construct, these mutations were also introduced into a vector that was used for the generation of intact particles. The reporter viruses carrying these mutations were subsequently used for the analysis of the transduction in untransfected cells, as well as in cells overexpressing SPOP and SPOP-depleted cells (4.5). These experiments (described in the following paragraph) were performed to examine the influence of SPOP on VP1 during co-expression of both proteins but also in the viral context, resembling the infection process.

4.4 Analysis of the interaction of SPOP and the VP1 SBC mutants

4.4.1 Co-immunoprecipitation of SPOP and the VP1 mutants

Analysis of the SPOP binding behavior with the SBC mutants was approached using co-IP. As SPOP expression was at low levels, co-IP was performed in the presence of 2 µM MG132 (4.2.1). The VP1 protein levels for the wild-type as well as for the mutants in the input were low. After immunoprecipitation using a VP1-specific antibody to bind and concentrate the protein, VP1 could be detected but the levels were still low (**Figure 21 B**). However, SPOP precipitation was successful for all of the mutants, but differences in the signal intensities were observed. The AAV2 VP1 PESSS bound SPOP at least as efficient as AAV2 wild-type, indicating that the aspartate to glutamate exchange did not influence the binding of SPOP. Even though the VP1 expression for PESSS was the weakest, a strong SPOP band was detected. As the negative control (bluescript + SPOP; see materials 2.2.1) did not show a SPOP-specific band, this result suggested a VP1-mediated immunoprecipitation. The lower levels of SPOP detected in the IP with the other mutants might be a hint on the interruption of the SPOP binding due to the mutations.

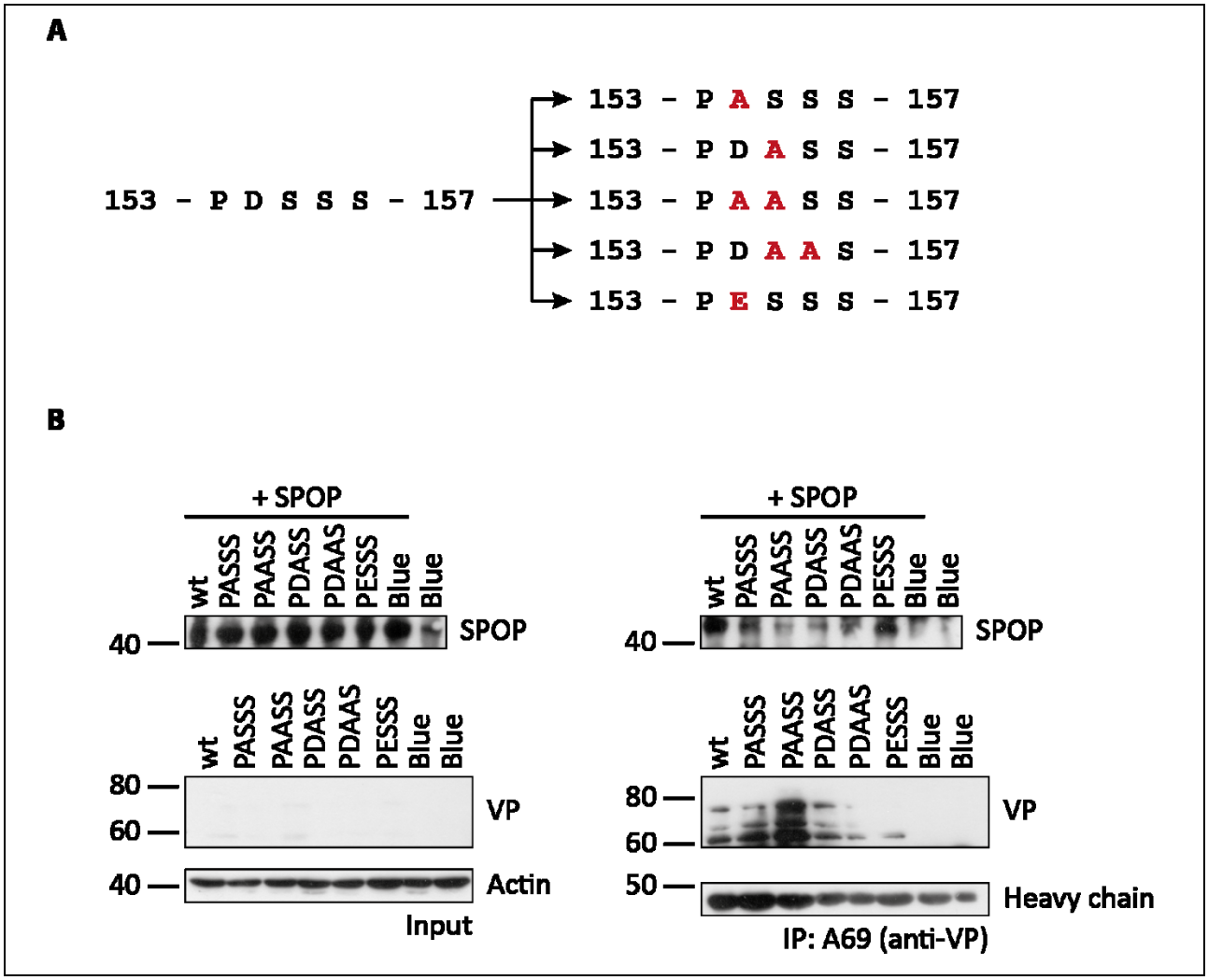

Figure 21: Analysis of the binding capability of VP1 SBC mutants to SPOP. A Amino acid exchanges in the putative SBC motif within the N-terminus of VP1 were introduced by site-directed mutagenesis resulting in two double mutants and three single mutants (mutations are marked in red; P1 = 153, P5 = 157). **B** Co-IP of SPOP with the VP1 SBC mutants. The SPOP expression construct was transfected together with one of the VP1 SBC mutant constructs into HeLa cells ($6*10^6$ cells/IP). After 48h of incubation, cell lysates were prepared and VP1 was immunoprecipitated with A69. Co-IP was analyzed by western blot using 10 µl of the cell lysates. VP1 expression in the input was very low, due to technical issues of the western blot, as previous experiments demonstrated that the amino acid exchanges in the putative SBC motif did not interfere with the VP1 expression. SPOP was detected via its myc-tag. Controls: bluscript and SPOP; bluescript alone. Antibodies: A69 (IP), anti-myc, anti-VP (B1) anti-actin

4.4.2 Co-localization of SPOP and the VP1 SBC mutants

To further analyze the influence of the mutations on SPOP binding co-localization studies by indirect immunofluorescence were performed. SPOP was co-expressed in HeLa cells in combination with one of the single VP1 SBC mutants and subsequently stained with fluorescently labelled antibodies. Image analysis was done using confocal microscopy.

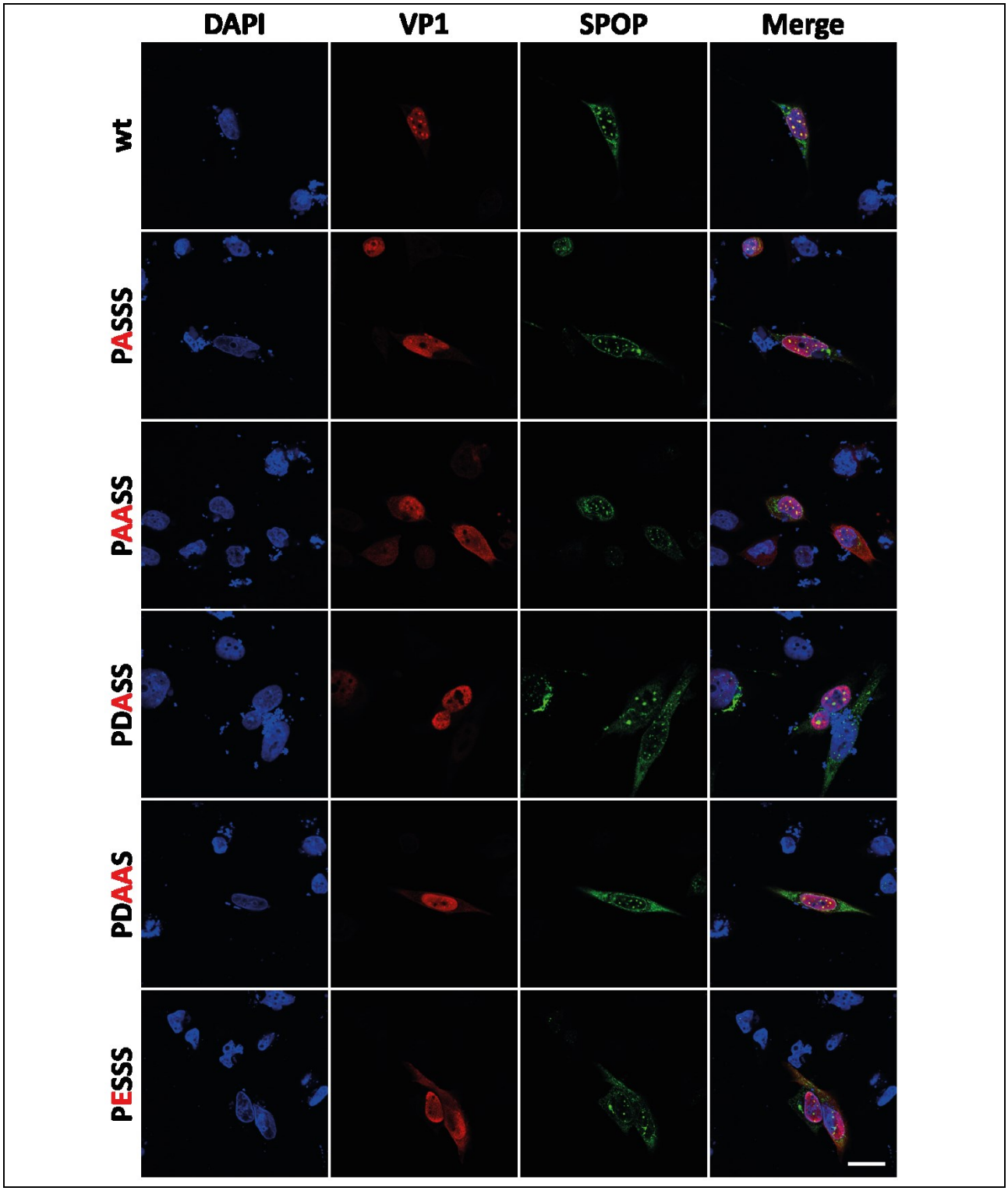

Figure 22: Analysis of the subcellular localization of SPOP and the VP1 SBC mutants after co-expression. HeLa cells were co-transfected with the SPOP expression construct (green) and one of the five different VP1 SBC mutant expression constructs, as well as VP1 wild-type (red) and stained with fluorescently labelled secondary antibodies (VP1: Alexa fluor 594; SPOP: Alexa fluor 488). As primary antibodies A69 and

an anti-myc antibody were used to detect VP1 or SPOP, respectively. DAPI (blue) was used to stain the nucleus. wt: wild-type. Scale bar: 20 µm

As can be seen in **Figure 22**, the AAV2 VP1 wild-type is located in speckles in the nucleus as described before (4.2.4), which co-localize with the speckled pattern of SPOP, indicating an interaction between these two proteins. The VP1 SBC mutants however only partially showed this distinct pattern. In some cells speckles were detected in the VP1 pattern that were co-localizing with the speckles formed by SPOP, but the level of the speckles was highly reduced. Also, cells showing the VP1 mutant proteins in speckles still showed a highly diffuse nuclear staining, indicating a weaker interaction between SPOP and VP1. Interestingly, the PESSS mutant did not show distinct speckles as it was observed for the wild-type, even though the mutation was supposed not to interrupt SPOP binding at high levels (**Figure 22**).

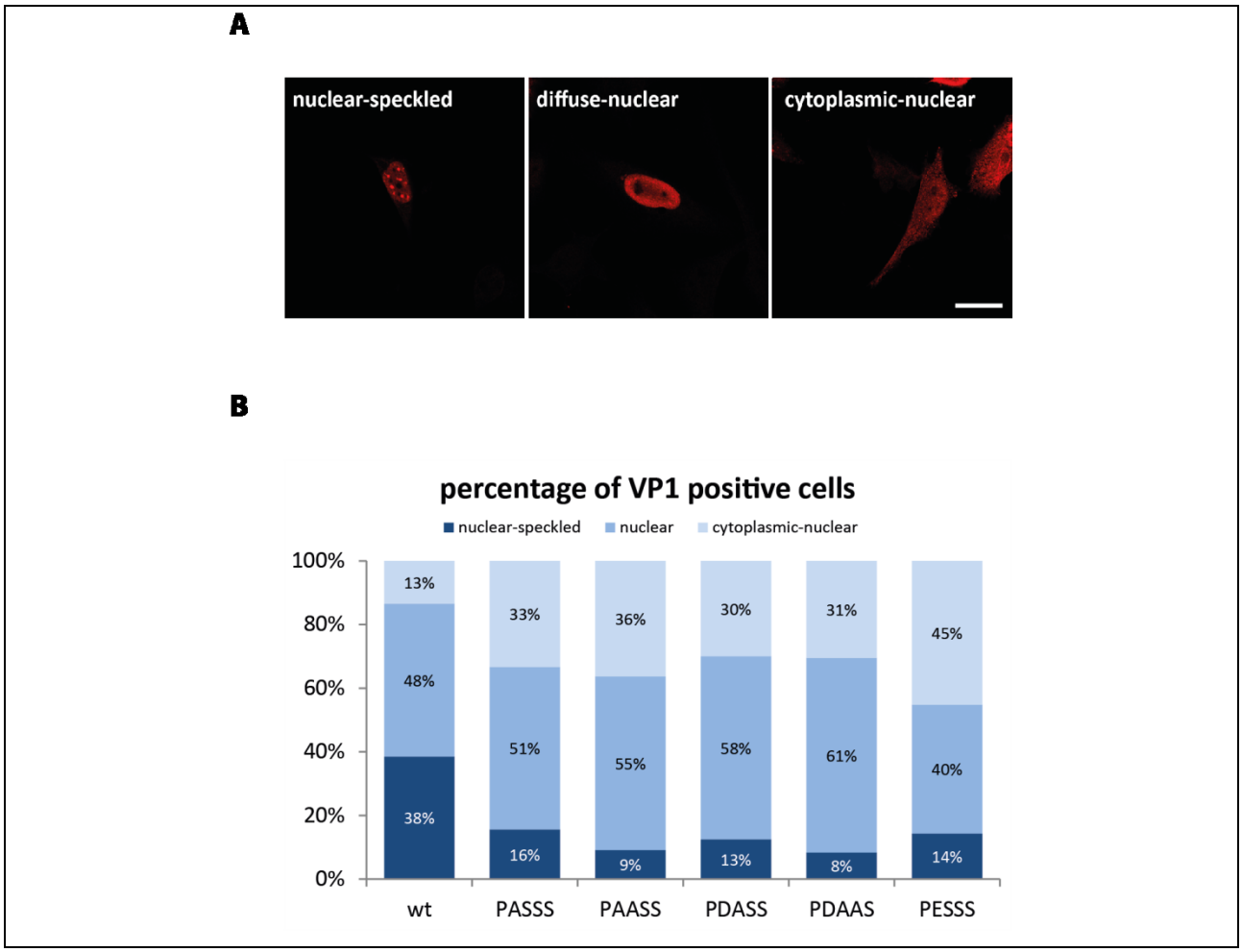

Figure 23: Abundance of different categories of VP1 distribution within the cell after co-expression with SPOP. A The observed subcellular distribution patterns for VP1 wild-type and the VP1 SBC mutants after co-expression with SPOP were categorized as follows: nuclear-speckled, nuclear-diffuse and cytoplasmic-nuclear. Scale bar: 20 µm **B** 129-135 individual cells co-expressing VP1 wild-type or one of the VP1 SBC

mutants with SPOP were counted and categorized according to the patterns described in A. The representation of the distinct distribution pattern categories is depicted in percent for each VP1 construct. The experiment was performed four times.

Counting of VP1 positive cells allowed calculating statistics on three different phenotypes of the VP1 distribution. These phenotypes were: nuclear speckles, diffuse-nuclear and cytoplasmic-nuclear (**Figure 23 A**). In 38% of the cells VP1 showed a nuclear speckled for the wild-type construct, followed by 13% – 16% for the single mutants (PASSS, PDASS and PESSS) and 8% – 9% for the two double mutants PAASS and PDAAS. The main pattern for all of the constructs was the diffuse-nuclear phenotype with 48% – 61% of the counted cells. The cytoplasmic-nuclear phenotype for the wild-type was very rare (13%), whereas for the mutants it was determined to be between 30% – 36% reflecting the normal average (~30%) as it was postulated for AAV2 wild-type when overexpressed in cells alone *(Popa-Wagner 2011)*. The only exception among the mutants was the PESSS mutant, showing a higher cytoplasmic-nuclear phenotype (45%) than the diffuse-nuclear phenotype (40%; **Figure 23 B**). Together, these results showed differences in the cellular distribution among the different VP1 SBC mutants. However, if this effect comes from a disturbed interaction with SPOP, could not be concluded.

4.4.3 Ubiquitination of newly synthesized VP1 proteins

SPOP is involved in the ubiquitin-proteasome system, mediating the turnover of various proteins (1.5.2). To analyze the ubiquitination status of newly synthesized wild-type VP1 compared to the VP1 SBC mutated forms, HeLa cells were co-transfected with a construct encoding for HA-tagged ubiquitin and one of the VP1 mutant constructs or the wild-type construct and incubated for 48h. Afterwards cell lysates were prepared and VP1 was immunoprecipitated using the VP1/2-specific A69 antibody coupled to sepharose beads. Ubiquitinated VP1 proteins could be detected via the HA-tag of the overexpressed ubiquitin. Overexpression of the ubiquitin was detected with bands covering the entire molecular weight range, indicating polyubiquitination of various proteins (**Figure 24**, upper left panel). High molecular weight signals in the immunoprecipitation blot were detected when stained with the HA-specific antibody (**Figure 24**, upper right panel). As this signal could not be detected for the negative control, where VP1 was not expressed (**Figure 24**, upper right panel, lane 12), these results suggest the ubiquitination of the VP1 proteins. Albeit no significant differences in the ubiquitin levels were detected for the VP1 wild-type and the VP1 SBC mutants, it seemed that the wild-type VP1 showed minimally reduced levels of ubiquitin; however this might be due to technical issues (**Figure 24**, upper right panel lane 1). Precipitation of VP1 was demonstrated, but if capsid ubiquitination occurred, one would expect to also see high molecular weight signals in the VP1 blot. In these experiments only the characteristic VP1 band was observed, but also very high

levels of degradation, indicating that ubiquitination might have occurred, but VP1 was immediately degraded by the proteasome. However, a repetition of this experiment with the addition of MG132 to avoid proteasomal degradation of high-molecular weight aggregates did not result in signals for VP1 which might account for accumulated ubiquitinated capsid proteins, but rather showed a similar pattern as observed in the previous experiment (data not shown). Together, this experiment suggests that a fraction of VP1 seems to be ubiquitinated but ubiquitination was not disturbed by the introduction of the amino acid exchanges. This further indicates that ubiquitination occurs independently of the identified motif.

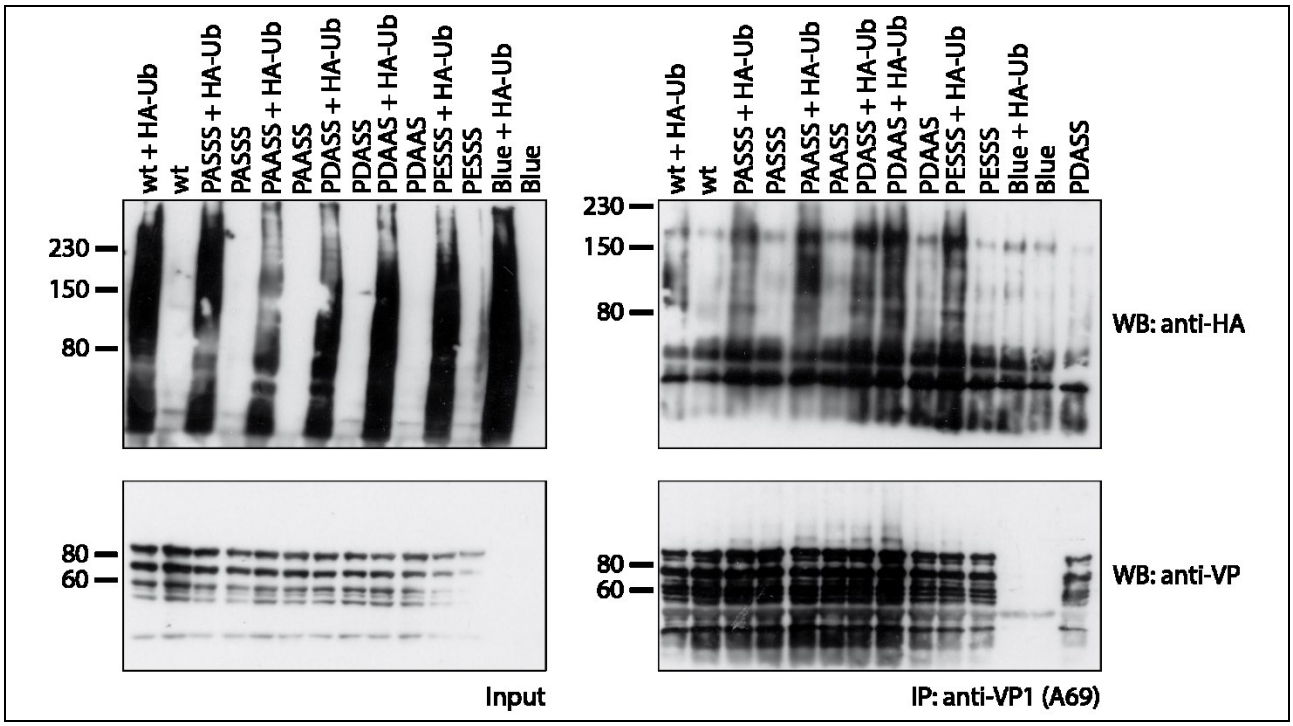

Figure 24 Ubiquitination of newly synthesized VP1, wild-type and mutants. The VP1 constructs (wild-type and mutants) were co-expressed with HA-tagged ubiquitin in HEK293TT cells ($4*10^6$ cells/construct). VP1 was immunoprecipitated using the VP1/2-specific antibody A69 (bound to sepharose beads) and probed for ubiquitination with an HA-tagged antibody in a western blot. Polyubiquitination was detected as smears on the western blot. VP1 was precipitated but ubiquitinated VP1 smears were not detected. Left panels: input, right panels: co-IP. Blue: bluescript, control vector.

4.5 Analysis of SPOP and the VP1 SBC mutants during viral infection

4.5.1 Generation of reporter viruses carrying mutations in the VP1 sequence

The experiments above demonstrated clear differences in the binding, as well as in the co-localization of SPOP between wild-type VP1 and the five VP1 mutants. This suggests that SPOP binding might be mediated by the identified SBC motif. To determine its influence on AAV2 infection, AAV2 reporter viruses displaying the above described mutations in their VP1 sequence and carrying renilla luciferase as reporter gene were generated. The aim was to investigate whether SPOP can be considered as host restriction factor (HRF) or host dependence factor (HDF). Generation of the viral particles was done by transfecting the VP1 constructs, adenoviral helper genes and the luciferase reporter gene into HEK293TT cells followed purification on an iodixanol step-gradient (3.5.3). Quantification of the viruses was performed by Barbara Leuchs, DKFZ using real time PCR, probing the CMV promoter of the packaged genome (3.5.4). As every particle only encapsidates one genome, the quantified genome number represents the number of intact and infectious viral capsids. **Table 4** shows the viral titers of all the various AAV2 productions. Packaging and production of all the viruses was successful, as they all showed titers within the average of a normal production of around 10^{11}–10^{12} viral genomes/ml. This further suggested that none of the mutations did interfere with capsid assembly or genome packaging, facilitating the use of these viruses for further experiments. Transduction experiments were performed in different contexts. The first approach aimed to analyze the ability of the SBC mutated reporter viruses to be able to transduce normal cells (4.5.2), while the other transduction experiments analyzed the influence of SPOP on transduction when overexpressed (4.5.3) or when knocked-out (4.5.4).

Table 4: Genome titers of the generated reporter viruses

Mutant	Titer (viral genomes/ml)
PDSSS (wt)	1,90E+11
PASSS	2,13E+11
PAASS	8,70E+11
PDASS	2,23E+11
PDAAS	3,51E+11
PESSS	1,80E+11

Viral genomes were quantified using real time PCR. Numbers represent viral genomes per ml.

4.5.2 Effect of the SPOP VP1/2 N-terminus interaction on the transduction of HEK293TT and HEK293 FlpIn™ cells

To analyze whether the generated reporter viruses (4.5.1) were able to transduce tissue culture cells, two different cell lines were infected at a multiplicity of infection (MOI) of 1000 with all of the different viruses. The cell lines used were HEK293TT cells and HEK293 FlpIn™ cells. The latter can be used for the generation of a cell line stably expressing a gene of interested under the control of a doxycycline-inducible promoter. Transduction was carried out for 24h, following cell lysis and measuring luciferase expression in the cell lysates. All viruses were able to transduce both of the cell lines however; clear differences in the transduction efficiencies were detected. The results of this experiment are summarized in **Figure 25**. Consistently among all different viruses was a slightly higher transduction rate of the HEK293 FlpIn™ cells. Comparison of the different viruses revealed that wild-type transduced with the highest efficiency in both cell lines. Strikingly, the two double mutants, PAASS and PDAAS, showed the weakest transduction, indicating a strong influence of the mutations on the AAV2 life-cycle. As expected, the PESSS mutant transduced with the highest efficiency among the mutants (showing 50% activity of wild-type), further suggesting that the aspartate to glutamate exchange did not interfere with the infection. The two remaining single mutants, PASSS and PDASS, transduced at similar levels with an efficiency between 5,8% and 13.1% compared to wild-type, depending on the mutant and the cell line (**Figure 25 B**). These results suggested that the identified motif seemed to be essential for the infection. However the influence of SPOP is not proven yet. Remarkably, the position of the exchanged amino acid was not important, as the D154A mutant, as well as the S155A mutant showed both similar levels of reduction in transduction efficiency, even though the serine at position three of the identified motif was postulated to be essential, while position four of the SBC could either be a serine or a threonine. AAV vectors carrying the amino acid exchanges PAASS or PDAAS both transduced with comparable efficiencies.

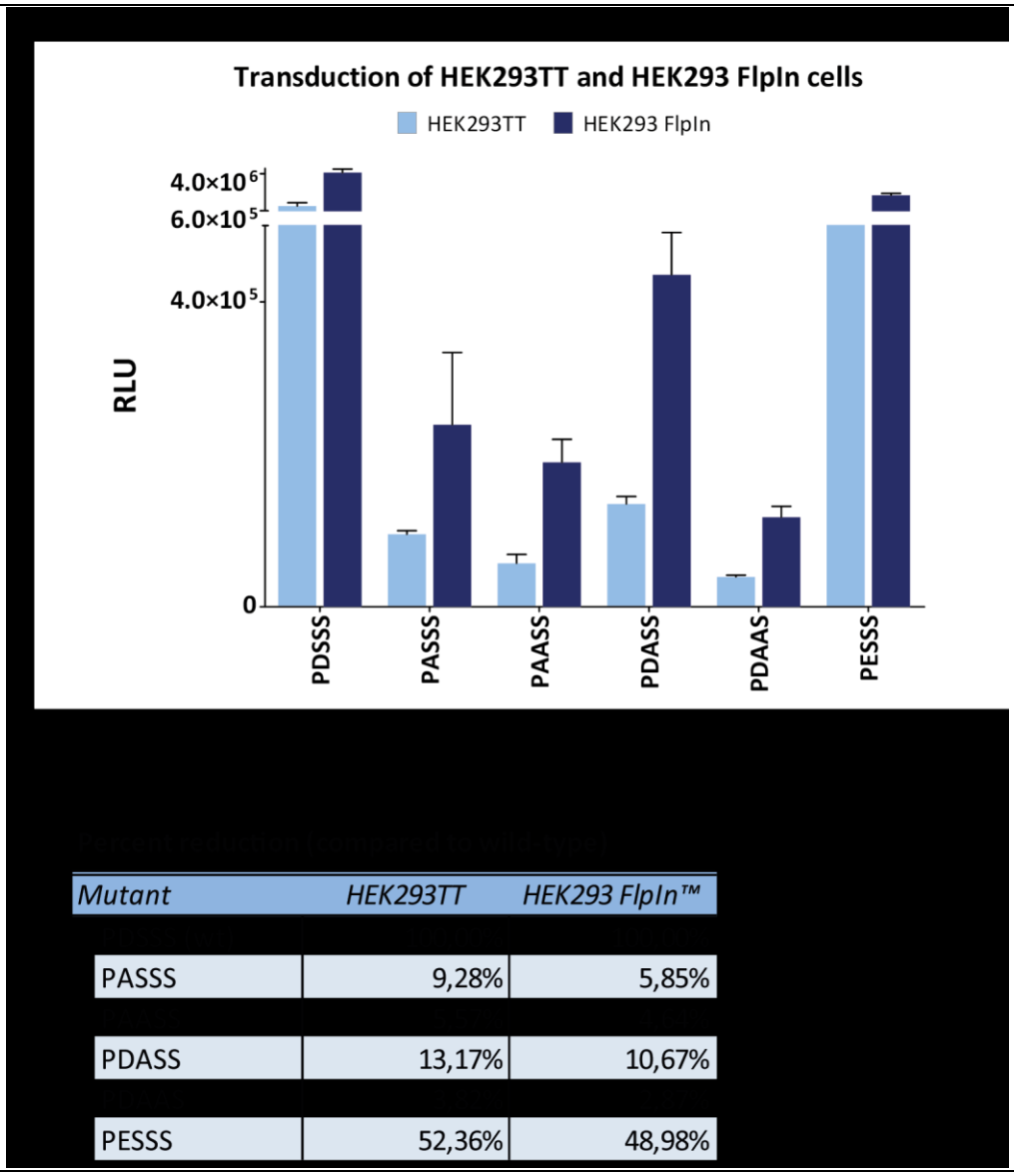

Mutant	HEK293TT	HEK293 FlpIn™
PASSS	9,28%	5,85%
PDASS	13,17%	10,67%
PESSS	52,36%	48,98%

Figure 25: Influence of the SBC region within the VP1 protein on the transduction of HEK293TT and HEK293 FlpIn™ cells with AAV2 reporter viruses. A HEK293TT and HEK293 FlpIn™ cells were transduced with AAV2 wild-type and AAV2 VP1 SBC mutants at an MOI of 1000. 24h post-transduction, cells were harvested and lysed. Renilla luciferase expression in the cell lysates was measured at the 1420 Multilabel Counter Viktor3. RLU: relative light units. The experiment was performed in triplicates, error bars represent the standard deviation. **B** Transduction efficiencies between wild-type and the VP1 SBC mutant viruses in comparison to the wild-type transduction.

4.5.3 Influence of SPOP over-expression on AAV transduction efficiency

As the different mutations in the VP1 gene led to a strong decrease in the transduction efficiencies of the corresponding viruses (**Figure 25 A**), further experiments aimed to examine whether SPOP is involved during AAV2 infection and if, in which context. For that, a cell line stably expressing SPOP

under the control of a doxycycline-inducible promoter was generated, which facilitated to specifically switch on the expression of SPOP within the cell. The generation of the stable SPOP cell line was done using the above mentioned HEK293 FlpIn™ parental cell line. These cells were modified to contain a specific genomic location a Flp-recombination target, allowing the integration of a gene of interest by Flp recombinase-mediated DNA recombination *(O'Gorman et al. 1991)*. The HEK293 FlpIn™ cells were transfected with a construct encoding for SPOP (2.2.1), flanked with Flp recombination sites and cultured under the selection of hygromycin B until single colonies were grown (3.1.7). Ten of these colonies (K1-K10) were cultured and tested for SPOP expression. Out of these, the two clones K1 and K5 showed a very strong expression of SPOP after induction with doxycycline (data not shown). K1 and K5 were further analyzed to find the minimum concentration of doxycycline that led to SPOP overexpression. A titration with different doxycycline concentrations for 48h resulted in a minimum concentration of 0.25 µg/ml doxycycline to be sufficient for the induction of high SPOP levels (**Figure 26 A**). However, as can be seen in **Figure 26 A**, the integration of the SPOP gene into the HEK293 FlpIn™ cell line led to a leaky expression of SPOP even in the absence of doxycycline.

For the analysis of the influence of SPOP on AAV2 transduction, both isolated clones (K1 and K5) were used. These cells were seeded in the presence of 0.25 µg/ml doxycycline for 48h, to overexpress SPOP, and subsequently the cells were infected with AAV2 wild-type, or one of the AAV2 VP1 SBC mutants at an MOI of 1000. Cells were harvested 24h post-transduction and the expression of renilla luciferase in the lysates was measured. As a control, un-induced cells were used. The pattern of the transduction efficiencies that was observed in this experiment reflected the result from the initial transduction experiment using HEK293TT and HEK293 FlpIn™ cells (**Figure 25**). AAV2 wild-type showed the highest transduction, followed by the PESSS mutant. The other two single mutants transduced at comparable levels among each other, but at reduced levels compared to wild-type, as observed in the first experiment. The lowest transduction was measured for the two double mutants. Albeit the expression of SPOP was induced in both clones, differences of the transduction between un-induced and induced cells were not detected for the wild-type for the VP1 SBC mutants (**Figure 26 B**). Also, the transduction efficiencies were in the same range as for the parental HEK293 FlpIn™ cell line tested above (**Figure 25 A**) although the SPOP levels in the un-induced K1 and K5 cell lines were elevated. This might suggest that overexpression of SPOP does not affect the infection ability of AAV2, and that the endogenous levels of SPOP might already be sufficient for its function on AAV2.

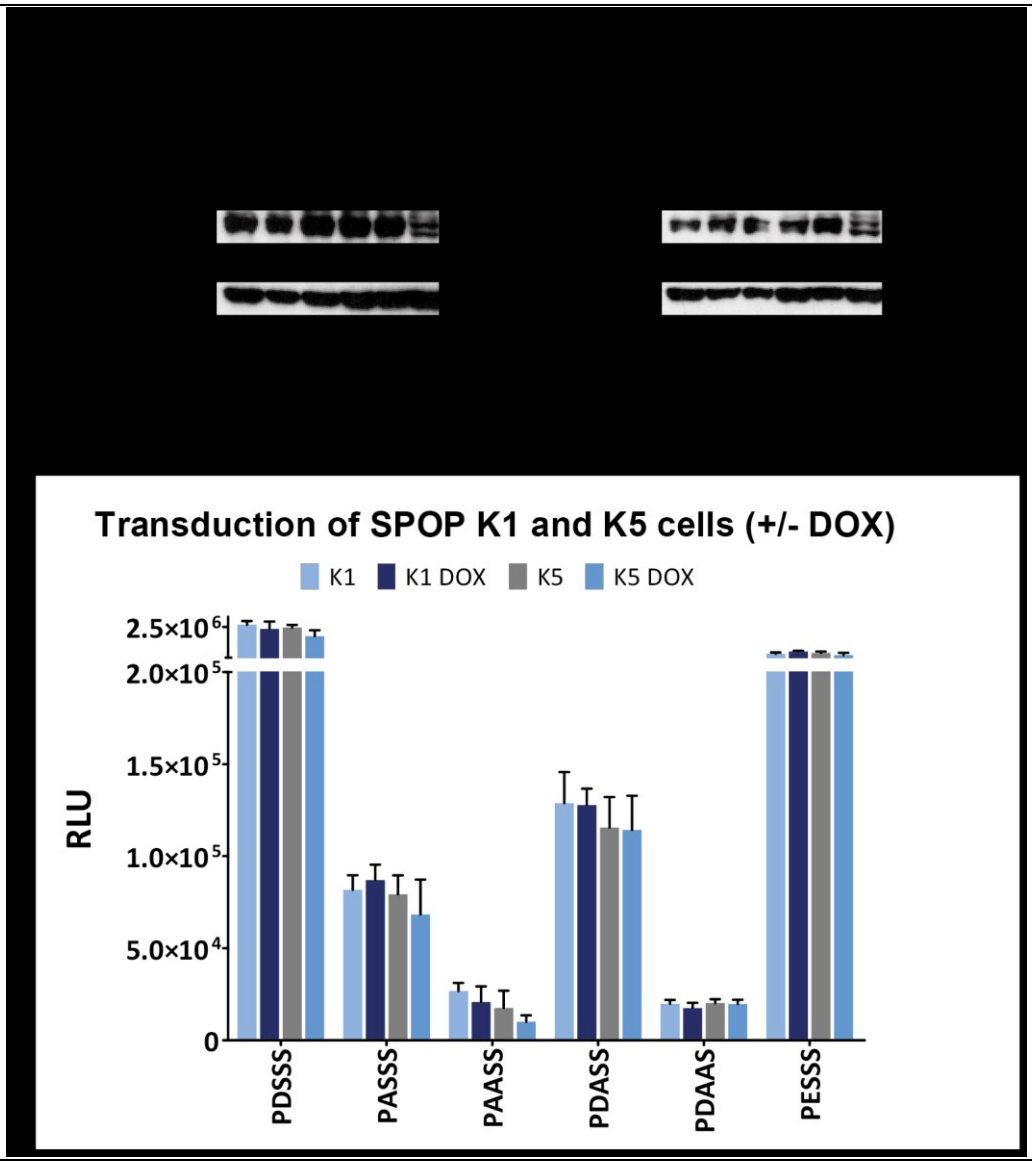

Figure 26: Transduction efficiency of the AAV2 wild-type and the AAV2 VP1 SBC mutant viruses in SPOP overexpressing cells. A Titration of doxycycline to determine the minimal concentration that induces SPOP expression in K1 and K5. Cells were treated with different concentrations of doxycycline (ranging from 2 – 0.25 µg/ml) for 48h and SPOP expression was analyzed by western blotting. **B** Induced and un-induced K1 and K5 cells were transduced with AAV2 wild-type or one of the VP1 SBC mutant reporter viruses for 48h. Renilla luciferase expression in the cell lysates was measured 24h post-transduction. The experiment was performed in triplicates; error bars represent the standard deviation. DOX: doxycycline

4.5.4 Influence of SPOP knockdown on AAV transduction

As overexpression of SPOP using the inducible stable SPOP cell line did not result in changes of the transduction efficiencies, AAV2 transduction in the absence of SPOP was analyzed. Hence, siRNA knockdown experiments were performed. For that, four different siRNAs targeting SPOP, as well as a control siRNA, not targeting any protein in the cell were used. Knockdown was performed at

conditions that were established with a so called cell death siRNA control. Successful transfection of cell death siRNA leads to a cytopathic effect. Under the established conditions, a cytopathic effect of approximately 90% was observed (data not shown). Knockdown was carried out for 48h in HeLa cells and these cells were subsequently infected with wild-type AAV2 or one of the VP1 SBC mutant reporter viruses for 24h. Cells were lysed and luciferase activity in the cell lysates was measured and analyzed. Luciferase values were normalized to the control transfection allowing calculating fold-change values among the different siRNAs. As depicted in **Figure 27 A**, the anti-SPOP #3 oligonucleotide led to a strong increase in AAV2 transduction, consistent for all of the vectors. However, the luciferase intensity among the different vectors varied. The strongest effect for example was observed for the PDAAS mutant with a fold-change of 7.22 (**Figure 27 A, table**). In contrast, AAV2 wild-type, as well as the PESSS mutant showed the lowest increase in transduction, however the fold-change was observed at similar levels among each other (1.69 and 2.05 for AAV2 wild-type and PESSS, respectively), supporting the hypothesis that the aspartate to glutamate exchange did not change the behaviour of AAV2, hence indicating that the effect of SPOP might be mediated by the identified SBC motif. A decrease of transduction was seen for the anti-SPOP #1 oligonucleotide consistent among all vectors. However this decrease was at negligible levels. The other two siRNAs used in this experiment did not show any effect. Transduction was slightly up- and down-regulated, but not in a consistent manner among the siRNAs themselves, hence these effects were not considered as siRNA-specific. Western blot analysis of the cell lysates proved a partial knockdown for all of the siRNAs (**Figure 27 B**). For the calculation of the percentage of SPOP knockdown, the signals were quantified using ImageJ (2.13). Calculated SPOP values were normalized with the respective actin values for each sample. Finally, normalized values were set into relation with the normalized values of the control siRNA transfection, allowing comparing the level of SPOP knockdown among the different samples (**Figure 27 B, table**). Interestingly, the strongest knockdown was observed for siRNA #4 with the PESSS mutant (~95%), but it did not show an effect on the transduction. Furthermore the overall SPOP level with this VP1 SBC mutant was highly reduced compared to the other VP1 SBC mutants. It needs to be determined, whether this observation was an artifact of the blot or a function by the mutant itself. Moreover, the knockdown with siRNA #3 was at comparable levels with the other siRNAs. However, as transfection with this siRNA was showing an effect on AAV transduction suggests that the observed effect was unspecific and hence probably mediated by off-target effects. But regarding the actin blots, strong differences between the single samples were detected which might indicate problems due to technical issues. Nonetheless, as the result from this experiment differed from the other transduction experiments in either untreated or SPOP overexpressing cells (**Figure 25**, **Figure 26**), and were consistent among three independent experiments, it seemed that down-regulation of SPOP at least partially influenced AAV transduction.

A

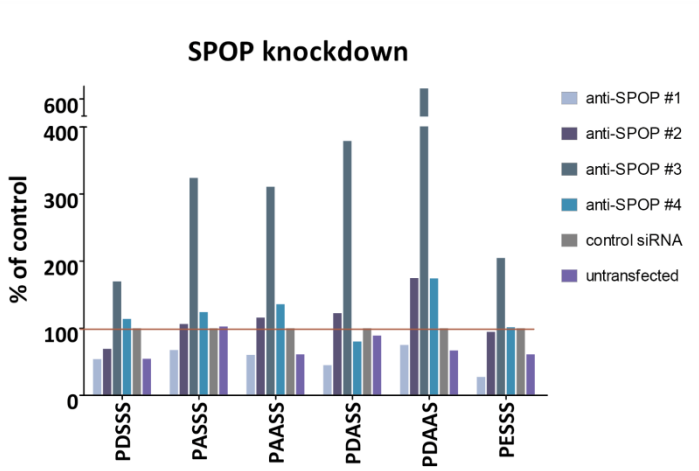

Fold change (compared to control transfection)

Vector	*siRNA*					
	anti-SPOP #1	**anti-SPOP #2**	**anti-SPOP #3**	**anti-SPOP #4**	**control siRNA**	**untransfected**
wt	0,54	0,69	1,69	1,14	1,00	0,54
PASSS	**0,67**	**1,06**	**3,24**	**1,24**	**1,00**	**1,03**
PAASS	0,60	1,16	3,11	1,36	1,00	0,61
PDASS	**0,45**	**1,22**	**3,79**	**0,80**	**1,00**	**0,89**
PDAAS	0,75	1,75	7,22	1,74	1,00	0,67
PESSS	**0,27**	**0,94**	**2,05**	**1,01**	**1,00**	**0,61**

B

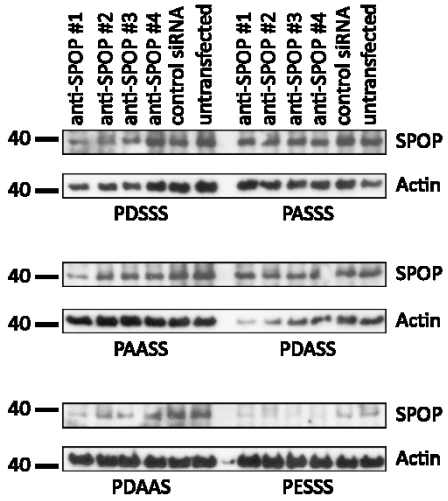

Quantification (percent of control transfection)

Vector	*siRNA*					
	anti-SPOP #1	**anti-SPOP #2**	**anti-SPOP #3**	**anti-SPOP #4**	**control siRNA**	**untransfected**
wt	76%	64%	60%	79%	100%	104%
PASSS	**63%**	**55%**	**81%**	**72%**	**100%**	**100%**
PAASS	37%	62%	67%	75%	100%	111%
PDASS	**473%***	**183%***	**99%**	**49%**	**100%**	**90%**
PDAAS	9%	37%	19%	43%	100%	80%
PESSS	**64%**	**60%**	**27%**	**5%**	**100%**	**200%**

Figure 27: SPOP knockdown following transduction with AAV2 and the VP1 SBC mutants. A Expression of endogenous SPOP was down-regulated using one of four SPOP-specific siRNAs, as well as a control siRNA. Knockdown was performed in HeLa cells for 48h following transduction of the cells with AAV2 wild-type or one of the VP1 SBC mutants at an MOI of 1000 for 24h. Luciferase expression in the cell lysates was measured and normalized to the control transfection to obtain fold-change values (table). Data represent three individual experiments, all performed in triplicates. **B** Western blot analysis of the SPOP knockdown. 10 µl of the cell lysates were analyzed by SDS-PAGE following western blot analysis. Signals were quantified using ImageJ (area under the curve) and normalized to the respective actin sample. To calculate the percentage of knockdown, normalized values were put into relation with the normalized control siRNA values. Values represent the percentage of remaining SPOP in the samples. Values marked with an asterisk do not represent the actual levels of the knockdown as the calculations might have been affected by the differences in the actin blot due to technical issues.

Taken together, the transduction experiments as well as the SPOP binding studies with the wild-type VP1 and the mutated VP1 SBC constructs suggested an influence of SPOP on the AAV2 life-cycle. Its effect and biological role for AAV2 will be discussed in the following.

5 Discussion

During the past years, AAV has gained great interest for the use as vector for gene therapy. The clinical value of AAV mainly derives from its lack of pathogenicity, low immunogenicity, replication deficiency and also its broad tropism, which altogether equip AAV to a unique viral vector superior to many others. However, despite its simple composition, the infection process is very complex. It comprises several steps that require interactions between the virus and cellular components, as well as structural rearrangements of the capsid to successfully infect the cell. Though AAV has been intensively studied during the past decades, some of the mechanisms during the infection are only partially or still poorly understood.

The AAV life-cycle begins with receptor attachment on the cell surface following receptor-mediated endocytosis, mediated by several pathways (reviewed in *Nonnenmacher and Weber 2012)*. Independently on the pathway for cellular uptake, AAV is transported through the cell within endosomes, where the capsid undergoes a conformational change to expose its VP1/2 N-terminus *(Kronenberg et al. 2005, Sonntag et al. 2006)*. This conformational change is a crucial step during the AAV life-cycle, as the VP1/2 N-terminus has been shown to comprise protein domains relevant for a successful infection. These domains are a phospholipase A2 domain acting in endosomal release and three basic regions involved in nuclear import *(Stahnke et al. 2011, Nicolson and Samulski 2013)*. Only capsids carrying an intact PLA2 are able to infect, ascribing a key role to the VP1/2 N-terminus *(Girod et al. 2002)* in the infection process. Following endosomal release the capsids accumulate in the perinuclear space until transportation into the nucleus through the nuclear pores occurs. Inside the nucleus, the genome is released followed by second-strand conversion, allowing the expression and synthesis of new infectious particles.

Detailed understanding of the complete infection process is a prerequisite for a precise development of effective therapeutic AAV vectors. To contribute to the knowledge of the biology of AAV, this study aimed to determine cellular proteins that are directly involved during the infection process. A recent study demonstrated the presence of several additional functional domains (SH2, SH3 and PDZ) on the VP1/2 N-terminus that might mediate protein-protein interactions involved in signal transduction to either facilitate capsid transport or elicit an immune response via the JAK/STAT pathway (through the SH2 domains *(Popa-Wagner 2011)*). Interacting proteins however, still need to be determined. As the exposure of the VP1/2 N-terminus has been shown to be indispensable for AAV infection, this study specifically focused on cellular proteins that are able to bind the VP1/2 N-terminus. With this approach it was possible to identify a subset of proteins supposed to

act on the AAV infection via ubiquitination, giving new evidence that during a certain step in the AAV life-cycle, capsids are influenced by the ubiquitin-proteasome system.

5.1 Isolation and identification of host cell proteins that interact with the VP1/2 N-termini of different AAV serotypes

Possible cellular interaction partners of the AAV VP1/2 N-termini were identified with the TAP-tag method. In this study, the five different AAV serotypes 2, 6, 8, 9 and 10 were used on the one hand to identify possible differences between interacting proteins among different serotypes and on the other hand to find overlapping proteins, which might indicate the use of similar pathways of the different serotypes. The VP1/2 N-terminus-specific amino acid sequence among these serotypes is highly conserved (84%), thus it was expected to identify a higher degree of similarity in the identified proteins. After elimination of unspecific contaminating proteins, such as keratins, immunoglobulins or proteins deriving from species different to human origin from the mass-spectrometry results, a list containing 51 distinct proteins was obtained. In contrast to the expectations, only seven of these proteins were co-eluted with all of the five serotypes used, whereas 19 of the proteins co-eluted with only one. Out of the 51 proteins 39 co-eluted with the VP1/2 N-terminus of AAV6, followed by AAV2 with 25. An explanation for this discrepancy between the expectations and the mass-spectrometry results might give the analysis of the purification procedure. Western blot analysis of the samples that were taken during the purification process showed a single VP1/2 N-terminus-specific band for AAV2 and AAV6. In contrast, for the other three serotypes beside the VP1/2 N-terminus-specific band strong signals of degradation were detected, which might have interfered with the purification process thus leading to a reduced yield. This assumption coincides with the mass-spectrometry results, where the lowest fraction of proteins (17) co-eluted with AAV9, which showed the highest degree of degradation by western blot (data not shown). This puts the yield of the mass-spectrometry into a direct proportion to the input of the target protein. Taken together, these results demonstrate the importance the specific purification procedure and also indicate that minor differences among the protein sequences are accompanied with differences in the interacting proteins. However, conclusions on specific interactions cannot be drawn by comparing the results of the different serotypes and hence other methods proving specificity are necessary. Nevertheless, initial hints on a putative function on AAV of the isolated proteins may derive by regarding their cellular function in more detail.

The 51 identified proteins could be grouped according to their function in the cell. Possible functions on the AAV life-cycle mediated by their interaction will be discussed in the following.

5.1.1 Proteins involved in the cell-cycle

Eight different proteins involved in the cell-cycle were identified by mass-spectrometry, of which three were found to interact with all of the five serotypes, namely Calpain 2, CDK1 and CDK2. The interaction between CDK2 is in agreement with the study of *Murphy et al. (2008)*, showing a strong interaction with CDK2 and AAV2 and AAV8 which is thought to negatively influence the AAV life-cycle. Both, CDK1 and CDK2 are involved in cell-cycle control either in the G2/M transition (CDK1) or the G1/S transition (CDK2). As AAV has been postulated to provoke cell-cycle arrest during infection, leading to the accumulation of the host cells in either the late S-phase or the G2-phase *(Winocour et al. 1988)*, both kinases are promising candidates for further interaction studies. Along with that, the calcium-dependent protease Calpain 2 also seems to be involved in cell-cycle progression as well as membrane fusion (reviewed in *Huang and Wang 2001)*. The latter is of particular interest, as the PLA2 of AAV depends on calcium to exert its activity inside the endosome. An interaction between AAV and Calpain 2 might be accompanied with a temporary accumulation of calcium, activating the PLA2 thus allowing AAV to escape the endosomes and simultaneously inhibiting the function of Calpain 2 leading to a blockage of cell-cycle progression. Another benefit of the interaction between AAV and Calpain 2 might be that AAV exploits the function of membrane fusion of Calpain 2 to further facilitate endosomal escape. Other calcium-binding proteins are S100 family members that are also involved in cell-cycle progression. The proteins S100 A1 and A2 have been identified in the screen for different serotypes. An interaction between AAV and these proteins probably also allows the accumulation of calcium for the activation of the viral PLA2. *In vitro* analysis of the proteolytic activity of the calcium proteases but also the PLA2 in the presence of VP1 under physiological calcium concentrations could be an approach to further study whether these proteins interact with VP1 and thereby influence each other.

5.1.2 Proteins involved in the nuclear pore/import

Nuclear import of the capsids has been controversially discussed since the beginning of AAV research. The general view however describes AAV to enter the nucleus as intact capsid where genome release occurs. *Grieger et al. (2006)* identified three basic regions on the VP1/2 N-terminus that were postulated to resemble a nuclear localization signal enabling AAV to enter the nucleus, the mechanism however, was still unknown. Recently, *Nicolson and Samulski (2013)* postulated that AAV interacts with the karyopherin beta family member Importin-β. Interaction with Importin-β was demonstrated to occur at basic region three of the AAV VP1/2 N-terminus, thus mediating active Ran-dependent nuclear import through the nuclear pores. This further implies that the interaction must occur after the exposure of the VP1/2 N-terminus, as before the basic regions are buried inside the capsids. In the underlying study, Importin 5 was identified as potential interaction

partner of the AAV VP1/2 N-terminus. Importin 5 is also a member of the karyopherin beta family that, together with the published data, provides further evidence on the specificity of the screening. As the interaction between Importin-β and basic region 3 was not published at the course of the screening, Importin 5 represented a promising candidate for further characterization, despite the fact that it was also isolated in the HPV16 L2 TAP-tag procedure. However, in contrast to the involvement of Importin-β in AAV nuclear import, a general study on parvoviruses claimed that parvoviruses interact with key nuclear proteins to induce nuclear envelope breakdown, resulting in nuclear import independently on mitosis *(Porwal et al. 2013)*. As AAV does not depend on dividing cells for successful infection this theory might account for it. However, the possible interaction with cell-cycle proteins that probably block cell-cycle progression and thus nuclear envelope breakdown argues against this hypothesis. Together these reasons might favor – at least for AAV – the theory of active nuclear import mediated by members of the karyopherin family. Further prove for an interaction between the AAV VP1/2 N-terminus and Importin 5 could derive from mutational analysis of the basic regions of AAV.

5.1.3 Proteins involved in translation/ribosomal proteins

The largest group containing 17 different proteins was composed of ribosomal proteins and proteins being involved in translation. The high presence of ribosomal subunits suggests that they might have co-eluted during VP1 translation, while the ribosome was still attached to the mRNA/partially translated protein, hence not necessarily VP1-specific. Another subset of proteins within the ribosomal/translational category was a group of different heat shock proteins. Heat shock proteins are chaperones, facilitating the folding of proteins. As in the screen the AAV VP1/2 N-terminus was used, only comprising around 28% of the full-length protein, folding in its native tertiary structure might have been compromised. In addition, the fusion of the TAP-tag could further influence protein folding, thereby leading to a higher prevalence of interaction with different heat shock proteins. Along with that comes, that other groups also identified ribosomal proteins to be highly purified in proteomic screens, claiming that these proteins might be identified due to their abundance in the cell *(Nash et al. 2009)* and not necessarily specific to the protein of interest. Furthermore, nine of these proteins were also isolated with the HPV16 L2 TAP-tag negative control and hence not further characterized.

5.1.4 Proteins involved in transport

Cytoskeletal proteins such as tubulins or actins are involved in the life-cycle of many viruses during almost every step. It has been shown that viruses hijack the cellular transport system to travel along intracellular tracks towards their destination, such as the nucleus (reviewed in *Radtke et al. 2006)*.

Intracellular trafficking of AAV is considered to be the rate-limiting step during the AAV life-cycle. Upon scission of the endosomal vesicle, retrograde transport towards the nucleus takes place *(Hirosue et al. 2007)*. In this screen different types of tubulin, as well as actin were identified, indicating that also AAV takes advantage of the cellular network. Interestingly, for all of the five serotypes used in the screen, copine 1 was co-eluted, a protein involved in membrane trafficking. The fact that copine 1 acts in a calcium-dependent manner suggests, that interaction between AAV VP1 and copine 1 might occur inside the endosome, facilitating the transport on the one hand but probably also helping in endosomal escape on the other. Copine 3, another member of the copine family, was isolated with four of the serotypes and hence further implicating a role in endosomal trafficking, as it is supposed to function in a similar way as copine 1 *(Creutz et al. 1998, Tomsig 2003)*. Vimentin and nestin, the two other identified candidates in the "transport group", both function in the rearrangement of intermediate filaments during mitosis. They both might be captured by AAV to rearrange the filaments in a way that possibly facilitates the movement of the virus to the nucleus. Consistent with the assumption that AAV hijacks the cellular transportation network is, that at least a fraction of AAV enters the cell in a dynamin-dependent mechanism that is associated to microtubules leading to retrograde transport to the trans-Golgi network (reviewed in *Nonnenmacher and Weber 2012)*. This makes it very likely that the identified proteins in the present study at least partially contribute to the transportation process, probably at different steps during the infection. However, these proteins were excluded from further analyses because four of this group (alpha-Tubulin, beta-Tubulin, beta-Actin and Vimentin) also co-eluted with HPV16 L2 full-length. Furthermore Copine 1 and Copine 3 both co-eluted with two fragments of HPV16 L2.

5.1.5 Proteins involved in ubiquitination

Based on several studies with specific proteasome inhibitors, ubiquitination has been described to influence the AAV life-cycle, functioning to inhibit the infection, probably due to a higher degree of capsid degradation *(Douar et al. 2001, Yan et al. 2002, Yan et al. 2004, Zhong et al. 2007)*. Specific proteins from the ubiquitin-proteasome system however (that are linked to AAV infection), have not been identified yet. Ultimately, in this study six different proteins from the UPS were isolated, indicating a role of ubiquitination in the AAV life-cycle. The two proteasomal subunits 11 and 12 that were co-eluted with AAV10 and AAV6, respectively, might indicate that a fraction of the overexpressed VP1/2 N-termini might have been directly degraded by the proteasome. Cullin 3 and Cullin 4a are two members of the Cullin-RING ligases that, together with a RING-box protein and a specific substrate recognition protein, act as scaffold for ubiquitination of substrates. SPOP has been identified to directly bind to Cullin 3, acting as a substrate recognition protein that recruits specific substrates for ubiquitination *(Genschik et al. 2013)*. The presence of Cullin 3 and SPOP

might suggest that SPOP promotes the binding to the VP1 N-terminus, thereby recruiting it to Cullin 3 which in turn mediates ubiquitination of VP1. This hypothesis suggests, that Cullin 3 might have eluted in a complex bound to SPOP. However, as in the present approach neither a RING-box protein nor an E2 ubiquitin-conjugation enzyme was isolated, might argue against this hypothesis. But the fact that the ubiquitination process is known to be very dynamic, where activation and deactivation of the Cullins occurs quite frequently, leading to the association and dissociation of the co-factors necessary for ubiquitination, might suggest that possible intermediate states of the complex were isolated during the screen. In addition, the presence of CAND1 further corroborates this argument, since it functions as specific substrate recognition protein exchange factor for the Cullins. Associated to a Cullin, CAND1 mediates the exchange of the substrate recognition protein, leading to intermediate states between Cullin, the substrate recognition protein and CAND1, in which the other co-factors for ubiquitination are dissociated from Cullin. The fact that CAND1 was co-eluted also with serotypes where neither a Cullin nor SPOP was identified might also suggest that its isolation was rather unspecific. However, as SPOP has been identified in a yeast-two-hybrid screen to bind to the AAV2 VP1/2 N-terminus *(Popa-Wagner 2011)* argues that SPOP binds to AAV, thus suggesting also an indirect interaction for CAND1.

The influence of ubiquitination on the AAV life-cycle is still highly controversial. As mentioned above, studies on proteasome inhibition suggested that ubiquitination directly leads to proteasomal degradation resulting in a reduced infection. Furthermore, a series of studies performed by *Zhong et al.* demonstrated a role for capsid phosphorylation, preferentially on tyrosine residues to accompany ubiquitination. More precisely, they demonstrated that epidermal growth factor receptor kinase (EGFR) mediates the phosphorylation of tyrosine residues on the capsid. In turn, these phosphorylated tyrosines serve as direct signal for ubiquitination. Consistent with this is the observation that removal of tyrosine residues on the capsid surface led to a strong increase in transduction, indicating the negative effect of both, phosphorylation and ubiquitination *(Zhong et al. 2007, Zhong et al. 2008, Zhong et al. 2008)*. However, if ubiquitination was detrimental for AAV, why did no ubiquitin-escape mutants evolve? Studies on other viruses demonstrated that interaction with CRLs and some of the viral proteins lead to a positive effect on their transduction. Interaction rather causes the degradation of antiviral cellular proteins, shielding the viruses from the host defense. This was demonstrated for several viruses including adenovirus, paramyxoviruses and HIV *(Harada et al. 2002, Ulane and Horvath 2002, Sheehy et al. 2003, Yu et al. 2003, Blanchette et al. 2004, Mehle et al. 2004, Precious et al. 2005)*. Besides degradation of host proteins, interaction with CRLs can also lead to ubiquitination of viral capsid proteins which facilitate the infection at certain stages. The latter was demonstrated for vaccinia virus interacting with Cullin 3 *(Mercer et al. 2012)*. Furthermore, ubiquitination does not always come along with proteasomal degradation. Depending

on the ubiquitination pattern (poly-, oligo-, multi-, or monoubiquitination) it functions in different ways, such as regulation of transport, signal transduction or replication and transcription *(Mukhopadhyay and Riezman 2007)*. Also the linkage between the single ubiquitin residues (lysine 48 or lysine 63) determines the fate of an ubiquitinated protein *(Hershko and Ciechanover 1992, Barriere et al. 2007)*. If SPOP and Cullin 3 ubiquitinated AAV, it would lead to proteasomal degradation and a reduced infection. But, if AAV recruited SPOP to force its own ubiquitination mediated by Cullin 3, it could help to degrade the capsid proteins for efficient genome release inside the nucleus. The fact that SPOP is located within the nucleus further suggests that SPOP-mediated ubiquitination of the capsid must either occur at late stages during the infection or after the synthesis of new capsid proteins. This is in line with the observation that the VP1/2 N-terminus is only accessible after its exposure during infection or when newly synthesized. As the field of ubiquitination is rather complex, it leaves the above discussed theories on its function on the AAV life-cycle as highly speculative. The results of the underlying thesis on a putative function of SPOP and AAV will be discussed in the following in more detail.

Upon identification of the aforementioned 51 proteins, I concentrated on the following proteins: CDK1, CDK2, Calpain 2, Importin 5, Cullin 3, CAND1 and SPOP. Furthermore the two orthologues Mad2 L1 and Mad2 L2 were included, because they were identified in the before mentioned yeast-two-hybrid screen at high prevalence. CDK2 has been described before to interact with AAV2 and AAV8, hence it was included as internal control. As SPOP was also identified in the yeast-two-hybrid screen for AAV2 it constituted an interesting hit for further analyses. Also, the presence of the SPOP-associated proteins, Cullin 3 and CAND1, further suggested a specific interaction between the ubiquitination proteins and VP1, hence these proteins were chosen, as well.

5.2 Validation of the interaction between the nine chosen proteins and VP1

Although the described proteins were found to interact with the AAV VP1/2 N-terminus in the TAP-tag procedure, experiments to confirm the specific interaction between VP1 and these proteins were performed. These experiments were co-immunoprecipitation and co-localization studies. For the validation experiments the full-length VP1 was used, as it should fold in its native conformation, as it most likely resembles conditions comparable to infection and synthesis of new capsid proteins. Furthermore, all the experiments were performed with AAV2 only, since it is the most extensively studied and best understood serotype and hence considered as the prototype among AAV. First, specific binding was analyzed by co-IP. As described in (4.2.2), the interaction between Mad2 L2, CDK1, CDK2, Cullin 3, Calpain 2 and SPOP was possible to confirm. Faint signals for CAND1 and Importin 5 were detected by western blot, however as these signals were slightly above the background, they were not considered as a specific interaction. Apparently, the weak signal of

CAND1 might be explained by the fact that it co-eluted in the TAP-tag only by indirect binding to VP1 via SPOP and Cullin 3. As mentioned above (1.5.3, **Figure 7**), CAND1 binds to Cullins, promoting substrate recognition protein exchange. During acting as exchange factor, intermediate states between Cullin, CAND1 and a substrate recognition protein may occur (**Figure 7**). As in the performed immunoprecipitation endogenous levels of Cullin 3 were present in the transfected cells, a weak interaction between VP1 and CAND1 might have been possible. Additionally, CAND1 has a high molecular mass making it rather challenging for detection by western blotting, particularly if the protein levels are at low concentrations. In contrast, as member of the Importin-beta family, Importin 5 was thought to directly interact with VP1, mediated by the basic regions of the VP1/2 N-terminus *(Nicolson and Samulski 2013)*, hence it was surprising that the interaction could not be confirmed by co-IP. Possible reasons for that might either be technical issues, as Importin 5 is also known to have a high molecular mass, but also a low affinity for its interaction with VP1.

Treatment of the cells with 2 μM MG132 for 4h before harvesting allowed the detection of SPOP in the input, as well as the specific interaction between SPOP and VP1 in the co-IP. The MG132-dependent accumulation of SPOP suggests that its turnover in the cell is high and tightly regulated by the proteasome. Furthermore, as the interaction between SPOP and VP1 was only detected while the proteasome was blocked also implies that under native conditions the interaction might be rather weak. Overexpression of both proteins could lead to a "forced" interaction that eventually constitutes an artificial than a physiological state of the cell. However, as SPOP was detected in two different assays before, the yeast-two-hybrid and the TAP-tag, to interact with AAV, supports a specific interaction that probably occurs at very low physiological levels.

For further confirmation of the interaction between VP1 and the identified candidate proteins immunofluorescence experiments were performed to determine whether the interacting proteins also co-localize in intact cells. Overexpression of VP1 and either of the proteins only revealed a distinct phenotype for VP1 when co-expressed with SPOP. The VP1 phenotype localized to a speckled pattern inside the nucleus as it was observed for SPOP alone *(Nagai et al. 1997)*, indicating that an interaction between SPOP and VP1 led to a redistribution of VP1 to the speckled nuclear localization of SPOP. Furthermore, SPOP co-localization was not observed for the VP1/2 N-terminus lacking VP3 protein indicating that the interaction with VP1 was specific and most likely mediated by the VP1/2 N-terminus. An interesting approach to further prove the specific interaction between VP1 and SPOP would be co-localization studies with different SPOP mutants, where either the substrate recognition site within the MATH domain of SPOP or its nuclear localization signal are mutated *(Zhuang et al. 2009)*. Changes in the VP1 distribution could further support the specificity between VP1 and SPOP. Also, it would be of great interest to analyze whether an interaction between VP1 and SPOP avoids the interaction of SPOP with its "natural" substrates. Interestingly,

in contrast to the co-IP, strong signals of SPOP were detected in the immunofluorescence without the treatment of MG132. This might be explained, that in intact cells targeting and degradation of SPOP has a minor role and further that proteasomal degradation more likely occurs when SPOP gets into the cytoplasm. For the other proteins the co-localization result was not as clear as for SPOP. The cellular distribution for these proteins was detected to be diffuse in the nucleus or both, nucleus and cytoplasm (**Figure 16**). As VP1 also mainly localizes to the nucleus as well, conclusions on co-localization were not possible. However, when overexpressed in combination with un-tagged SPOP and VP1, Mad2 L1, Cullin 3 and Calpain 2 showed a speckled pattern inside the nucleus overlapping with VP1, suggesting a specific interaction. The strong co-localization of Cullin 3 (completely localized to speckles in the nucleus) and VP1 in combination with SPOP could either derive through an interaction between Cullin 3 and SPOP which would mirror the biological function of SPOP acting as substrate recognition protein recruiting substrates to Cullin 3 (1.5.2). But it could also be a direct binding between VP1 and Cullin 3. An interesting approach to test whether Cullin 3 interaction is direct or indirect would be mutational analysis of Cullin 3, analyzing whether a mutation in the SPOP binding site leads to reduced co-localization and interaction between Cullin 3 and VP1. Tyrosine 62 within Cullin 3 has been demonstrated to be essential for SPOP binding, thus constituting a promising target *(Kwon et al. 2006)*. Interestingly, Mad2 L1 did not bind to VP1 in the co-IP but co-localized with VP1, rather indicating a dynamic than a steady-state interaction that is probably dependent on the cell-cycle, where Mad2 L1 is known to function. This comes along with the observation that only a small fraction of the stained cells showed the speckled phenotype for Mad2 L1 when co-expressed with SPOP and VP1. Synchronization of the cells might be a possibility to increase this fraction allowing drawing conclusions on this hypothesis. In contrast to Mad2 L1, Mad2 L2 showed a specific interaction in the co-IP, but not in the immunofluorescence, which might probably also be linked to the cell-cycle. Both CDKs did not co-localize with VP1, even though CDK2 was described before to bind to AAV2 *(Murphy et al. 2008)*. As both CDKs function in cell-cycle progression an interaction with AAV seems to be obvious to provoke cell-cycle arrest which is needed for efficient transduction *(Winocour et al. 1988)*. However, cell-cycle arrest might be necessary during infection but not mandatory for the expression of new capsid proteins and also capsid assembly. Overexpression of VP1 might resemble the infection process at a very late stage, after uncoating of the genome occurred and the virus already generates progeny, which might occur independently of cell-cycle arrest. Controversial to that is that both CDKs were found in the co-IP to bind to VP1, although it was overexpressed in this experiment with the same plasmid and hence mimicking the same step of the viral life-cycle. Also, as in the VP1 construct, expression of VP2 and VP3 is repressed, capsids cannot be formed, and thus the VP1/2 N-terminus might be accessible, similar as during infection after the conformational change within the endosome. However, interaction between VP1 and the CDKs might also occur in a time- and space-

dependent manner, making it difficult to detect via immunofluorescence. Moreover, the interaction between SPOP and VP1 might interfere with the binding of the CDKs, probably due to a sterical hindrance. The fact that CAND1 did not co-localize in this approach might also be explained by its indirect binding, as well as its function as substrate recognition protein exchange factor as described above. Here, an interesting approach would be the transfection of a combination of VP1, SPOP, Cullin 3 and CAND1 to promote co-localization of CAND1 to VP1. Interaction between CAND1 and VP1 in this experiment would mirror the ubiquitination complex as it was described before (1.5.3). Furthermore, it would be interesting to analyze the SPOP binding of AAV capsids during infection of cells that overexpress VP1 and SPOP. The interaction between SPOP and expressed VP1 might lead to a depletion of free SPOP and hence influencing the infection.

Taken together, these experiments demonstrated the complexity of protein-protein interactions, clearly showing that interactions depend on a subset of functions and states of the cell. Overexpression of the proteins might force the interaction with VP1 in a way that does not necessarily reflect the situation as it is under physiological conditions. However, it allows gaining an impression on possible natural interactions whose influences on AAV can be studied by functional analysis. Also, using several different approaches to demonstrate the interaction between VP1 and the chosen proteins resulted in robust data for some of the identified proteins, strongly suggesting an interaction and hence involvement in the AAV life-cycle.

5.3 Influence of SPOP on the AAV2 life-cycle

Ubiquitination was postulated to influence the AAV2 life-cycle; key proteins however still remain unidentified. As the TAP-tag screen revealed the ubiquitination complex of SPOP, Cullin 3 and CAND1, as well as the fact that SPOP led to a possible recruitment of VP1 to speckles inside the nucleus, these proteins were promising candidates for further studies on their function on the AAV2 life-cycle. As discussed above, SPOP was assumed to be the direct binding partner of VP1, mediating its recruitment to Cullin 3 for ubiquitination. This theory was strongly supported by the identification of a putative SPOP binding consensus in the VP1/2 N-terminus. The high level of conservation among the different serotypes that was observed in this region further suggested an important role of the identified motif and SPOP in the AAV life-cycle. The fact that neither AAV5 nor AAV12 displayed this motif in their VP1 sequences might indicate that these two serotypes are probably able to infect independently of an interaction with SPOP and may be considered as natural mutants. However, experiments to follow this theory still need to be done, as the putative SBC was not confirmed completely in the present study. To analyze the influence of the identified SBC motif on AAV2, several mutations were introduced within this motif. Apparently, as the VP1 sequence of AAV9 displayed an alanine at P5 of the putative SBC motif but SPOP was identified in the TAP

screen with AAV9 (**Figure 20**), this exchange was considered as natural mutation, not influencing the SPOP binding properties. Hence, this mutation was not introduced in the AAV2 SBC motif. It was rather decided to change the aspartate on P2, as well as the two serines on P3 and P4 either to alanines or to glutamate (**Figure 21**). In total, five different VP1 SBC mutants were cloned for further analyses. Two of these VP1 SBC mutants carried double mutations. The D154E mutant was expected to resemble the wild-type as the aspartate to glutamate exchange did not result in a change of the polarity, thus the SBC motif was supposed not to be disturbed. The proline at P1was not mutated, as the restriction to a non-polar amino acid of the postulated SBC motif allowed the highest degree of freedom, indicating a minor role for this amino acid. The restriction to either a polar amino acid or to serine or threonine (P2 – P5) narrowed the variance and hence made these mutations more interesting. The influence of the introduced mutations on the SPOP binding, as well as on the infection of AAV2 was analyzed by a subset of experiments (4.4, 4.5) and will be discussed in detail in the following.

5.4 Analysis of the interaction of SPOP and the VP1 SBC mutants during overexpression of VP1

The co-IP of SPOP and the VP1 SBC mutants gave hints on the relevance of the putative SBC motif to be recognized by SPOP. The D154E mutant showed similar SPOP levels in the co-IP compared to wild-type. Furthermore, also the D154A mutant was still able to bind SPOP at high levels. This indicated that a mutation of the aspartate does not interfere with SPOP binding. Regarding the other VP1 SBC mutants, all displaying a mutation at P3, the levels of precipitated SPOP were highly reduced, indicating a major role of the serine in this motif. This is also in line with the postulated SBC motif, as the serine at P3 is the only position that is restricted to a particular amino acid, namely serine. However, as the SBC motif was not clearly confirmed to mediate SPOP binding, conclusions on direct effects of the mutations and SPOP binding cannot be drawn. It is also likely, that other cellular factors might have been influenced by these mutations, thus leading to the observed results. Although in this experiment the overexpression of the VP1 constructs was weak, VP1-specific bands in the immunoprecipitation were detected. However, the precipitation of VP1 varied strongly among the different VP1 SBC mutants, which might have influenced the result partially. According to other experiments, an influence of the mutations on the expression of VP1 can be excluded, as similar levels were observed for all of the VP1 SBC mutants before (data not shown). Strikingly, despite the fact that the weakest precipitation of VP1 was observed for the D154E mutant, it still showed a strong precipitation of SPOP. As the VP1-negative, SPOP-positive sample did not give a SPOP signal in the immunoprecipitation western blot, the D154E result can be interpreted as specific interaction with VP1. Moreover, as the strongest VP1 signal was observed in the DS154AA double

mutant, that in contrast showed the weakest precipitation of SPOP, further suggests that the differences among the VP1 precipitation were likely due to technical issues in the detection and hence not influencing the experiment.

Contradictory to the co-IP were the results from the co-localization studies between SPOP and the VP1 SBC mutants. The wild-type showed the highest prevalence of SPOP co-localization, with a distribution in the SPOP speckles as observed before (4.4.2). The D154E mutant however had a reduced formation of nuclear speckles, although the SPOP binding did not seem to be disturbed by the mutation (4.4.1). Additionally, the overall distribution of this VP1 SBC mutant was rather different, as 45% of the cells showed a cytoplasmic-nuclear staining. Normally, around 30% of transfected VP1 localizes to the cytoplasm *(Popa-Wagner 2011)*. This proposes that the aspartate at P2 in the putative SBC might not be necessary for the binding of SPOP, but it possibly interferes with the interaction of other, yet unidentified proteins. However, the fact that the other two aspartate P2 mutants (D154A and DS154AA) were found to be distributed in the cytoplasm at "normal" levels, does not account for the necessity of the aspartate at P2 for AAV2 VP1 in regard to its subcellular distribution. Interestingly, the two double mutants showed the lowest number of speckles, which reflected the interaction result that was observed in the co-IP. To see whether the differences in the cellular distribution, especially for the D154E mutant, rise from the mutation itself or from a disruption of the SPOP binding, overexpression of the VP1 SBC mutants alone would be an approach to follow up. Although endogenous SPOP is still expressed in the cell, a similar distribution of the VP1 SBC mutants would account for the influence of other proteins, as under physiological SPOP levels, VP1 was not seen to be located into speckles. In contrast, a "normal" distribution (70% nuclear, 30% cytoplasmic-nuclear) would suggest a disruption of the binding between SPOP and VP1 and thus leading to a disturbed cellular distribution of the VP1 SBC mutants. Furthermore, as VP1 is was not found in speckles under physiological SPOP levels it could also be that binding of SPOP leads to a shuttling between the speckles and the nucleoplasma. This could have a regulatory function, as the binding of SPOP through VP1 might also lead to a temporary accumulation of other cellular proteins that are regulated by SPOP, which could be advantageous for AAV.

The ubiquitination co-IP did not reveal differences between wild-type and the different VP1 SBC mutants. Even though strong levels of VP1 degradation were observed, repetition under treatment with MG132 did not result in accumulation of ubiquitinated VP1 bands, but in similar levels of degradation as without MG132. These observations might have several reasons. First, if capsid proteins are ubiquitinated it is likely, that ubiquitination only occurs at distinct time points during infection and not when new capsid proteins are produced. Therefore, analysis of capsid ubiquitination while entering the cell would be an interesting approach to analyze. Secondly, these

results might suggest, that the interaction between VP1 and SPOP is independently of ubiquitination, hence supposing a role in targeting and subcellular localization mediated by the indirect interaction between VP1 and Cullin 3 through SPOP (5.6).

Taken together, the results in the performed experiments demonstrated the complexity of ubiquitination, and furthermore the importance and necessity of analyzing various time points of the viral infection to get an impression on how ubiquitination is involved in the AAV life-cycle.

5.5 Analysis of SPOP and the VP1 SBC mutants during viral infection

To identify the influence of the SBC motif on viral transduction, reporter viruses carrying the above described mutations in the VP1 protein of their capsids were generated. The titers of the VP1 SBC mutant virus preparations were at similar concentrations with the wild-type preparation, suggesting that neither capsid assembly nor viral protein expression was influenced by these mutations. Moreover, the similar titers allowed using comparable volumes for transduction experiments, avoiding an overload of interfering empty capsids within one approach. Hence, the observed results for all of the performed experiments were considered as capsid-specific and differences in the transduction efficiency were likely mediated by the mutations interfering with the viral infection.

Transduction of HEK293TT and HEK293 FlpIn™ cells under physiological levels of SPOP revealed differences in the efficiencies among the different viruses. The result partially reflected the differences that were observed for SPOP binding in the co-IP. Wild-type AAV2 transduced the cells with the highest efficiency, followed by the D154E mutant, indicating that the introduction of the glutamate did neither interfere with transduction nor with a possible SPOP interaction. However, as these mutations occurred at a highly sensitive part of the capsid, namely the VP1/2 N-terminus, playing a major role during infection, also other functions or interactions might be disturbed. For example, the amino acid exchange(s) might change the chemical properties of the capsid in a way that the exposure of the VP1/2 N-terminus through the 5-fold axis was impeded and only occurred partially, leaving a fraction of the viruses trapped within the endosomes and subsequently targeted for lysosomal degradation. VP1/2 N-terminus externalization of the VP1 SBC mutants would be possible to test in a cell free assay by limited temperature treatment up to 65°C *(Bleker et al. 2005, Kronenberg et al. 2005)*. Here, the capsids are spotted on a nitrocellulose membrane and VP1/2 N-terminus externalization, as well as the presence of intact capsids, can be detected with different VP-specific antibodies. Differences between the wild-type and the VP1 SBC mutants would give further insights into the influence of the mutations on the infection. Furthermore, different efficiencies in the release of DNA from viral capsids after infection with the different vectors could be measured by time-course experiments in combination with quantitative real-time PCR. Reduced DNA levels of the

VP1 SBC mutants could account for the above mentioned lysosomal degradation. Ultimately, the overall transduction in this experiment was about double as efficient in the HEK293 FlpIn™ cells as in the HEK293TT cells. However, as it was consistent among all serotypes indicated that the HEK293 FlpIn™ cells were more prone to viral infections and hence this observation was not further followed up.

Transduction of cells overexpressing SPOP did not result in different transduction efficiencies compared to the transduction of cells with physiological SPOP levels (4.5.2, **Figure 25**). This might either indicate that the infection of AAV2 is SPOP independent or that physiological SPOP concentrations are already sufficient to influence the infection in either direction. Moreover, the cells that were used as negative control, not overexpressing SPOP, had slightly elevated levels of SPOP compared to their parental cell line, likely due to a leaky expression of the introduced SPOP gene, which might already have led to levels of SPOP saturation (4.5.3, **Figure 26**). Consistent with that is the fact, that the transduction efficiencies were in the same order of magnitude as observed in the first experiment, supporting that endogenous levels of SPOP are sufficient for influencing AAV infection. Concluding, the results of these two experiments suggested that if SPOP interacts with AAV2 during infection, interaction already occurs at low levels and hence rather elimination of SPOP might influence the infection, either positively or negatively.

Preliminary experiments on the SPOP knockdown were done with four different siRNAs. Western blot analysis of the knockdown revealed that all of the siRNAs were down-regulating the endogenous SPOP levels at a similar degree. As it was shown in **Figure 27**, treatment of cells with siRNA #3 had an influence on AAV2 for all of the VP1 SBC mutants and AAV2 wild-type, leading to enhanced transduction. All alanine VP1 SBC mutants showed a strong reaction on the knockdown with siRNA #3, whereas the influence on the wild-type and the D154E mutant was the weakest among all vectors used. These results might indicate that SPOP has a negative effect on AAV2 transduction, as the experiments on SPOP overexpression did not change the viral transduction compared to physiological SPOP levels. The fact that the wild-type and the D154E mutant showed the lowest reaction on the knockdown might be explained by the intact SBC motif which both viruses possess. This could allow binding of SPOP with high affinity, as it was observed in the co-IP experiments. As SPOP was only partially down-regulated in the knockdown experiment, the remaining levels could still bind to the VP1/2 N-termini. Because the SPOP levels were lower compared to physiological levels and hence limited, one could imagine that binding might occur in a “competitive” manner, meaning that proteins with a higher binding affinity are targeted by SPOP more likely than proteins with a lower binding affinity. That could lead to an enhanced interaction between wild-type and the D154E mutant, which was reflected in the lower effect of the knockdown. Along with that, the alanine VP1 SBC mutants showed lower binding affinity to SPOP in the co-IP, supporting the

theory that during SPOP competition these VP1 SBC mutants might interact to a lower extent with SPOP, thus leading to a higher increase in transduction when SPOP is limited. Ultimately, the strongly reduced SPOP levels after transduction with the D154E mutant suggested an influence of the new capsid composition on SPOP. However, analysis of cells that were infected with this VP1 SBC mutant could not reproduce this result, hence it was considered as blotting artifact (data not shown). As these observations come from preliminary data further knockdown experiments need to be done for concrete conclusions. To further analyze the SPOP knockdown, quantification by real time PCR would be an approach allowing drawing conclusions on the relative SPOP levels within the cells after treatment with the different siRNAs.

5.6 Possible functions of SPOP on AAV

Taken together, the mutational analysis of the putative SBC motif showed the following impacts on AAV: reduced binding between SPOP and VP1, differences in the cellular distribution and reduced transduction. Contradictory, down-regulation of SPOP led to an increase in transduction for the wild-type, as well as for the VP1 SBC mutants, making it challenging to put these results in a functional connection. However, regarding the biology of the recognition sequences for substrate recognition proteins of E3 substrates, also called degrons, it was postulated that they frequently undergo post-translational modifications. A common modification has been found to be phosphorylation. It has been shown, that for example Cullin 3 - SPOP mediated ubiquitination of Src-3 depends on degron phosphorylation for efficient recognition of Src-3 by SPOP *(Varshavsky 1991, Ferry et al. 2011, Li et al. 2011)*. On the other hand, other studies demonstrated that phosphorylation of the degrons rather inhibits the recruitment of CRL3s *(Lo et al. 2006)*. Along with that *Zhuang et al. (2009)* showed that substitutions with phospho-serine or phospho-threonine in substrate degrons led to a reduced binding of SPOP.

Transferring the first theory of degron phosphorylation on the AAV2 life-cycle, considering that phosphorylation as signal for ubiquitination has been postulated to be detrimental for AAV, it is likely that phosphorylation might occur at the putative SBC motif or in its proximity, facilitating SPOP binding and hence degradation (**Figure 28 B**). Regarding the putative SBC motif in the VP1/2 N-terminus, the three serines are very prone to be phosphorylated by a serine/threonine kinase *(personal communication with Dr. A. Alonso, DKFZ)*, making this theory very likely. Mutations of this motif should escape cellular phosphorylation and thus leading to a reduced binding of SPOP, avoiding ubiquitination and degradation. Contradictory to that was the observation that the mutations of the serines led to a reduced transduction even though SPOP binding seemed to be impeded. This either suggests a positive role for SPOP on AAV2 transduction (probably on genome

uncoating or capsid trafficking) or it might indicate that also other factors influence the infection. Furthermore also the amino acid exchanges might have has an impact on capsid integrity.

The second theory, suggesting that degron phosphorylation inhibits the binding of SPOP, would support the observations of the present study, where wild-type and the D154E mutant showed the highest levels of transduction and also the lowest increase after SPOP knockdown, pointing towards a negative effect of SPOP on AAV2 transduction. However, contradictory to that was the enhanced binding of SPOP in the co-IP, as well as the strong co-localization of SPOP and VP1, at least for wild-type.

Regarding the fact that the approaches in the present study aimed on the analysis of two different stages of the AAV2 infection might explain these contradictory results: With the overexpression of VP1, the synthesis of capsid proteins after efficient entry and uncoating was mimicked. Despite the fact, that this process might not reflect natural conditions completely, as the expression of VP2 and VP3 was repressed and hence capsids could not be assembled, it still partially resembled a late step of the AAV2 life-cycle. However, the fact that the VP1/2 N-terminus was possibly accessible for a longer period of time in this approach might have influenced the results in these experiments. On the other side, the transduction experiments allowed determining early steps of the AAV2 life-cycle, showing possible influences of SPOP on the externalization of the VP1/2 N-terminus and probably genome uncoating.

To get a general view on how the CRL3 complex might act on AAV2, studies that were conducted on vaccinia virus may give further information. For vaccina virus, Cullin 3 dependent stages during infection have been demonstrated. Here, the virus exploits the UPS at two different stages of its life-cycle. While virion assembly, core proteins become ubiquitinated by CRL3s. These ubiquitin residues are then shielded from the proteasome by the envelope of the virus. After infection of a cell, the envelope fuses with the endosomal membrane and subsequently the ubiquitin residues attached to the core get accessible for the proteasome. Proteasomal degradation then leads to a fast and facilitated genome uncoating, allowing an efficient infection for the virus *(Mercer et al. 2012)*.

For AAV2 it might be slightly more difficult, as it is a non-enveloped virus, thereby direct ubiquitination of the capsid during or after assembly could be challenging. However, regarding the studies on the phosphorylation of the substrate degron discussed above, a possible scenario might be that during protein synthesis and capsid assembly, the VP1/2 N-terminus gets “primed” through phosphorylation at distinct residues, probably the serines in the SBC motif. As the VP1/2 N-terminus is buried inside the capsid before the virus enters the cell, also the phosphorylated residues are hidden. During infection, VP1/2 N-terminus exposure occurs within the endosome, allowing endosomal escape and import of the complete capsids into the nucleus, where SPOP is

located. Inside the nucleus, two possibilities are given: i) SPOP is either unable to bind to or ii) SPOP might be attracted by the phosphorylated VP1/2 N-termini.

If SPOP was not able to bind the phosphorylated VP1/2 N-termini would suggest, that if phosphorylation occurred during assembly, it might help the virus to prevent proteasomal degradation at different stages during infection (**Figure 28 B**). Attraction might lead to CRL3 mediated ubiquitination and subsequent degradation of the capsids leading to genome release, thereby facilitating viral infection. Moreover, CRL3s not only target substrates for degradation, but also control their subcellular localization *(*reviewed in *Genschik et al. 2013)*. This might also suggest another possibility of SPOP influencing AAV2. If the interaction led to a distinct nuclear localization of the capsid proteins, controlling their subcellular distribution, it could probably facilitate capsid assembly, by organizing the three capsid proteins, as well as AAP (**Figure 28 A**). Also, if ubiquitination of newly synthesized VP1 occurred, ubiquitin residues (mono- or multi-ubiquitination) could probably be buried inside the capsid and help the virus during trafficking and uncoating independently of phosphorylation. However, as the AAV2 capsid is with approximately 25 nm in diameter rather small, the packaging of ubiquitin residues might be challenging for the virus. Nonetheless, these possible scenarios all imply a SPOP dependent step during synthesis of the capsid proteins and a Cullin 3 dependent step during entry. Experiments to rule out whether these theories might apply to AAV2 would be of great importance. The presence of phosphorylated, as well as ubiquitinated VP1/2 N-termini, could easily be demonstrated in the before mentioned cell free assay, where the VP1/2 N-termini can be experimentally exposed by limited temperature treatment. Detection with different phosphorylation- or ubiquitination-specific antibodies (phospho-tyrosine, phospho-serine or phospho-threonine, anti-ubiquitin (lysine-48 or lysine-63)) would allow the identification of post-translational modified VP1/2 N-termini. Also, overexpression and analysis of VP1 under the treatment with specific inhibitors that either block the activity of tyrosine and/or serine/threonine kinases would further give rise on VP1/2 N-terminus phosphorylation. Ultimately, production of viruses under the same conditions and also in combination with proteasome inhibitors following transduction experiments would further reveal phosphorylation and ubiquitination dependent steps in the AAV2 life-cycle. Another interesting approach to study the function of SPOP on AAV would be the generation of AAV particles in SPOP-knockout cells following functional analysis on their infectivity, as well as on post-translational modifications of the Vp1/2 N-terminus.

As a last scenario how SPOP might be involved in the AAV life-cycle, a recruitment of SPOP by VP1 might be possible. Binding of SPOP by VP1 could lead to a temporary inhibition of the function of SPOP and thus blocking the regulation of other cellular proteins that might function in innate immunity. With a mechanism like this, AAV would be able to overcome the cellular defense during entry and thereby facilitating its infection (**Figure 28 C**).

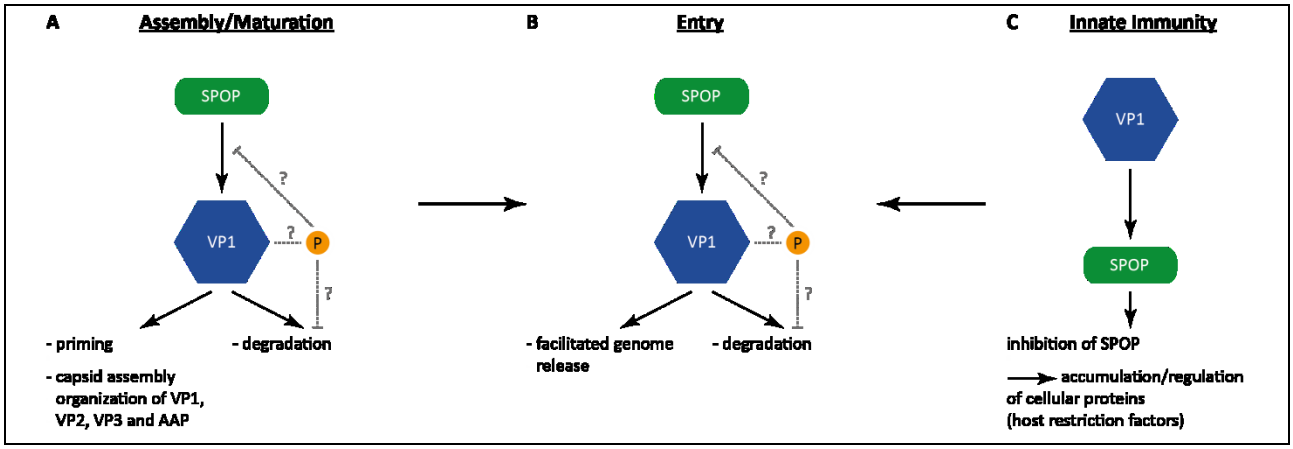

Figure 28: Hypothetical model of the function of SPOP on AAV2. Three different possible scenarios how SPOP influences AAV2 are shown. **A** SPOP interaction occurs during capsid assembly and maturation. Capsid proteins are phosphorylated to either attract or inhibit SPOP. Binding of SPOP to VP1 during protein synthesis regulates the subcellular distribution of the capsid proteins VP1, VP2, VP3 and AAP thereby facilitating and organizing capsid assembly. Furthermore, changes in the SPOP binding during viral entry due to phosphorylation can influence the infection. **B** Influence of SPOP during entry. Interaction with SPOP either leads to degradation of the capsids and preventing the infection or helps during genome release. (Prior) phosphorylated VP1 could increase or inhibit SPOP binding. **C** VP1 recruits SPOP for a temporary inhibition thus regulating the turnover of cellular proteins. This mechanism can help to overcome the cellular immune response, helping AAV to infect the host cell. All scenarios described are not proven experimentally.

Finally, not only the binding of SPOP indicates the involvement of CRL3s in the AAV2 life-cycle. Also the finding of Cullin 3, as well as the confirmed interaction with VP1 indicates its function on the AAV life-cycle. Overexpression, as well as knockdown experiments on Cullin 3 itself might further help understanding the role of CRL3s for AAV2 and probably also support the results of this work.

5.7 Conclusions

In the underlying study, several proteins that might be able to interact with the VP1/2 N-termini of different AAV were isolated and identified, suggesting influencing AAV infection. A subset of nine different proteins was chosen for further characterization on their ability to bind the AAV2 VP1/2 N-terminus. Among those proteins, Cullin 3, SPOP and CAND1 were further analyzed for their function on AAV2, as they were found to act in the ubiquitin proteasome system as Cullin-RING ligase 3. A direct interaction between SPOP and the N-terminus of VP1 was demonstrated. Furthermore, a 5-residue motif that resembles a SPOP binding consensus and might mediate SPOP binding was identified. Mutational analysis within this motif revealed differences in the binding of SPOP, as well as in the subcellular distribution of VP1. Moreover, transduction

analysis revealed differences in the efficiencies among the VP1 SBC mutants suggesting a possible role for SPOP in the AAV2 life-cycle.

The performed experiments demonstrated the complexity of a very simply organized virus to enter the cell. Infection seems to be tightly regulated during the whole course of the infection. Regulation might either occur through viral "tools", such as the VP1/2 N-terminus and its functional domains, or through the ability of the virus to exploit the host cell machinery. On the other side, the cell needs to defend and overcome viral infections with very complex mechanisms. For an efficient infection, AAV needs to harmonize the host cell defense and use certain mechanisms of this defense complex simultaneously. A major mechanism that is highly discussed within the AAV field is ubiquitination of the capsids during infection. Core proteins of the UPS were identified in this study, indicating a function during the infection; however the experiments did not give a clear result that allowed drawing final conclusions on their function. It still remained unclear whether the identified proteins act as host restriction or host dependence factors, as the results were partially contradictory. However, these studies indicated that these proteins might be involved at different steps during infection, both during entry and capsid assembly. Time course experiments to trace the virus all over its infection would be of great importance to analyze the function of the CRL3 on the AAV2 life cycle and furthermore to identify possible steps where the interactions occur. This would reveal so far unknown steps and add one more piece to the challenging puzzle of the AAV life-cycle.

6 References

Akache, B., D. Grimm, K. Pandey, S. R. Yant, H. Xu and M. A. Kay (2006). "The 37/67-kilodalton laminin receptor is a receptor for adeno-associated virus serotypes 8, 2, 3, and 9." J Virol **80**(19): 9831-9836.

Akache, B., D. Grimm, X. Shen, S. Fuess, S. R. Yant, D. S. Glazer, J. Park and M. A. Kay (2007). "A two-hybrid screen identifies cathepsins B and L as uncoating factors for adeno-associated virus 2 and 8." Molecular Therapy **15**(2): 330-339.

Asokan, A., J. B. Hamra, L. Govindasamy, M. Agbandje-McKenna and R. J. Samulski (2006). "Adeno-associated virus type 2 contains an integrin alpha5beta1 binding domain essential for viral cell entry." J Virol **80**(18): 8961-8969.

Atchison, R. W., Casto, B. C., Hammon, W. (1965). "Adeno-Associated Defective Virus Particles." Science **149**: 754-756.

Barriere, H., C. Nemes, K. Du and G. L. Lukacs (2007). "Plasticity of polyubiquitin recognition as lysosomal targeting signals by the endosomal sorting machinery." Mol Biol Cell **18**(10): 3952-3965.

Bartlett, J. S., R. Wilcher and R. J. Samulski (2000). "Infectious entry pathway of adeno-associated virus and adeno-associated virus vectors." J Virol **74**(6): 2777-2785.

Becerra, S. P. (1988). "Synthesis of Adeno-Associated Virus Structural Proteins Requires Both Alternative mRNA Splicing and Alternative Initiations from a Single Transcript." Journal of Virology **62**(8): 2745-2754.

Berns, K. I., T. C. Pinkerton, G. F. Thomas and M. D. Hoggan (1975). "Detection of adeno-associated virus (AAV)-specific nucleotide sequences in DNA isolated from latently infected Detroit 6 cells." Virology **68**(2): 556-560.

Bevington, J. M., P. G. Needham, K. C. Verrill, R. F. Collaco, V. Basrur and J. P. Trempe (2007). "Adeno-associated virus interactions with B23/Nucleophosmin: identification of sub-nucleolar virion regions." Virology **357**(1): 102-113.

Blanchette, P., C. Y. Cheng, Q. Yan, G. Ketner, D. A. Ornelles, T. Dobner, R. C. Conaway, J. W. Conaway and P. E. Branton (2004). "Both BC-box motifs of adenovirus protein E4orf6 are required to efficiently assemble an E3 ligase complex that degrades p53." Mol Cell Biol **24**(21): 9619-9629.

Bleker, S., F. Sonntag and J. A. Kleinschmidt (2005). "Mutational analysis of narrow pores at the fivefold symmetry axes of adeno-associated virus type 2 capsids reveals a dual role in genome packaging and activation of phospholipase A2 activity." Journal of Virology **79**(4): 2528-2540.

Boname, J. M. a. L., P.J. (2008). "The Ubiquitination-Proteasome System and Disease." WILEY-VCH **4**.

Carter, B. J., C. J. Marcus-Sekura, C. A. Laughlin and G. Ketner (1983). "Properties of an adenovirus type 2 mutant, Ad2dl807, having a deletion near the right-hand genome terminus: failure to help AAV replication." Virology **126**(2): 505-516.

Chang, L. S. and T. Shenk (1990). "The adenovirus DNA-binding protein stimulates the rate of transcription directed by adenovirus and adeno-associated virus promoters." J Virol **64**(5): 2103-2109.

Chang, L. S., Y. Shi and T. Shenk (1989). "Adeno-associated virus P5 promoter contains an adenovirus E1A-inducible element and a binding site for the major late transcription factor." J Virol **63**(8): 3479-3488.

Cheung, A. K., M. D. Hoggan, W. W. Hauswirth and K. I. Berns (1980). "Integration of the adeno-associated virus genome into cellular DNA in latently infected human Detroit 6 cells." J Virol **33**(2): 739-748.

Chiorini, J. A., F. Kim, L. Yang and R. M. Kotin (1999). "Cloning and characterization of adeno-associated virus type 5." J Virol **73**(2): 1309-1319.

Chiorini, J. A., L. Yang, Y. Liu, B. Safer and R. M. Kotin (1997). "Cloning of adeno-associated virus type 4 (AAV4) and generation of recombinant AAV4 particles." J Virol **71**(9): 6823-6833.

Chua, Y. S., B. K. Boh, W. Ponyeam and T. Hagen (2011). "Regulation of cullin RING E3 ubiquitin ligases by CAND1 in vivo." PLoS One **6**(1): e16071.

Creutz, C. E., J. L. Tomsig, S. L. Snyder, M. C. Gautier, F. Skouri, J. Beisson and J. Cohen (1998). "The copines, a novel class of C2 domain-containing, calcium-dependent, phospholipid-binding proteins conserved from Paramecium to humans." J Biol Chem **273**(3): 1393-1402.

Daya, S. and K. I. Berns (2008). "Gene therapy using adeno-associated virus vectors." Clin Microbiol Rev **21**(4): 583-593.

Douar, A. M., K. Poulard, D. Stockholm and O. Danos (2001). "Intracellular trafficking of adeno-associated virus vectors: routing to the late endosomal compartment and proteasome degradation." J Virol **75**(4): 1824-1833.

Duan, D., Q. Li, A. W. Kao, Y. Yue, J. E. Pessin and J. F. Engelhardt (1999). "Dynamin is required for recombinant adeno-associated virus type 2 infection." J Virol **73**(12): 10371-10376.

Duan, D., P. Sharma, L. Dudus, Y. Zhang, S. Sanlioglu, Z. Yan, Y. Yue, Y. Ye, R. Lester, J. Yang, K. J. Fisher and J. F. Engelhardt (1999). "Formation of adeno-associated virus circular genomes is differentially regulated by adenovirus E4 ORF6 and E2a gene expression." J Virol **73**(1): 161-169.

Duan, D., P. Sharma, J. Yang, Y. Yue, L. Dudus, Y. Zhang, K. J. Fisher and J. F. Engelhardt (1998). "Circular intermediates of recombinant adeno-associated virus have defined structural characteristics responsible for long-term episomal persistence in muscle tissue." J Virol **72**(11): 8568-8577.

Duan, D., Y. Yue, Z. Yan, J. Yang and J. F. Engelhardt (2000). "Endosomal processing limits gene transfer to polarized airway epithelia by adeno-associated virus." J Clin Invest **105**(11): 1573-1587.

Duda, D. M., L. A. Borg, D. C. Scott, H. W. Hunt, M. Hammel and B. A. Schulman (2008). "Structural insights into NEDD8 activation of cullin-RING ligases: conformational control of conjugation." Cell **134**(6): 995-1006.

Ferrari, F. K., T. Samulski, T. Shenk and R. J. Samulski (1996). "Second-strand synthesis is a rate-limiting step for efficient transduction by recombinant adeno-associated virus vectors." J Virol **70**(5): 3227-3234.

Ferry, C., S. Gaouar, B. Fischer, M. Boeglin, N. Paul, E. Samarut, A. Piskunov, G. Pankotai-Bodo, L. Brino and C. Rochette-Egly (2011). "Cullin 3 mediates SRC-3 ubiquitination and degradation to control the retinoic acid response." Proc Natl Acad Sci U S A **108**(51): 20603-20608.

Fisher, K. J., G. P. Gao, M. D. Weitzman, R. DeMatteo, J. F. Burda and J. M. Wilson (1996). "Transduction with recombinant adeno-associated virus for gene therapy is limited by leading-strand synthesis." J Virol **70**(1): 520-532.

Genschik, P., I. Sumara and E. Lechner (2013). "The emerging family of CULLIN3-RING ubiquitin ligases (CRL3s): cellular functions and disease implications." EMBO J.

Geoffroy, M. C. and A. Salvetti (2005). "Helper functions required for wild type and recombinant adeno-associated virus growth." Curr Gene Ther **5**(3): 265-271.

Georg-Fries, B., S. Biederlack, J. Wolf and H. zur Hausen (1984). "Analysis of proteins, helper dependence, and seroepidemiology of a new human parvovirus." Virology **134**(1): 64-71.

Girod, A., C. E. Wobus, Z. Zadori, M. Ried, K. Leike, P. Tijssen, J. A. Kleinschmidt and M. Hallek (2002). "The VP1 capsid protein of adeno-associated virus type 2 is carrying a phospholipase A2 domain required for virus infectivity." Journal of General Virology **83**: 973-978.

Grieger, J. C. and R. J. Samulski (2012). "Adeno-associated virus vectorology, manufacturing, and clinical applications." Methods Enzymol **507**: 229-254.

Grieger, J. C., S. Snowdy and R. J. Samulski (2006). "Separate basic region motifs within the adeno-associated virus capsid proteins are essential for infectivity and assembly." J Virol **80**(11): 5199-5210.

Harada, J. N., A. Shevchenko, A. Shevchenko, D. C. Pallas and A. J. Berk (2002). "Analysis of the adenovirus E1B-55K-anchored proteome reveals its link to ubiquitination machinery." J Virol **76**(18): 9194-9206.

Hermonat, P. L., M. A. Labow, R. Wright, K. I. Berns and N. Muzyczka (1984). "Genetics of adeno-associated virus: isolation and preliminary characterization of adeno-associated virus type 2 mutants." J Virol **51**(2): 329-339.

Hernandez-Munoz, I., P. Taghavi, C. Kuijl, J. Neefjes and M. van Lohuizen (2005). "Association of BMI1 with polycomb bodies is dynamic and requires PRC2/EZH2 and the maintenance DNA methyltransferase DNMT1." Mol Cell Biol **25**(24): 11047-11058.

Hershko, A. and A. Ciechanover (1992). "The ubiquitin system for protein degradation." Annu Rev Biochem **61**: 761-807.

Hershko, A. and A. Ciechanover (1998). "The ubiquitin system." Annual Review of Biochemistry **67**: 425-479.

Hirosue, S., K. Senn, N. Clement, M. Nonnenmacher, L. Gigout, R. M. Linden and T. Weber (2007). "Effect of inhibition of dynein function and microtubule-altering drugs on AAV2 transduction." Virology **367**(1): 10-18.

Hoggan, M. D., N. R. Blacklow and W. P. Rowe (1966). "Studies of small DNA viruses found in various adenovirus preparations: physical, biological, and immunological characteristics." Proc Natl Acad Sci U S A **55**(6): 1467-1474.

Huang, M. M. and P. Hearing (1989). "Adenovirus early region 4 encodes two gene products with redundant effects in lytic infection." J Virol **63**(6): 2605-2615.

Huang, Y. and K. K. Wang (2001). "The calpain family and human disease." Trends Mol Med **7**(8): 355-362.

Janik, J. E., M. M. Huston, K. Cho and J. A. Rose (1989). "Efficient synthesis of adeno-associated virus structural proteins requires both adenovirus DNA binding protein and VA I RNA." Virology **168**(2): 320-329.

Johnson, J. S., M. Gentzsch, L. Zhang, C. M. Ribeiro, B. Kantor, T. Kafri, R. J. Pickles and R. J. Samulski (2011). "AAV exploits subcellular stress associated with inflammation, endoplasmic reticulum expansion, and misfolded proteins in models of cystic fibrosis." PLoS Pathog **7**(5): e1002053.

Johnson, J. S. and R. J. Samulski (2009). "Enhancement of adeno-associated virus infection by mobilizing capsids into and out of the nucleolus." J Virol **83**(6): 2632-2644.

Kashiwakura, Y., K. Tamayose, K. Iwabuchi, Y. Hirai, T. Shimada, K. Matsumoto, T. Nakamura, M. Watanabe, K. Oshimi and H. Daida (2005). "Hepatocyte growth factor receptor is a coreceptor for adeno-associated virus type 2 infection." J Virol **79**(1): 609-614.

Kern, A., K. Schmidt, C. Leder, O. J. Muller, C. E. Wobus, K. Bettinger, C. W. Von der Lieth, J. A. King and J. A. Kleinschmidt (2003). "Identification of a heparin-binding motif on adeno-associated virus type 2 capsids." J Virol **77**(20): 11072-11081.

Kim, B., H. J. Nam, K. E. Pyo, M. J. Jang, I. S. Kim, D. Kim, K. Boo, S. H. Lee, J. B. Yoon, S. H. Baek and J. H. Kim (2011). "Breast cancer metastasis suppressor 1 (BRMS1) is destabilized by the Cul3-SPOP E3 ubiquitin ligase complex." Biochem Biophys Res Commun **415**(4): 720-726.

King, J. A., R. Dubielzig, D. Grimm and J. A. Kleinschmidt (2001). "DNA helicase-mediated packaging of adeno-associated virus type 2 genomes into preformed capsids." EMBO J **20**(12): 3282-3291.

Kronenberg, S., B. Bottcher, C. W. von der Lieth, S. Bleker and J. A. Kleinschmidt (2005). "A conformational change in the adeno-associated virus type 2 capsid leads to the exposure of hidden VP1 N termini." J Virol **79**(9): 5296-5303.

Kronenberg, S., J. A. Kleinschmidt and B. Bottcher (2001). "Electron cryo-microscopy and image reconstruction of adeno-associated virus type 2 empty capsids." Embo Reports **2**(11): 997-1002.

Kwon, J. E., M. La, K. H. Oh, Y. M. Oh, G. R. Kim, J. H. Seol, S. H. Baek, T. Chiba, K. Tanaka, O. S. Bang, C. O. Joe and C. H. Chung (2006). "BTB domain-containing speckle-type POZ protein (SPOP) serves as an adaptor of Daxx for ubiquitination by Cul3-based ubiquitin ligase." J Biol Chem **281**(18): 12664-12672.

Levy, H. C., V. D. Bowman, L. Govindasamy, R. McKenna, K. Nash, K. Warrington, W. Chen, N. Muzyczka, X. Yan, T. S. Baker and M. Agbandje-McKenna (2009). "Heparin binding induces conformational changes in Adeno-associated virus serotype 2." J Struct Biol **165**(3): 146-156.

Li, C., J. Ao, J. Fu, D. F. Lee, J. Xu, D. Lonard and B. W. O'Malley (2011). "Tumor-suppressor role for the SPOP ubiquitin ligase in signal-dependent proteolysis of the oncogenic co-activator SRC-3/AIB1." Oncogene **30**(42): 4350-4364.

Liu, J., M. Furukawa, T. Matsumoto and Y. Xiong (2002). "NEDD8 modification of CUL1 dissociates p120(CAND1), an inhibitor of CUL1-SKP1 binding and SCF ligases." Mol Cell **10**(6): 1511-1518.

Lo, S. C., X. Li, M. T. Henzl, L. J. Beamer and M. Hannink (2006). "Structure of the Keap1:Nrf2 interface provides mechanistic insight into Nrf2 signaling." EMBO J **25**(15): 3605-3617.

Lusby, E., K. H. Fife and K. I. Berns (1980). "Nucleotide sequence of the inverted terminal repetition in adeno-associated virus DNA." J Virol **34**(2): 402-409.

Lydeard, J. R., B. A. Schulman and J. W. Harper (2013). "Building and remodelling Cullin-RING E3 ubiquitin ligases." EMBO Rep **14**(12): 1050-1061.

McMahon, M., K. Itoh, M. Yamamoto and J. D. Hayes (2003). "Keap1-dependent proteasomal degradation of transcription factor Nrf2 contributes to the negative regulation of antioxidant response element-driven gene expression." J Biol Chem **278**(24): 21592-21600.

McPherson, R. A., L. J. Rosenthal and J. A. Rose (1985). "Human cytomegalovirus completely helps adeno-associated virus replication." Virology **147**(1): 217-222.

Mehle, A., B. Strack, P. Ancuta, C. Zhang, M. McPike and D. Gabuzda (2004). "Vif overcomes the innate antiviral activity of APOBEC3G by promoting its degradation in the ubiquitin-proteasome pathway." J Biol Chem **279**(9): 7792-7798.

Mercer, J., B. Snijder, R. Sacher, C. Burkard, C. K. Bleck, H. Stahlberg, L. Pelkmans and A. Helenius (2012). "RNAi Screening Reveals Proteasome- and Cullin3-Dependent Stages in Vaccinia Virus Infection." Cell Rep **2**(4): 1036-1047.

Metzger, M. B., J. N. Pruneda, R. E. Klevit and A. M. Weissman (2014). "RING-type E3 ligases: master manipulators of E2 ubiquitin-conjugating enzymes and ubiquitination." Biochim Biophys Acta **1843**(1): 47-60.

Michelfelder, S. and M. Trepel (2009). "Adeno-Associated Viral Vectors and Their Redirection to Cell-Type Specific Receptors." Tissue-Specific Vascular Endothelial Signals and Vector Targeting, Part A **67**: 29-60.

Mitchell, A. M., S. C. Nicolson, J. K. Warischalk and R. J. Samulski (2010). "AAV's anatomy: roadmap for optimizing vectors for translational success." Curr Gene Ther **10**(5): 319-340.

Mitchell, A. M. and R. J. Samulski (2013). "Mechanistic insights into the enhancement of adeno-associated virus transduction by proteasome inhibitors." J Virol.

Mori, S., L. Wang, T. Takeuchi and T. Kanda (2004). "Two novel adeno-associated viruses from cynomolgus monkey: pseudotyping characterization of capsid protein." Virology **330**(2): 375-383.

Moskalenko, M., L. Chen, M. van Roey, B. A. Donahue, R. O. Snyder, J. G. McArthur and S. D. Patel (2000). "Epitope mapping of human anti-adeno-associated virus type 2 neutralizing antibodies: implications for gene therapy and virus structure." J Virol **74**(4): 1761-1766.

Mouw, M. B. and D. J. Pintel (2000). "Adeno-associated virus RNAs appear in a temporal order and their splicing is stimulated during coinfection with adenovirus." J Virol **74**(21): 9878-9888.

Mukhopadhyay, D. and H. Riezman (2007). "Proteasome-independent functions of ubiquitin in endocytosis and signaling." Science **315**(5809): 201-205.

Muramatsu, S., H. Mizukami, N. S. Young and K. E. Brown (1996). "Nucleotide sequencing and generation of an infectious clone of adeno-associated virus 3." Virology **221**(1): 208-217.

Murphy, S. L., A. Bhagwat, S. Edmonson, S. Zhou and K. A. High (2008). "High-throughput screening and biophysical interrogation of hepatotropic AAV." Mol Ther **16**(12): 1960-1967.

Nagai, Y., T. Kojima, Y. Muro, T. Hachiya, Y. Nishizawa, T. Wakabayashi and M. Hagiwara (1997). "Identification of a novel nuclear speckle-type protein, SPOP." FEBS Letters **418**(1-2): 23-26.

Nam, H. J., B. L. Gurda, R. McKenna, M. Potter, B. Byrne, M. Salganik, N. Muzyczka and M. Agbandje-McKenna (2011). "Structural studies of adeno-associated virus serotype 8 capsid transitions associated with endosomal trafficking." J Virol **85**(22): 11791-11799.

Nash, K., W. Chen, M. Salganik and N. Muzyczka (2009). "Identification of cellular proteins that interact with the adeno-associated virus rep protein." J Virol **83**(1): 454-469.

Naumer, M. (2011). "Implications of capsid modifications by selected peptide ligands on rAAV-mediated gene transduction."

Nicolson, S. C. and R. J. Samulski (2013). "Adeno-Associated Virus Utilizes Host Cell Nuclear Import Machinery to Enter the Nucleus." Molecular Therapy **21**: S30-S30.

Nonnenmacher, M. and T. Weber (2011). "Adeno-Associated Virus 2 Infection Requires Endocytosis through the CLIC/GEEC Pathway." Cell Host & Microbe **10**(6): 563-576.

Nonnenmacher, M. and T. Weber (2012). "Intracellular transport of recombinant adeno-associated virus vectors." Gene Therapy.

O'Gorman, S., D. T. Fox and G. M. Wahl (1991). "Recombinase-mediated gene activation and site-specific integration in mammalian cells." Science **251**(4999): 1351-1355.

Ogston, P., K. Raj and P. Beard (2000). "Productive replication of adeno-associated virus can occur in human papillomavirus type 16 (HPV-16) episome-containing keratinocytes and is augmented by the HPV-16 E2 protein." J Virol **74**(8): 3494-3504.

Opie, S. R., K. H. Warrington, Jr., M. Agbandje-McKenna, S. Zolotukhin and N. Muzyczka (2003). "Identification of amino acid residues in the capsid proteins of adeno-associated virus type 2 that contribute to heparan sulfate proteoglycan binding." J Virol **77**(12): 6995-7006.

Petroski, M. D. and R. J. Deshaies (2005). "Function and regulation of cullin-RING ubiquitin ligases." Nat Rev Mol Cell Biol **6**(1): 9-20.

Popa-Wagner, R. (2011). "Funktionelle Analyse infektionsrelevanter Proteinsequenzmotive des VP1/2 N-Terminus vom Adeno-assoziierten Virus Typ 2."

Porwal, M., S. Cohen, K. Snoussi, R. Popa-Wagner, F. Anderson, N. Dugot-Senant, H. Wodrich, C. Dinsart, J. A. Kleinschmidt, N. Pante and M. Kann (2013). "Parvoviruses cause nuclear envelope breakdown by activating key enzymes of mitosis." PLoS Pathog **9**(10): e1003671.

Precious, B., K. Childs, V. Fitzpatrick-Swallow, S. Goodbourn and R. E. Randall (2005). "Simian virus 5 V protein acts as an adaptor, linking DDB1 to STAT2, to facilitate the ubiquitination of STAT1." J Virol **79**(21): 13434-13441.

Qing, K., B. Khuntirat, C. Mah, D. M. Kube, X. S. Wang, S. Ponnazhagan, S. Zhou, V. J. Dwarki, M. C. Yoder and A. Srivastava (1998). "Adeno-associated virus type 2-mediated gene transfer: correlation of tyrosine phosphorylation of the cellular single-stranded D sequence-binding protein with transgene expression in human cells in vitro and murine tissues in vivo." J Virol **72**(2): 1593-1599.

Qing, K., C. Mah, J. Hansen, S. Zhou, V. Dwarki and A. Srivastava (1999). "Human fibroblast growth factor receptor 1 is a co-receptor for infection by adeno-associated virus 2." Nat Med **5**(1): 71-77.

Radtke, K., K. Dohner and B. Sodeik (2006). "Viral interactions with the cytoskeleton: a hitchhiker's guide to the cell." Cell Microbiol **8**(3): 387-400.

Rigaut, G., A. Shevchenko, B. Rutz, M. Wilm, M. Mann and B. Seraphin (1999). "A generic protein purification method for protein complex characterization and proteome exploration." Nat Biotechnol **17**(10): 1030-1032.

Rose, J. A., J. V. Maizel, Jr., J. K. Inman and A. J. Shatkin (1971). "Structural proteins of adenovirus-associated viruses." J Virol **8**(5): 766-770.

Rutledge, E. A., C. L. Halbert and D. W. Russell (1998). "Infectious clones and vectors derived from adeno-associated virus (AAV) serotypes other than AAV type 2." J Virol **72**(1): 309-319.

Saha, A. and R. J. Deshaies (2008). "Multimodal activation of the ubiquitin ligase SCF by Nedd8 conjugation." Mol Cell **32**(1): 21-31.

Salganik, M., F. Aydemir, H. J. Nam, R. McKenna, M. Agbandje-McKenna and N. Muzyczka (2014). "Adeno-associated virus capsid proteins may play a role in transcription and second-strand synthesis of recombinant genomes." J Virol **88**(2): 1071-1079.

Salganik, M., B. Venkatakrishnan, A. Bennett, B. Lins, J. Yarbrough, N. Muzyczka, M. Agbandje-McKenna and R. McKenna (2012). "Evidence for pH-dependent protease activity in the adeno-associated virus capsid." J Virol **86**(21): 11877-11885.

Samulski, R. J. and T. Shenk (1988). "Adenovirus E1B 55-Mr polypeptide facilitates timely cytoplasmic accumulation of adeno-associated virus mRNAs." J Virol **62**(1): 206-210.

Sanlioglu, S., P. K. Benson, J. Yang, E. M. Atkinson, T. Reynolds and J. F. Engelhardt (2000). "Endocytosis and nuclear trafficking of adeno-associated virus type 2 are controlled by rac1 and phosphatidylinositol-3 kinase activation." J Virol **74**(19): 9184-9196.

Sarikas, A., T. Hartmann and Z. Q. Pan (2011). "The cullin protein family." Genome Biol **12**(4): 220.

Schlehofer, J. R., M. Ehrbar and H. zur Hausen (1986). "Vaccinia virus, herpes simplex virus, and carcinogens induce DNA amplification in a human cell line and support replication of a helpervirus dependent parvovirus." Virology **152**(1): 110-117.

Schmidt, M., A. Voutetakis, S. Afione, C. Zheng, D. Mandikian and J. A. Chiorini (2008). "Adeno-associated virus type 12 (AAV12): a novel AAV serotype with sialic acid- and heparan sulfate proteoglycan-independent transduction activity." J Virol **82**(3): 1399-1406.

Schulman, B. A. and J. W. Harper (2009). "Ubiquitin-like protein activation by E1 enzymes: the apex for downstream signalling pathways." Nat Rev Mol Cell Biol **10**(5): 319-331.

Sheehy, A. M., N. C. Gaddis and M. H. Malim (2003). "The antiretroviral enzyme APOBEC3G is degraded by the proteasome in response to HIV-1 Vif." Nat Med **9**(11): 1404-1407.

Shi, Y., E. Seto, L. S. Chang and T. Shenk (1991). "Transcriptional repression by YY1, a human GLI-Kruppel-related protein, and relief of repression by adenovirus E1A protein." Cell **67**(2): 377-388.

Sonntag, F., S. Bleker, B. Leuchs, R. Fischer and J. A. Kleinschmidt (2006). "Adeno-associated virus type 2 capsids with externalized VP1/VP2 trafficking domains are generated prior to passage through the cytoplasm and are maintained until uncoating occurs in the nucleus." Journal of Virology **80**(22): 11040-11054.

Sonntag, F., K. Kother, K. Schmidt, M. Weghofer, C. Raupp, K. Nieto, A. Kuck, B. Gerlach, B. Bottcher, O. J. Muller, K. Lux, M. Horer and J. A. Kleinschmidt (2011). "The assembly-activating protein promotes capsid assembly of different adeno-associated virus serotypes." J Virol **85**(23): 12686-12697.

Sonntag, F., K. Schmidt and J. A. Kleinschmidt (2010). "A viral assembly factor promotes AAV2 capsid formation in the nucleolus." Proc Natl Acad Sci U S A **107**(22): 10220-10225.

Srivastava, A., E. W. Lusby and K. I. Berns (1983). "Nucleotide sequence and organization of the adeno-associated virus 2 genome." J Virol **45**(2): 555-564.

Stahnke, S., K. Lux, S. Uhrig, F. Kreppel, M. Hosel, O. Coutelle, M. Ogris, M. Hallek and H. Buning (2011). "Intrinsic phospholipase A2 activity of adeno-associated virus is involved in endosomal escape of incoming particles." Virology **409**(1): 77-83.

Summerford, C., J. S. Bartlett and R. J. Samulski (1999). "AlphaVbeta5 integrin: a co-receptor for adeno-associated virus type 2 infection." Nat Med **5**(1): 78-82.

Summerford, C. and R. J. Samulski (1998). "Membrane-associated heparan sulfate proteoglycan is a receptor for adeno-associated virus type 2 virions." J Virol **72**(2): 1438-1445.

Tomsig, J. L. (2003). "Identification of Targets for Calcium Signaling through the Copine Family of Proteins. CHARACTERIZATION OF A COILED-COIL COPINE-BINDING MOTIF." Journal of Biological Chemistry **278**(12): 10048-10054.

Ulane, C. M. and C. M. Horvath (2002). "Paramyxoviruses SV5 and HPIV2 assemble STAT protein ubiquitin ligase complexes from cellular components." Virology **304**(2): 160-166.

Varshavsky, A. (1991). "Naming a targeting signal." Cell **64**(1): 13-15.

Wallen, A. J., G. A. Barker, D. E. Fein, H. Jing and S. L. Diamond (2011). "Enhancers of adeno-associated virus AAV2 transduction via high throughput siRNA screening." Mol Ther **19**(6): 1152-1160.

Walz, C., A. Deprez, T. Dupressoir, M. Durst, M. Rabreau and J. R. Schlehofer (1997). "Interaction of human papillomavirus type 16 and adeno-associated virus type 2 co-infecting human cervical epithelium." J Gen Virol **78 (Pt 6)**: 1441-1452.

Ward, P., F. B. Dean, M. E. O'Donnell and K. I. Berns (1998). "Role of the adenovirus DNA-binding protein in in vitro adeno-associated virus DNA replication." J Virol **72**(1): 420-427.

Weitzman, M. D., S. R. Kyostio, R. M. Kotin and R. A. Owens (1994). "Adeno-associated virus (AAV) Rep proteins mediate complex formation between AAV DNA and its integration site in human DNA." Proc Natl Acad Sci U S A **91**(13): 5808-5812.

Wenzel, D. M., K. E. Stoll and R. E. Klevit (2011). "E2s: structurally economical and functionally replete." Biochem J **433**(1): 31-42.

Winocour, E., M. F. Callaham and E. Huberman (1988). "Perturbation of the cell cycle by adeno-associated virus." Virology **167**(2): 393-399.

Wu, P., W. Xiao, T. Conlon, J. Hughes, M. Agbandje-McKenna, T. Ferkol, T. Flotte and N. Muzyczka (2000). "Mutational analysis of the adeno-associated virus type 2 (AAV2) capsid gene and construction of AAV2 vectors with altered tropism." J Virol **74**(18): 8635-8647.

Xiao, P. J. and R. J. Samulski (2012). "Cytoplasmic trafficking, endosomal escape, and perinuclear accumulation of adeno-associated virus type 2 particles are facilitated by microtubule network." J Virol **86**(19): 10462-10473.

Xiao, W., N. Chirmule, S. C. Berta, B. McCullough, G. Gao and J. M. Wilson (1999). "Gene therapy vectors based on adeno-associated virus type 1." J Virol **73**(5): 3994-4003.

Xiao, W., K. H. Warrington, Jr., P. Hearing, J. Hughes and N. Muzyczka (2002). "Adenovirus-facilitated nuclear translocation of adeno-associated virus type 2." J Virol **76**(22): 11505-11517.

Xie, Q., W. Bu, S. Bhatia, J. Hare, T. Somasundaram, A. Azzi and M. S. Chapman (2002). "The atomic structure of adeno-associated virus (AAV-2), a vector for human gene therapy." Proc Natl Acad Sci U S A **99**(16): 10405-10410.

Yakobson, B., T. A. Hrynko, M. J. Peak and E. Winocour (1989). "Replication of adeno-associated virus in cells irradiated with UV light at 254 nm." J Virol **63**(3): 1023-1030.

Yakobson, B., T. Koch and E. Winocour (1987). "Replication of adeno-associated virus in synchronized cells without the addition of a helper virus." J Virol **61**(4): 972-981.

Yalkinoglu, A. O., R. Heilbronn, A. Burkle, J. R. Schlehofer and H. zur Hausen (1988). "DNA amplification of adeno-associated virus as a response to cellular genotoxic stress." Cancer Res **48**(11): 3123-3129.

Yan, Z., R. Zak, Y. Zhang, W. Ding, S. Godwin, K. Munson, R. Peluso and J. F. Engelhardt (2004). "Distinct classes of proteasome-modulating agents cooperatively augment recombinant adeno-associated virus type 2 and type 5-mediated transduction from the apical surfaces of human airway epithelia." J Virol **78**(6): 2863-2874.

Yan, Z. Y., R. Zak, G. W. G. Luxton, T. C. Ritchie, U. Bantel-Schaal and J. F. Engelhardt (2002). "Ubiquitination of both adeno-associated virus type 2 and 5 capsid proteins affects the transduction efficiency of recombinant vectors." Journal of Virology **76**(5): 2043-2053.

Yu, X., Y. Yu, B. Liu, K. Luo, W. Kong, P. Mao and X. F. Yu (2003). "Induction of APOBEC3G ubiquitination and degradation by an HIV-1 Vif-Cul5-SCF complex." Science **302**(5647): 1056-1060.

Zadori, Z., J. Szelei, M. C. Lacoste, Y. Li, S. Gariepy, P. Raymond, M. Allaire, I. R. Nabi and P. Tijssen (2001). "A viral phospholipase A(2) is required for parvovirus infectivity." Developmental Cell **1**(2): 291-302.

Zheng, J., X. Yang, J. M. Harrell, S. Ryzhikov, E. H. Shim, K. Lykke-Andersen, N. Wei, H. Sun, R. Kobayashi and H. Zhang (2002). "CAND1 binds to unneddylated CUL1 and regulates the formation of SCF ubiquitin E3 ligase complex." Mol Cell **10**(6): 1519-1526.

Zhong, L., B. Li, G. Jayandharan, C. S. Mah, L. Govindasamy, M. Agbandje-McKenna, R. W. Herzog, K. A. Weigel-Van Aken, J. A. Hobbs, S. Zolotukhin, N. Muzyczka and A. Srivastava (2008). "Tyrosine-phosphorylation of AAV2 vectors and its consequences on viral intracellular trafficking and transgene expression." Virology **381**(2): 194-202.

Zhong, L., B. Li, C. S. Mah, L. Govindasamy, M. Agbandje-McKenna, M. Cooper, R. W. Herzog, I. Zolotukhin, K. H. Warrington, Jr., K. A. Weigel-Van Aken, J. A. Hobbs, S. Zolotukhin, N. Muzyczka and A. Srivastava (2008). "Next generation of adeno-associated virus 2 vectors: point mutations in tyrosines lead to high-efficiency transduction at lower doses." Proc Natl Acad Sci U S A **105**(22): 7827-7832.

Zhong, L., W. Zhao, J. Wu, B. Li, S. Zolotukhin, L. Govindasamy, M. Agbandje-McKenna and A. Srivastava (2007). "A dual role of EGFR protein tyrosine kinase signaling in ubiquitination of AAV2 capsids and viral second-strand DNA synthesis." Mol Ther **15**(7): 1323-1330.

Zhuang, M., M. F. Calabrese, J. Liu, M. B. Waddell, A. Nourse, M. Hammel, D. J. Miller, H. Walden, D. M. Duda, S. N. Seyedin, T. Hoggard, J. W. Harper, K. P. White and B. A. Schulman (2009). "Structures of SPOP-substrate complexes: insights into molecular architectures of BTB-Cul3 ubiquitin ligases." Mol Cell **36**(1): 39-50.

7 Appendix

7.1 Table of figures

7.2 Abbreviations

A

A	alanine
Å	angstrom
AAP	assembly-activating protein
AAV(s)	adeno-associated virus(es)
Ad	Adenovirus
al.	alteres
APS	ammonium persulfate
Asp	aspartate

B

Bidest.	Bidestillatus
bp	base pairs
BR	basic region(s)
BSA	bovine serum albumin
BTB	Bric-a-brac, Tramtrack, Broad-complex

C

CAND1	Cullin-associated neddylation dissociated protein 1
CAV	caveolar-mediated
CBP	calmodulin binding peptide
CCP	clathrin-mediated
CDK	cyclin-dependent kinase
cDNA	complementary DNA
CLIC/GEEC	clathrin-independent carriers/GPI-enriched endocyctic compartment
cm	centimeter
Co-IP	co-immunoprecipitation
CRL(s)	Cullin-RING ligase(s)
CRL3	Cullin-RING ligase 3
CSN	signalosome
CTD	C-terminal domain
Cul	Cullin

D

°C	degree centigrade
D	aspartate
d	day(s)
DAGPO	Donkey-anti-goat coupled with HRP
DAPI	4',6-diamidino-2-phenylindole
Daxx	Death-associated protein
DCAF	DDB1-Cul4 associated factor
DDB1	DNA damage-binding protein 1
DMEM	dulbecco's modified eagle's minimal essential medium

DMSO	dimethylsulfoxide
DNA	desoxy-ribonucleic acid
dNTP	desoxy-ribonucleotide triphosphate
DOX	doxycycline
DTT	dithiothreitol

E

E	glutamate
E. coli	Escherichia coli
e.g.	example given
EDTA	ethylendiaminetetraacetic acid
EE	early endosomes
ER	endoplasmatic reticulum
EtOH	ethanol

F

Fbw8	F-box and WD repeat domain protein 8
FCS	fetal calf serum
FRT	Flp recombinase target
Fwd.	forward

G

g	gram
GAMPO	goat anti mouse peroxidase
GARPO	goat anti rabbit peroxidase
GDP	guanidine diphosphate
GPCF	Genomics & Proteomics Core Facility
GST	glutathione-S-transferase
GTP	guanidine triphosphate

H

h	hour(s)
HA	hemagglutinin
HDF	host dependence factor
HEK	human embryonic kidney (cells)
HeLa	Henrietta Lacks (cells)
HEPES	4-(2-hydroxyethyl)-1-piperazineethanesulfonic acid
HIV	human immunodeficiency virus
HPV	human papilloma virus
HRF	host restriction factor
HRP	horseradish peroxidase
HSPG	heparan sulfate proteoglycane

I

i.e.	in example
IgG	immunoglobuline G
IP	immunoprecipitation
ITR	inverted terminal repeat

K

kb	kilo bases
kDa	kilo Dalton
KOD	pyrococcus kodakaraensis
kV	kilo Volt

L

l	liter(s)
LB	luria broth
LB-Amp	Luria Broth ampicillin
LE	late endosomes
LSM	laser scanning microscope

M

M	molar
mA	milli Ampère
Mad2	mitotic arrest deficient 2
MATH	Merpin and TRAF homology
MeOH	methanol
µg	micro gram
µl	micro liter
µM	micro molar
µm	micrometer
min	minutes
ml	milli liter
mM	milli molar
mm	millimeter
MOI	multiplicity of infection
mol	mole
MP	macropinocytosis
mRNA	messenger RNA
MS	mass-spectrometry
ms	milli seconds

N

NaAc	sodium acetate
NLS	nuclear localization signal
nM	nano molar
nm	nanometer
No	nucleolus
Np	nucleoplasm
NPC	nuclear pore complex
Nt	nucleotide(s)
Nuc	nucleus

O

ORF	open reading frame

P

P	proline
P/S	penicillin/streptavidine
PBS	phosphate buffered saline
PBS-MK	phosphate buffered saline-magnesia potassium
PBS-T	phosphate buffered saline-tween
PCR	polymerase chain reaction
PFA	paraformaldehyde
PLA2	phospholipase A2
PNRE	perinuclear recycling endosomes
Pro	proline

R

RBE	rep binging element
Rev.	reverse
RING	really interesting new gene
RLU	relative light units
RNA	ribonucleic acid
ROC	regulator of Cullins
Rpm	rounds per minute
RT	room temperature

S

S	serine
SBC	SPOP binding consensus
SCF	Skp, Cullin, F-box containing complex
SDS	sodium dodecyl sulfate
SDS-PAGE	sodium dodecyl sulfate polyacrylamide gel electrophoresis
Ser	serine
sec.	seconds
siRNA	short interference RNA
Skp1	S-phase kinase associated protein 1
SN	supernatant
SOCS-box	Suppressors of cytokine signaling-box
SPOP	Speckle-type POZ protein
ss	single-stranded

T

TAE	tris-acetate EDTA
TAP	tandem-affinity purification
TEMED	tetramethylethylenediamine
TEV	tobacco etch virus
TGN	trans-Golgi network
TGS	tris-glycine SDS
Thr	threonine
Trs	terminal resolution site

U

U	units
Ub	ubiquitin
UPS	ubiquitin-proteasome system
UV	ultra violet

V

V	Volt
v/v	volume/volume
VHL-box	von Hippel-Lindau box
Vif	HIV-1 virion infectivity factor
VP	viral protein

W

w/v	weight/volume
wt	wild-type

X

X-Gal	bromo-chloro-indolyl-galctopyranoside

Y

YFP	yellow fluorescent protein

Acknowledgements

I would like to express my gratefulness to all those who supported me during my time as a PhD student.

Above all, I would like to thank Prof. Dr. Martin Müller for giving me the opportunity to work on this promising project and complete my thesis in his lab. I also want to thank him for his supervision, scientific input and his great and enduring support during those three years.

I am also grateful to PD Dr. Oliver Müller for agreeing to be my second reviewer, as well as for his scientific support and advice during my TAC meetings.

I would also like to express my gratitude to Prof. Dr. Oliver Gruß and PD Dr. Suat Özbek for joining my thesis evaluation committee.

I am very thankful to Prof. Dr. Jürgen Kleinschmidt for all his scientific advice, input and most of all AAV-specific answers and help throughout my time as PhD student. Furthermore I want to thank Dr. Michael Pawlita for all the input during my TAC meetings. I also would like to thank Prof. Dr. Angel Alonso for all the personal conversations about my project, helping to see it from a different point of view.

Many thanks to Barbara Leuchs for all the AAV titer quantifications she did for me in the last years. I also want Dr. Martina Schnölzer and Dr. Tore Kempf for conducting the mass-spectrometry analysis.

A big "Thank You" to all the members of my lab 2.114, especially to Lis Müller for the mental support every day, her helping hand and all the motivating conversations. Patrick Kammer, Kathatrina Henrich and Gian Mario Dore for the experimental help in the last weeks of my thesis. Petra Galmbacher, Caroline Odenwald, Lorenzo Bulli, Gloria Spagnoli and Dr. Christina Hölscher for a great time and nice working atmosphere in the lab. I also want to thank all former lab members for their help, especially Dr. Anna Sacher for all her support over the years and for introducing me to and accompanying me in the field of AAV. Many thanks to the whole department "2. OG West", especially to Dr. Daniele Viarisio, Dr. Paola Zanna, Birgit Aengeneyndt and Susanne Latzko for many funny moments and open ears. Thanks to Madeleine Sporleder for all the organizational help during the last years.

I am very grateful to all former ATV members, Dr. Lysann Schädlich for her support and help during the last years. I also would like to thank the former Kleinschmidt group, Dr. Ruth Wagner, Dr. Matthias Naumer and Dr. Karl Varadi for all the answers, support and guidance concerning AAV. Many thanks to Patrick Schulz for the numerous motivating coffee breaks with all the discussions about science and society.

Moreover, I want to thank all my friends inside and outside of Heidelberg who always supported me during my PhD time.

I want to express my gratitude to my parents, Antje and Rolf, and my brothers, Stefan and Jörg, for all the support, motivation and strength they spent every day to keep me going.

And last but not least, I want to thank my girlfriend Anja for her support, her patience and always being with me throughout all the ups and downs within this time, making it possible for me to accomplish this thesis.